2014

Measurements and transient multistep outflow simulation of soil-water characteristic curve for soils modified with biopolymers

Xiaoyi Zhao

Department:

MEASUREMENTS AND TRANSIENT MULTISTEP OUTFLOW SIMULATION OF SOIL-WATER CHARACTERISTIC CURVE FOR SOILS MODIFIED WITH BIOPOLYMERS

by

XIAOYI ZHAO

A THESIS

Presented to the Faculty of the Graduate School of the

MISSOURI UNIVERSITY OF SCIENCE AND TECHNOLOGY

In Partial Fulfillment of the Requirements for the Degree

MASTER OF SCIENCE IN CIVIL ENGINEERING

2014

Approved by

Bate Bate, Advisor
Ronaldo Luna
Jeffery Volz

ABSTRACT

In recent decades, biopolymers have shown promising applications in soil modification due to its environmental friendly nature. Most of the studies, however, focused on mechanical properties at saturated or unsaturated conditions. The study on unsaturated soil behaviors under controlled pore air and pore water pressures were limited. Soil-water characteristic curve (SWCC), relating water content with matric suction is a key property to evaluate unsaturated soils. With SWCC, other soil properties, such as hydraulic conductivity and shear strength can be estimated. In this study, SWCC of sands modified with different biopolymers were measured with both Tempe cell and Fredlund SWCC device. An elevation-controlled low suction (0.01 to 5 kPa) horizontal tube was developed to accurately measure SWCC of sands. Corrections for air diffusion and evaporation were performed. The results were fitted by both Fredlund and Xing and van Genutchen equations. In addition, inverse simulation of SWCC based on one-step or multistep SWCC measurements were carried out with software Hydrus 1D, finite element software. The measured SWCC results of mine tailing were used as an example. The inverse model can significantly reduce the time to measure a SWCC curve, especially for soils with low hydraulic conductivity (clay and silt). Three different input outflow methods were used, namely multiple single-step outflow method (MSOM), one-step outflow method (OOM), and multiple-step outflow method (MOM). Their performance was evaluated by both SWCC results and outflow vs. time curves. It was found that MOM provided the most accurate SWCC, while MSOM yielded the most accurate Flux – Time results.

ACKNOWLEDGMENTS

I want to thank my advisor, Dr. Bate Bate, for his patience and guidance. Also I want to thank my committee member. Dr. Ronaldo Luna, a knowledgeable professor and teaching the best foundation course and geotechnical earthquake engineering. Dr. Jeffery Volz, a professor knows how to make student laugh every time. Finally, I want to send my best wishes to my Amazing Smart wife Nan Zhang and the love from my parents.

TABLE OF CONTENTS

LIST OF ILLUSTRATIONS

Page

LIST OF TABLES

Page

NOMENCLATURE

Symbol	Description
β	Contact Angle
ψ	Soil Suction
T_s	Surface Tension
ρ	Density
g	Gravity Constant
r	Pore Size
μ	Viscosity
κ	Soil Permeability
K	Soil Hydraulic Conductivity
S	Degree of Saturation
θ	Volumetric Water Content
a	Factor for Fredlund and Xing Model
n	Factor for Fredlund and Xing Model
m	Factor for Fredlund and Xing Model
δ	Factor for Van Genutchten Model
λ	Factor for Van Genutchten Model
η	Factor for Van Genutchten Model

1. INTRODUCTION

1.1. BIOPOLYMER MODIFICATION

Recent developments of using organic agents for soil stabilization have shown promising results. Organic agents, such as polymers (polyacrylamide, PAM), biopolymers (xanthan gum), and surfactants, have exhibited their abilities to improve the shear strength, stiffness, and erosion resistance behaviors of geomaterials. Besides, PAM and xanthan gum show great impact in enhanced oil recovery. In spite of the extensive amount of work that has been done in soil modification with chemical and microbial methods, most of the work focused on evaluating the swelling/shrinkage, large strain strength, small strain stiffness, and hydraulic conductivity properties in either saturated or unsaturated condition.

1.2. SOIL-WATER CHARACTERISTIC CURVE (SWCC)

Only a few studies controlled the unsaturation conditions, such as matric suction (Puppala et al., 2006). In the field condition, soils are not always saturated due to seasonal groundwater level change, precipitation, evaporation, and evapotranspiration. Once desaturation occurs, soils become unsaturated. The above mentioned mechanical properties of organically modified geomaterials could change drastically (Fredlund and Rahardjo, 1993; Fredlund et al., 2012). It is crucial, therefore, to quantify these changes. These changes are primarily due to the surface tension, contact angle and viscosity of water changes with the addition of biopolymers. Soil-water characteristic curve (SWCC) is a description between water content and matric suction which is a key property to evaluate unsaturated soils. With SWCC, other soil properties, such as hydraulic conductivity and shear strength can be estimated. SWCC can be used in earth dams, contaminant transport and nutrition absorption of plant. These three problems are all about unsaturated water flow which can be related to SWCC. Besides unsaturated water flow, due to the matric suction inside soil, the shear strength of soil will be increased which will show a good result of designing geotechnical projects. Most of the engineering projects are designed in saturation condition which is more conservative.

Since unsaturated condition is changing all the time, there is no guarantee that the matric suction is always inside the soil.

1.3. HYDRUS 1D NUMERICAL ANALYSIS

On the other hand, determination of SWCC experimentally is time consuming, especially for fine-grained soils. Alternatively, numerical estimations from grain size distribution, pore size distribution, and inverse modeling were proposed. The reliability of pore size based methods is not satisfactory. Wayllace and Lu (2012) used inverse modeling for estimating SWCC with a transient water release and imbitions method (TRIM) for rapidly measuring wetting and drying SWCC and hydraulic conductivity functions. The inverse modeling can significantly reduce the time to measure a SWCC curve, especially for soils with low hydraulic conductivity (clay and silt).

1.4. OBJECTIVES OF STUDY

The first objective of this study is to elucidate the mechanisms of the effects of biopolymers on the water holding capacity of sands. To realize this objective, the following tasks will be performed.

1. Use both Tempe cell and Fredlund SWCC device to measure soil-water characteristic curve (SWCC) of geomaterials (sands, kaolinite, and mine tailing) that were modified with different biopolymers.
2. Develop an elevation-controlled low suction (0.01 to 4 kPa) horizontal tube to accurately measure SWCC of sands. Corrections for air diffusion and evaporation were performed.
3. Use Fredlund and Xing (1994) and Van Genutchen (1980) SWCC models to fit the measured SWCC results with least square method. The fitting parameters will be compared, and Scanning Electron Microscope (SEM) images will be taken to evaluate the effects of biopolymers on the pore morphology (size, size distribution, connectivity, and tortuosity) of the biopolymer-modified geomaterials.
4. Measure the contact angle, surface tension, and viscosity of biopolymer solutions. Then use Laplace equation to calculate the pore size distributions. Together with

the results from Task 3, the influence of biopolymers on the pore fabric and bulk solutions will be better understood.

The second objective of this study is to propose transient outflow methods to predict SWCC of geomaterials with different particle size ditributions. There methods will save the time-consuming procedure of SWCC measurements. To realize this objective the following tasks will be performed.

5. Use the recorded outflow-time relationship to predict SWCC and relative hydraulic conductivity using inverse modeling method by Hydrus 1D (Wayllace and Lu, 2012), a finite element software. With the measured SWCC results of a mine tailing as an example, three different input outflow methods, namely multiple single-step outflow method (MSOM), one-step outflow method (OOM), and multiple-step outflow method (MOM) were used.
6. Compare the performance of these methods in terms of R^2 of both SWCC results and outflow vs. time curves.

1.5. LAYOUT OF THESIS

Section 2 is literature review. This section contains different soil modification methods, including both advantages and disadvantages for each method. The advantages of for bio-polymer modification for sand will be exhibited.

Section 3 is soil and solutions' index properties about all the materials used in the SWCC test. They are uniform sand with different grain size, kaolinite and mine tailings. All biopolymers solutions' properties include surface tension, contact angle and viscosity.

Section 4 is the introduction for basic theory of unsaturated soil and SWCC, including sample preparation, test device introduction, model for SWCC and correction.

Section 5 is the SWCC results for different grain size uniform sands with water and biopolymers, mine tailings and kaolinite with biopolymer.

Section 6 will exhibit the numerical analysis results from soil physical parameters and by using HYDRUS-1D, the SWCC will be reversed calculated which will save a lot of time for SWCC test.

Section 7 is the conclusion and future work.

2. LITERATURE REVIEW

2.1. BIOPOLYMER MODIFICATION

Recent developments in the use of organic agents for soil stabilization show promising results. Organic agents, such as polymers (polyacrylamide, PAM), biopolymers (xanthan gum), and surfactants, have exhibited their abilities to improve the shear strength, stiffness, and erosion resistance behaviors of geomaterials (Briscoe and Klein, 2007; Yoshizawa et al., 1993; Bate et al., 2014; Bate et al., 2013; Kang et al., 2014; Martin et al., 1996; Kavazanjian et al., 2009; Cabalar and Canakci, 2005; Nugent et al., 2011). Briscoe and Klein (2007) observed that under water hydration, the slip plane during shearing between two surfactant coated mica surfaces is at the interface of surfactant head and the mica surface. Bate et al. (2013; 2014) found that the addition of a surfactant with long carbon chain (C_{16}) onto montmorillonite can increase the friction angle up to 60^{o}, and increase the shear wave velocity up to 154 m/s at a mean normal stress of 50 kPa. Adsorbed surfactant reduced net surface charge (indicated by the zeta potential) of the soil particle, condensed the soil, and increased the interfacial friction. Xanthan gum, a polysaccharide derived from the bacteria coat of *Xanthomonas campestris*, is reported to increase shear strength of a sand from 30 kPa to 190 kPa with only up to 5% (by weight) addition (Cabalar and Canakci, 2005). The study by Martin et al. (1996) showed that mixing silt with 0.3 weight percent of xanthan gum increased shear strength by up to 30%. In addition, Xanthan gum was also used in increasing wind and coastal stream erosion resistance (Kavazanjian et al., 2009; Nugent et al., 2011). Polyacrylamide (PAM), an industrial polymer, has been widely used in highway erosion control and soil reservation and recovery. Furthermore, increasing number of studies on organically modified soils were also reported in drilling slurry (Mazzieri et al. 2010), slurry wall, mineral separation (Chandraprabha et al., 2004), and geosynthetic clay liner (Lake and Rowe, 2005). Chen and Zhang (2013) using xanthan gum and guar gum to stabilize mine tailings, the effect of biopolymer is building the bonding between mine tailing particles which will stabilize mine tailing. Voordouw (2012) showed that oil sand tailings can be stabilized by using a positive charged biopolymer.

In spite of the extensive amount of work done in soil modification with chemical and microbial methods, most of the work focused on evaluating the swelling, large strain strength, small strain stiffness, and hydraulic conductivity properties in either saturated or unsaturated condition. Only a few studies controlled the unsaturation conditions, such as matric suction (Puppala et al., 2006). In the field condition, soils are not always saturated due to seasonal groundwater level change, precipitation, evaporation, and evapotranspiration. Once desaturation occurs, soils become unsaturated. The above mentioned mechanical properties of organically modified geomaterials could change drastically (Fredlund and Rahardjo, 1993; Fredlund et al., 2012). It is crucial, therefore, to quantify these changes. These changes are primarily due to the surface tension, contact angle and viscosity of water changes with the addition of bio-polymers (Adamson and Gast, 1967). The solution properties are important factors for SWCC test. Surface tension (T_s), contact angle (α), pore size (r), density (ρ) and gravity constant (g) are related to matric suction(ψ):

$$\psi = \frac{2 \cdot T_s \cdot \cos\alpha}{\rho \cdot g \cdot r} \qquad \text{Eq. 2.1}$$

Viscosity is related to the hydraulic conductivity for a porous media with the same pore structure (permeability, κ, hydraulic conductivity, K) but with different pore fluid (viscosity,μ):

$$\kappa = K \frac{\mu}{\rho \cdot g} \qquad \text{Eq. 2.2}$$

Biopolymers can modify these three properties, which leads to changes in the water retention ability of the same porous media with different biopolymer solutions. The water retention capability can be quantified by measurement of soil-water characteristic curve (SWCC).

2.2. UNSATURATED SAND PROPERTIES

The unsaturated soil properties of natural geomaterials have been widely studied. Imre (2008) studied SWCC of both well graded and poorly graded sands. Due to the low water hold capacity, sand will start loss water before 1 kPa and almost drained out under matric suction at 100 kPa. Figure 2.1 showed the SWCC result.

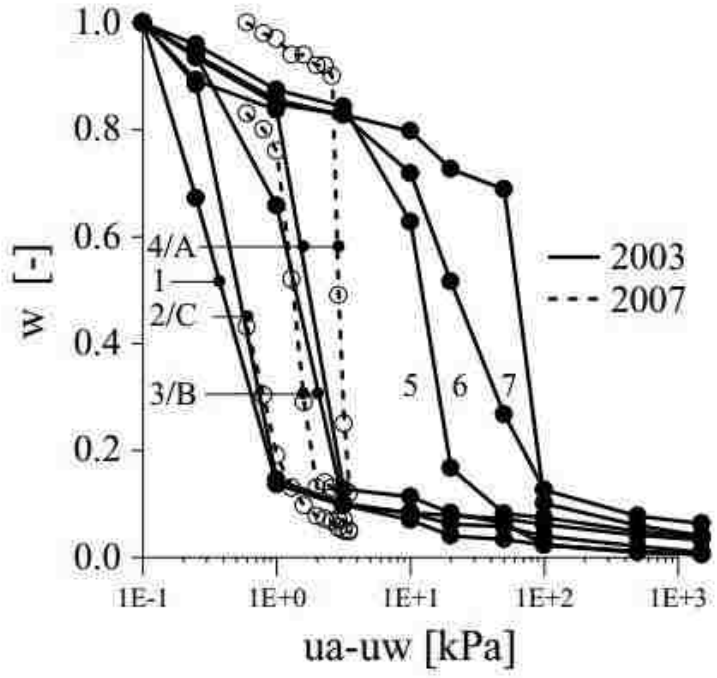

Figure 2.1 SWCC result for Imre (2003,2007)

2.3. INTRODUCTION OF SOIL-WATER CHARACTERISTIC CURVE

Soil suction is generated by unsaturation soil behavior. All soil beneath underground water table is in saturation condition, but soil above water table will stay in unsaturated condition. The principle is the same as capillarity tube. The pore between each soil particles connect with each other and form capillary tube which will lead to water lift up. Usually, the water content used in soil mechanics is gravimetric water content. The definition of volumetric water content is the volume of water remaining in soil divided by total volume of soil sample. Figure 2.2 shows SWCC result for No.125 sand.

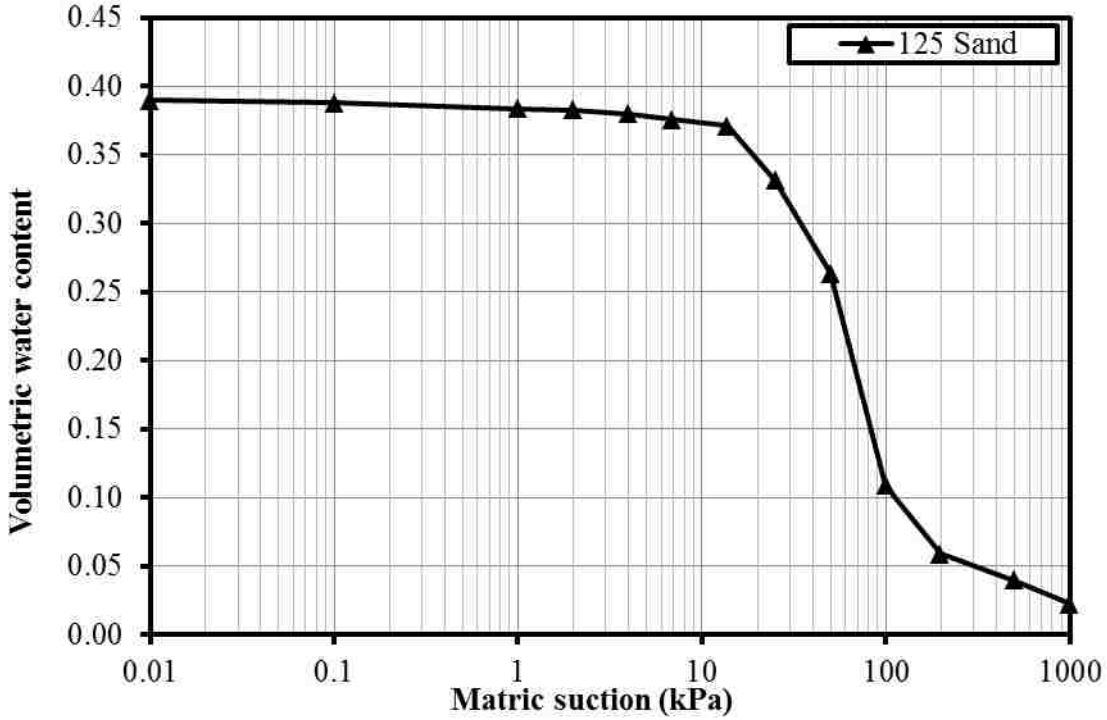

Figure 2.2 SWCC for No. 125 Sand

Soil-Water Characteristic Curve (SWCC) exhibits the relationship between matric suction and volumetric water content inside a soil (Williams, 1982). There are two types of suction in soil, namely matric suction (ψ) and osmotic suction. Matric suction is the difference between air pressure (u_a) and water pressure (u_w), i.e. $\psi = u_a - u_w$. Osmotic suction is only related to the chemical properties of bulk solution. Comparing to matric suction, osmotic suction is usually small and can be neglected in most cases with diluted solutions and coarse-grained geomaterials. SWCC varies with pore size distribution, mineralogy, and bulk fluid.

A typical SWCC was shown in Figure 2.3. Air entry value (AEV) of soil is the suction that cause air starts to get into the largest pores. The major water desaturation occurs between AEV and residual matric suction (ψ_r). The water content at residual matric suction is termed residual water content (ψ_r). The determination of AEV is draw two tangent line of initial SWCC and desorption curve, the value of cross is AEV. Residual water content is the cross between desorption curve and residual SWCC.

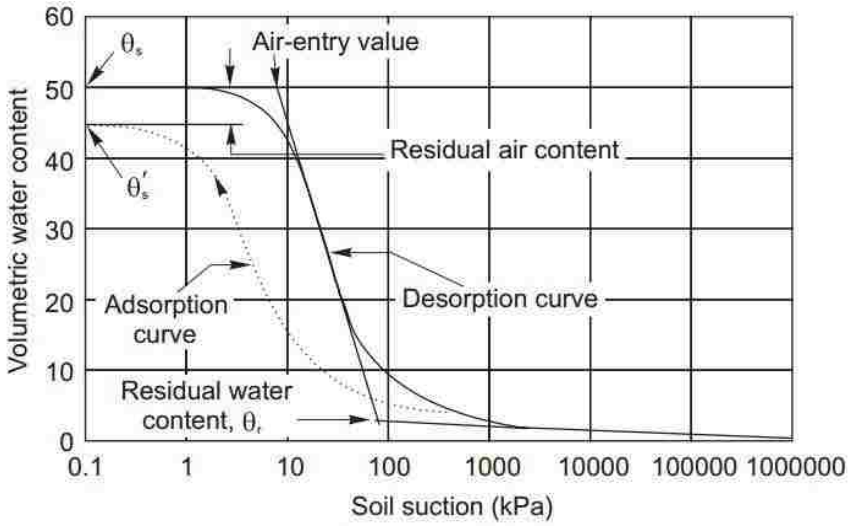

Figure 2.3 Fredlund and Xing model for SWCC (1994)

Previously, many researchers proposed SWCC models as summarized by Ba-Te (2005) and in Table 2.1.

Table 2.1 Previous SWCC model (Ba-Te, 2005)

Model name	**Model**	**Parameters**
Gardner (1922)	$*\ \theta = \frac{B}{\psi} - D$	B, D =parameters
Burdine(1953)	$**\ S = \frac{1}{\left(1+(a\psi)^n\right)^{1-2/n}}$	a, n =parameters
Gardner (1958)	$S = \frac{1}{1+a\psi^n}$	a, n =curve-fitting parameters
Brooks and Corey (1964)	$\theta = \left(\frac{\psi_{aev}}{\psi}\right)^{\lambda}$	ψ_{aev} =air-entry value, λ =pore-size distribution index
Brutsaert model (1966)	$S = \frac{1}{1+\left(\frac{\psi}{a}\right)^n}$	a, n =parameters
Normal distribution	$S = \frac{1}{2} erfc\left(\frac{\psi-\mu}{\sqrt{2}s}\right)$	μ ,s =parameters

Mualem (1976)	$S = \frac{1}{\left(1+(a\psi)^n\right)^{1-1/n}}$	a, n =parameters
Van Genuchten (1980)	$S = \frac{1}{\left(1+(a\psi)^n\right)^m}$	a, n, m = parameters
Williams et al. (1983)	$\ln\psi = a_1 + b_1 \ln\theta$	a_1, b_1 =curve fitting parameters
McKee and Bumb (1987) (Modified Boltzman)	$S = \exp\left(-\frac{\psi}{B}\right)$	B =parameters
Fredlund and Xing (1994)	$S = \frac{1}{\left(\ln\left(e+\left(\frac{\psi}{a}\right)^n\right)\right)^m}$	a, n, m = parameters
Kosugi (1994) (Modified Tani)	$S = \frac{1}{2} erfc\left(\frac{\ln\left(\frac{\psi_{aev}-\psi}{\psi_{aev}-\psi_{mode}}\right)-s^2}{\sqrt{2}\pi s}\right)$	s= parameter related to the standard deviation of pore size distribution, Ψ_{mode} =the mode of the pore size distribution, erfc =the complimentary error function
* : θ =normalized water content ($\theta = (\theta-\theta_r)/(\theta_s-\theta_r)$, where θ_s and θ_r are the saturated and residual volumetric water contents, respectively), ** : S =degree of saturation		

Table 2.1 Previous SWCC model (Ba-Te, 2005) (cont.)

The water retention capability is very important in agriculture, and the soil water characteristic curve in agriculture literature is referred to as water retention curve (van Genuchten, 1980). van Genuchten (1980) model is a continuous SWCC model as shown in Table 2.1:

$$S = \left[\frac{1}{1+(\alpha\psi)^n}\right]^m \qquad \text{Eq. 2.3}$$

The model fits the degree of saturation versus soil suction data over the entire range of soil suction. The equation uses three fitting parameters: *a*, *n* and *m*. The parameter *a* is related to the inverse of the air-entry value (AEV); the *n* parameter is

related to the pore size distribution of the soil and the *m* parameter is related to the asymmetry of the model.

Fredlund and Xing (1994) proposed a SWCC model as shown in Eq. 2.4:

$$\theta = \theta_r + \frac{\theta_s - \theta_r}{\left\{\ln\left[e + \left(\frac{\psi}{\alpha}\right)^n\right]\right\}^m} \qquad \text{Eq 2.4}$$

Where *a* represents air entry value (AEV), the larger *a* represents the higher AEV. Parameter *m* relates to the asymmetry of the model. Parameter *n* is a description of the pore size distribution; the larger *n* will result in a steep SWCC curve which indicates that geomaterial is uniform. Figures 2.4 – 2.6 show the effect of different *a*, *m*, and *n* parameters.

Fredlund and Xing (1994) model with residual suction correction term is as follows:

$$C(\psi) = \frac{-\ln(1 + \psi / \psi_r)}{\ln\left[1 + (1000000 / \psi_r)\right]} + 1 \qquad \text{Eq. 2.5}$$

Where soil suction in residual condition that can be computed (Vanapalli et al. 1998) or assumed to be a value such as 1500 kPa or 3000 kPa. In this study, residual suction is taken as 1500 kPa.

The parameter *a* is related to, but greater than the air entry value of the soil, and has the units of suction. Parameter *a* does not affect the overall shape of the curve but shifts the curve toward the higher soil suction region as *a* increases (Figure 2.4).

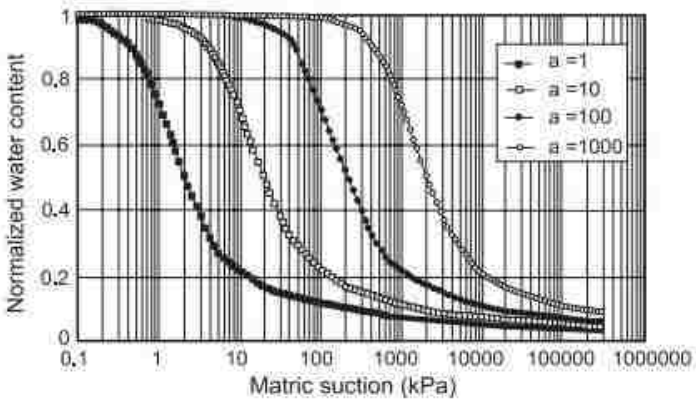

Figure 2.4 Effect of AEV (Fredlund and Xing,1994)

The *n* value corresponds to the inflection point on the curve and it is related to the pore size distribution of the soil. The more uniform the pore sizes in the soil, the larger the value of *n*.

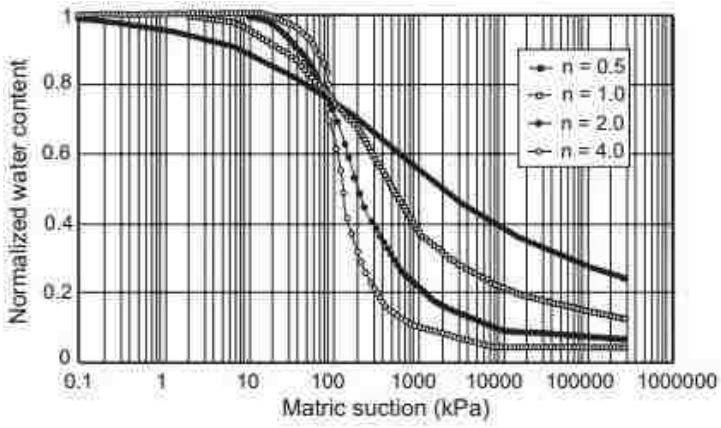

Figure 2.5 Effect of parameter *n* (Fredlund and Xing,1994)

The parameter *m* is related to the asymmetry of the model. Small values of *m* result in a moderate slope in the low suction range and a steeper slope in the high suction range.

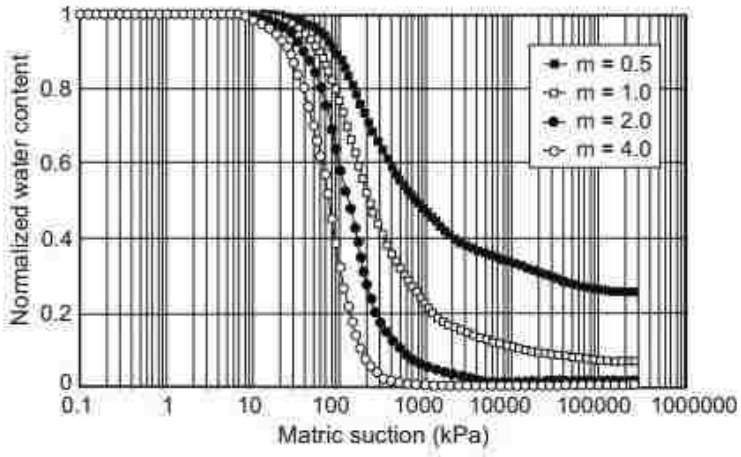

Figure 2.6 Effect of parameter *m* (Fredlund and Xing,1994)

Among all these models, the two most popular ones are Van Genuchten (1980) and Fredlund and Xing (1994) model, which will be used in the analysis of the results in this study. As shown in Figure 2.4-2.6, all the data points are calculated through Fredlund

and Xing model. These two models are continuous so you can use these two model to fit the entire suction range of soil samples.

2.4. APPLICATION OF SWCC

Laboratory studies showed that SWCC can be related to other unsaturated soil properties (Fredlund and Rahardjo, 1993). Unsaturated soil permeability can be estimated through combining saturated permeability and SWCC together (Mualem, 1976). Shear strength estimation is also proposed in a similar way (Fredlund and Rahardjo, 1993). Unsaturated soils permeability is an important factor for many engineering applications, such as water flow in vadose zone, dam engineering, and seepage in slopes. Many researchers have explored the prediction of the permeability with using SWCC (Brooks and Corey 1964; Van Genuchten 1980; McKee and Bumb 1984; Fredlund and Xing 1994). After observing the similarities in different soils behaviors, some of them proposed equations for estimation of SWCC and predict the variation of unsaturated coefficient of permeability with respect to soil suction.

SWCC can be used to predict shear strength. The variation between soil shear strength and matric suction has been well established by Fredlund and Morgenstern (1978), Fredlund and Rahardjo (1993) and Lu and Likos (2006). It was reported that matric suction increase will cause an increase the shear strength. This is due to an additional capillarity-induced stress, either termed as matric suction or suction stress, which provided an additional strength term in addition to the effective stress. It was also shown that a nonlinear increment of shear strength with matric suction was widely reported. Fredlund and Morgenstern (1978) related used SWCC to predict the shear strength gain.

2.5. DETERMINATION OF SWCC

SWCC can be determined from laboratory measurements, particle size distribution, pore size distribution, or inverse modeling. Laboratory testing contains Tempe cell, Fredlund cell and WP4. Tempe and Fredlund cell is using air pressure to desaturation soil sample. WP4 is measuring the relative humidity of air above sample, at temperature equilibrium, relative humidity is a direct measurement of water potential. In

the field, tensiometer is widely used. Laboratory testing is usually time consuming, especially for fine-grained soils with low hydraulic conductivity. To facilitate quick and reliable determination of SWCC, numerical methods were proposed. Theoretical derivations from either particle sizes or pore size distributions are proposed (Fredlund et al., 2002; Wolf et al., 2013; Xiao et al., 2009). However, the deviation from the laboratory measurements was large in general. One-step outflow method (OOM), which uses the outflow vs. time curve at one matric suction value as input to inversely solve for SWCC, was proposed as well (Wayllace and Lu, 2012; details in Section 6). Reasonably results can be obtained. In this study, both laboratory and inverse-simulation were used to determine SWCC.

3. SOIL AND SOLUTION INDEX PROPERTIES

3.1. SOIL PROPERTIES

There are four types of materials used in this study.

1. Ottawa 20-30, 50-70, and 125 sands (US Silica, Ottawa, Illinois, USA)
2. Georgia RP-2 kaolinite (Active Minerals, Cockeysville, MD)
3. Mine Tailing (Doe Run site, MO)
4. Mixture of three of above mentioned geo-materials were also used.

The experimental matrix shows all the testing material and solution (Table 3.1).

Table 3.1 Experimental matrix

		DI-water	PEO	SA		Agar	Xanthan	PAM	PAA	Chitosan
Concentra-tion (g/L)			10	2	20	2	2	2	2	2
Ottawa Sand	20-30	Y	Y	Y	Y	Y	Y	Y	Y	Y
	50-70	Y								
	125	Y								
Ottawa Sand mixture		Y					Y	Y	Y	
Mine tailing		Y								
Kaolinite		Y	Y							
50-70 sand with Kaolinite		Y								

DI water: Deionized water

PEO: Polyethylene oxide

SA: Sodium alginate

PAA: Polyacrylic acid

PAM: Polyacrylamide

The grain size distributions of Ottawa sands 20-30, 50-70 and 125 were shown in Figure 3.1 and the sieve analysis result is shown in Table 3.2, Table 3.3 and Table 3.4 individually.

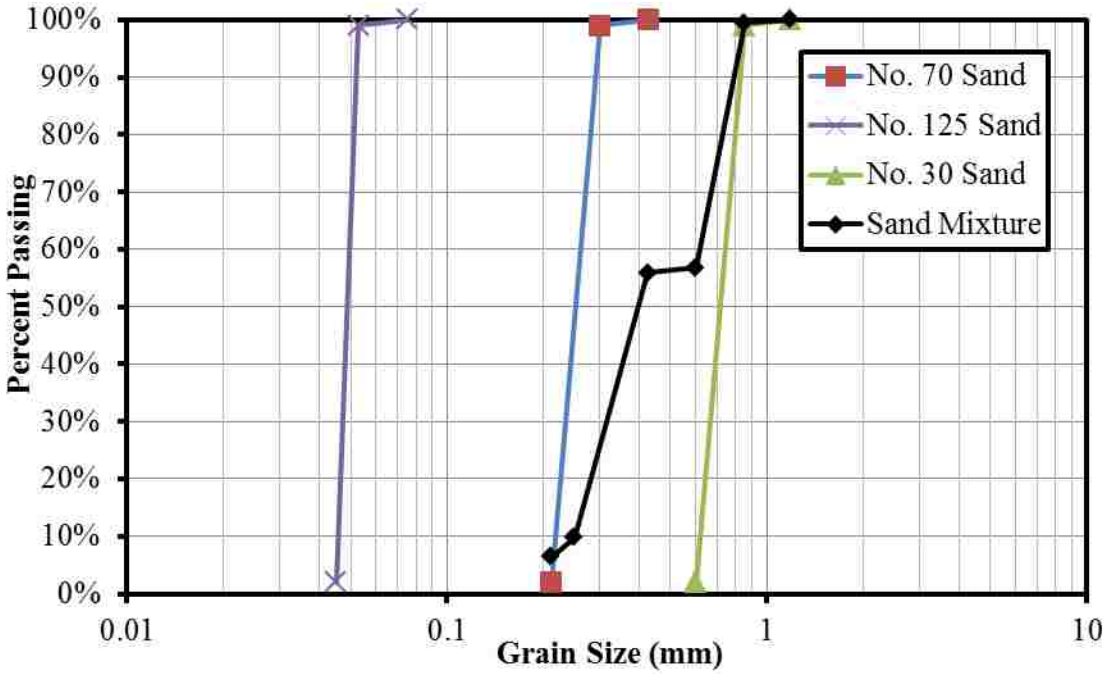

Figure 3.1 Grain size distribution of Ottawa Sand

Table 3.2 Sieve analysis of Ottawa 20-30 sand (Ottawa Sand Manual)

Sieve No.	Sieve Diameter (mm)	Percent Retained Cumulative	Percent Passing
16	1.18	0.0%	100.0%
20	0.85	1.0%	99.0%
30	0.6	97.0%	2.0%
Pan		2.0%	0.0%

Table 3.3 Sieve analysis of Ottawa 50-70 sand (Ottawa Sand Manual)

Sieve No.	Sieve Diameter (mm)	Percent Retained Cumulative	Percent Passing
40	0.425	0.0%	100.0%
50	0.3	1.0%	99.0%
70	0.212	97.0%	2.0%
Pan		2.0%	0.0%

Table 3.4 Sieve analysis of Ottawa 125 sand (Ottawa Sand Manual)

Sieve No.	Sieve Diameter (mm)	Percent Retained Cumulative	Percent Passing
200	0.075	0.0%	100.0%
270	0.053	1.0%	99.0%
325	0.045	97.0%	2.0%
Pan		2.0%	0.0%

Table 3.5 Property of RP-2 Kaolinite (Kang, Kang, Bate, 2014)

	This study
Soil type	Georgia kaolinite
Source	Active Minerals International, Hunt Valley, MD, USA
Trade name	ACTI-MIN RP-2
Color	cream
Specific gravity	2.6***
Liquid limit	54.8
Plastic limit	32.1
Main cation	Sodium
CEC (mequiv./100 g)	-
pH	neutral

Conductivity (mS/cm)	0.07 (10% solids)
D_{50} (micron)	0.36***
Surface area, m^2/g	22 - 35****
Max moisture content (mass %)	1%***
Oil absorption (ASTM D 281) (g/100g clay)	40***
Slurry consolidation pressure (kPa)	100
Vertical effective stress (K_0 loading) (kPa)	0 - 800
Mean effective stress (triaxial loading) (kPa)	-
Void ratio	1.278 - 0.933
Compression index, C_c	0.49 (0.005 mol/l); 0.38 (1 mol/l)
Critical state effective friction angle (degree)	19.8
Testing technique	BE

Table 3.5 Property of RP-2 Kaolinite (Kang, Kang, Bate, 2014) (cont.)

3.2. INDEX PROPERTIES

Hydrometer analysis tests were performed according to ASTM D422. The resulting grain size distribution is shown in Figure 3.2.

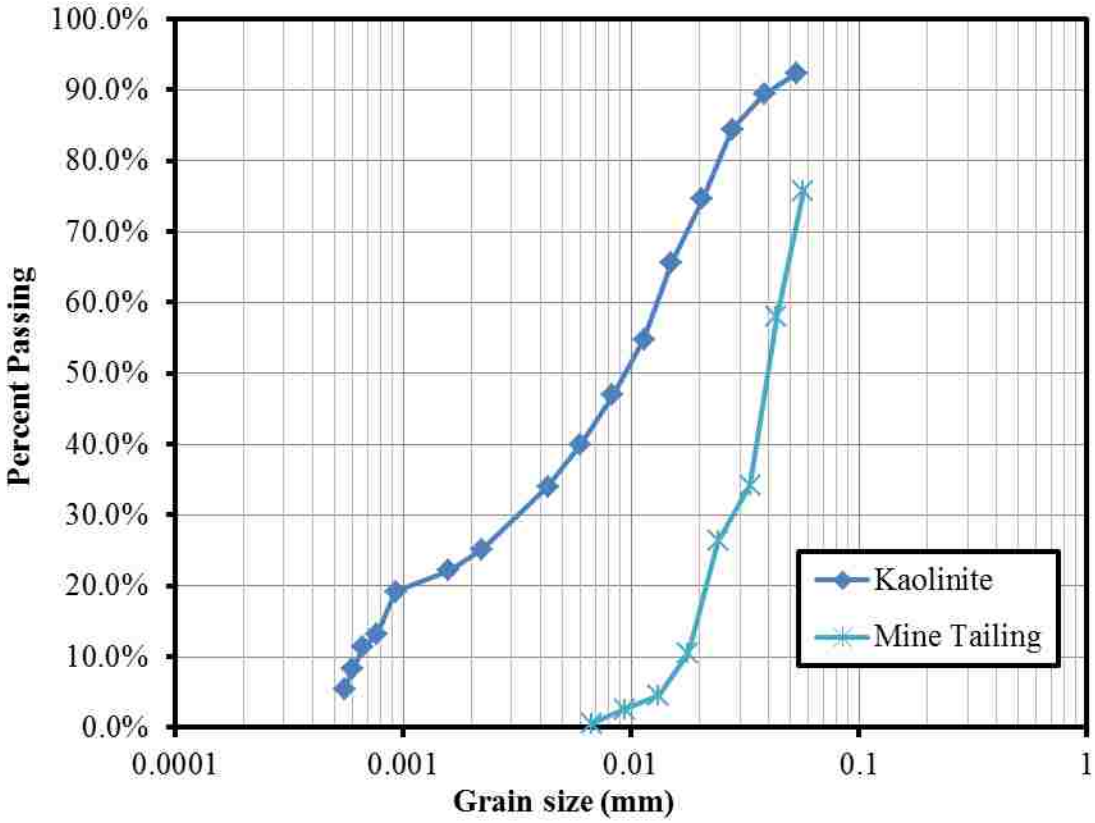

Figure 3.2 Grain size distribution of kaolinite and mine tailing by hydrometer test

Atterberg limits tests were performed according to ASTM D4318-05, and the results were shown in Tables 3.6 and 3.7, and in Figure 3.3. The liquid and plastic limits are 54.83% and 32.08%, respectively.

Table 3.6 PL test result

Kaolinite		
PL = 32.08%		
Trial	1	2
Wt_{tare}	11.8	11.68
Total Wt_{wet}	23.64	23.19
Wt_{wet}	11.84	11.51

Total Wt_{dry}	20.81	20.35
Wt_{dry}	9.01	8.67
Water Content	31.41	32.76

Table 3.6 PL test result (cont.)

Table 3.7 LL test result

Kaolinite				
LL = 54.83%				
Blow Count	17	22	31	39
Wt_{tare}	13.93	14.27	11.88	11.71
Total Wt_{wet}	29.73	32.65	34.98	28.88
Wt_{wet}	15.80	18.38	23.10	17.17
Total Wt_{dry}	23.96	26.06	27.05	23.10
Wt_{dry}	10.03	11.79	15.17	11.39
Water Content	57.53	55.89	52.27	50.75

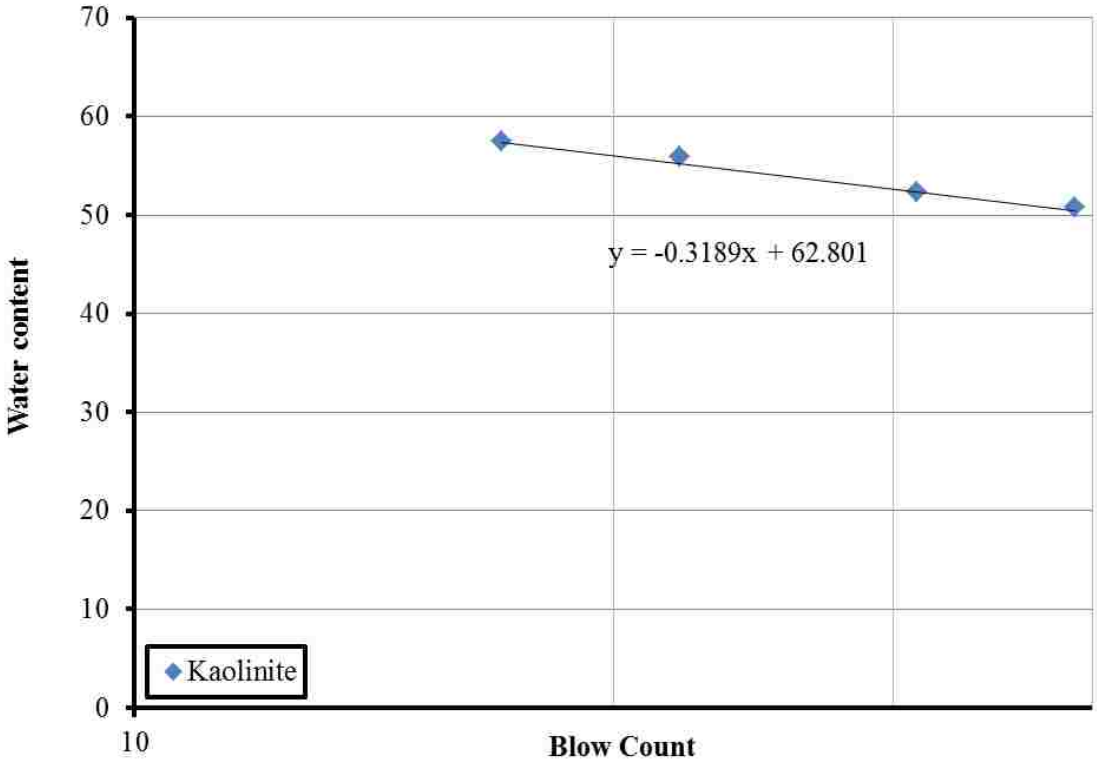

Figure 3.3 Blow Count – Water Content relationship

3.3. BIOPOLYMER SOLUTION PROPERTIES

A series of biopolymers were used as listed in Table 3.1. Their solutions were mixed with geo-materials to modify the water retention capability. Surface tension, contact angle, and viscosity of biopolymer solutions were quantified. The procedures are shown in the following sections.

3.3.1. Surface Tension Measurement. Surface tension is a contractive tendency of liquid surface which allows it to resist external force. Surface tension is an important factor which has a significant impact on the ecosystem. For example, water strider is able to float or move along the water surface (Fredlund and Rahardjo, 1993). Microscopically, in the liquid, each molecule is attracted equally in every direction by neighboring liquid molecules. The molecules at the surface do not have other molecules on all sides of them and therefore are pulled inwards. The loss of top forces creates internal pressure and forces liquid surfaces to contract, thus forming surface tension. Addition of biopolymer molecules will change the existing balance, and yielded different surface tension values. For examples, surface active agents (surfactants), such as soap, are well-known in reducing the surface tension of aliphatic substances that was attached on clothes, and was used widely for detergent.

Surface tension can be measured in torque method or bubble pressure method. The device used for measurement is SensaDyne QC 6000 Surface Tensiometer (Figure 3.4).

Figure 3.4 SensaDyne QC 6000 surface tensiometer (SensaDyne Instrument)

The principle of measurement is applied maximum bubble pressure (Physical Chemistry of Surface, Wiley). This method works by blowing a bubble through a liquid and measuring the maximum pressure of the bubble. This method is more accurate than that of ring tensiometer. The ring method will be affected by surface contamination or moving surface.

In practice, the measurement device uses Nitrogen gas which slowly bubbled through two probes of different radii that are immersed in the test fluid. The bubbling of nitrogen through two probes produces a differential pressure signal which is directly related to the surface tension of the fluid. The two probes should be kept at the same immersion depth to eliminate error caused by different amounts of hydraulic head at the probes. In this process, air is pumped through a capillary in the liquid to be analyzed. A special sensor measures the internal pressure of the developed bubble on the capillary peak. The dynamic surface tension is calculated by making up the difference of the maximum and minimum bubble pressure and the usage of the calibration factor k: (Manual for SensaDyne QC 6000)

$$\sigma = k * \Delta p \qquad \text{Eq. 3.1}$$

$$\Delta p = p_{max} - p_{min} \quad \text{Eq. 3.2}$$

After calibration the device with deionized water and alcohol, the calibration factor will be automatically stored by computer program. The measurement results are shown in Table 3.8.

Table 3.8 Surface Tension measurement results

Solution	Concentration (g/L)	Test 1 (dyne/cm)	Test 2 (dyne/cm)	Test 3 (dyne/cm)	Average (dyne/cm)
Deionized Water	0	73.1	73	73.1	73.1
PEO	1	63.8	63.7	63.8	63.8
PEO	10	61.7	61.9	61.7	61.8
SA	2	77.3	77.2	77.2	77.2
SA	20	80.5	80.5	80.5	80.5
Agar	2	76.1	76	76.1	76.1
Chitosan	2	74	74	74	74.0
PAA	2	74.2	74.1	74	74.1
PAM	2	76	76.2	76.1	76.1
Xanthan	2	76	75.9	76.1	76.0

3.3.2. Contact Angle Measurement. Where a liquid/vapor phase meets a solid phase meets, such as water on a glass plate, the interface forms a contact angle. Contact angles are extremely sensitive to surface contamination. Values of contact angle can be only obtained under laboratory conditions with purified liquids and very clean solid surfaces. If the liquid molecules are strongly attracted to the solid molecules then the liquid drop will completely spread out on the solid surface and therefore corresponding to a contact angle of zero degree. Generally, if the water contact angle is smaller than 90°, the solid surface is considered hydrophilic. Otherwise, it is hydrophobic.
Many polymers exhibit hydrophobic surfaces.

The solid surface condition of test is quartz (Fisher Scientific), which is also the major component of Ottawa sands in this study. Table 3.9 contains all the sand property information from US silica and Chemglass.

Table 3.9 Chemical property of Ottawa sand (from US Silica and Chemglass data)

	Percent of SiO_2
Quart Slide (Chemglass)	99.8%
20-30 Ottawa Sand	99.8%
50-70 Ottawa Sand	99.7%
125 Ottawa Sand	99.7%

The main element for Ottawa sand and quartz slide are both SiO_2, the same chemical material will provide the same surface condition which is the reasonable replacement for Ottawa sand.

Sessile drop method was used to measure contact angle. By using sessile drop, the spreading of solution can be avoided and therefore get a better result. Contact angle was measured by a contact angle goniometer with an optical system to capture the profile of a high purity liquid on a solid surface such as quartz slide (Wikipedia, 2014). The angle formed between the liquid/solid interface and the liquid/vapor interface is the contact angle. The current generation goniometer equipped with high resolution cameras and software to capture and analyze the contact angle (Figure 3.5). Table 3.10 listed all the measurement value of contact angle.

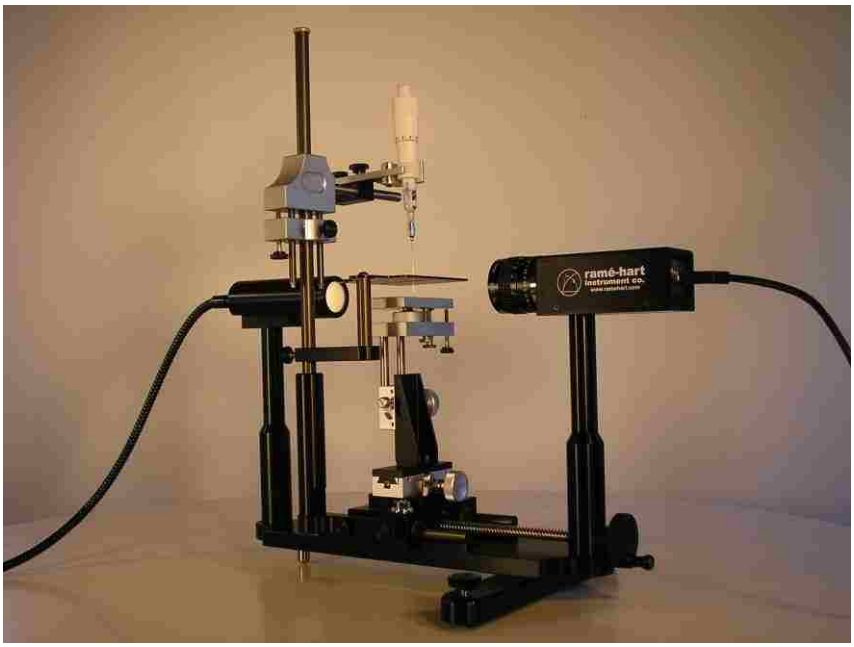

Figure 3.5 Rame-hart goniometer (Wikipedia, 2014)

Table 3.10 Contact angle measurement results

Solution	Concentration (g/L)	Test 1 (degree)	Test 2 (degree)	Test 3 (degree)	Test 4 (degree)	AVG (degree)
Deionized Water		38.4	37.5	38.2	38.1	38.1
PEO	1	39.9	39.2	39.4	39.9	39.6
PEO	10	37	37.5	37.1	37.3	37.2
SA	2	40.5	40.5	40.7	40.8	40.6
SA	20	41	41.6	41.2	41.3	41.3
Agar	2	37.7	37.1	37.9	37.8	37.6
Chitosan	2	31.6	31.5	31.9	31.8	31.7
PAA	2	38.6	38.9	38.4	38.3	38.6
PAM	2	21.1	21.2	21.5	21.4	21.3
Xanthan	2	34.5	35.1	35	34.7	34.8

3.3.3. Viscosity Measurement. The solutions' viscosity values are measured by Anton Paar MCR302 rheometer under room temperature and normal pressure. Spindle rotation method is the normal measurement been used for viscosity test. This method requires the condition of solution is uniform. Since solubility of each biopolymer is not same therefore some of the solutions have suspensions inside so spindle method is not operational. The testing device provides another method called peddle plate method to measure the viscosity of suspension solution. The principle of this method is measuring the torque of the top peddle plate and transfer torque into shear stress. The rotation velocity will be transferred to shear rate. All the measurement, data collection and interpretation will be finished by computer program automatically.

The following Figure 3.6 exhibits the relationship between shear rate and shear stress.

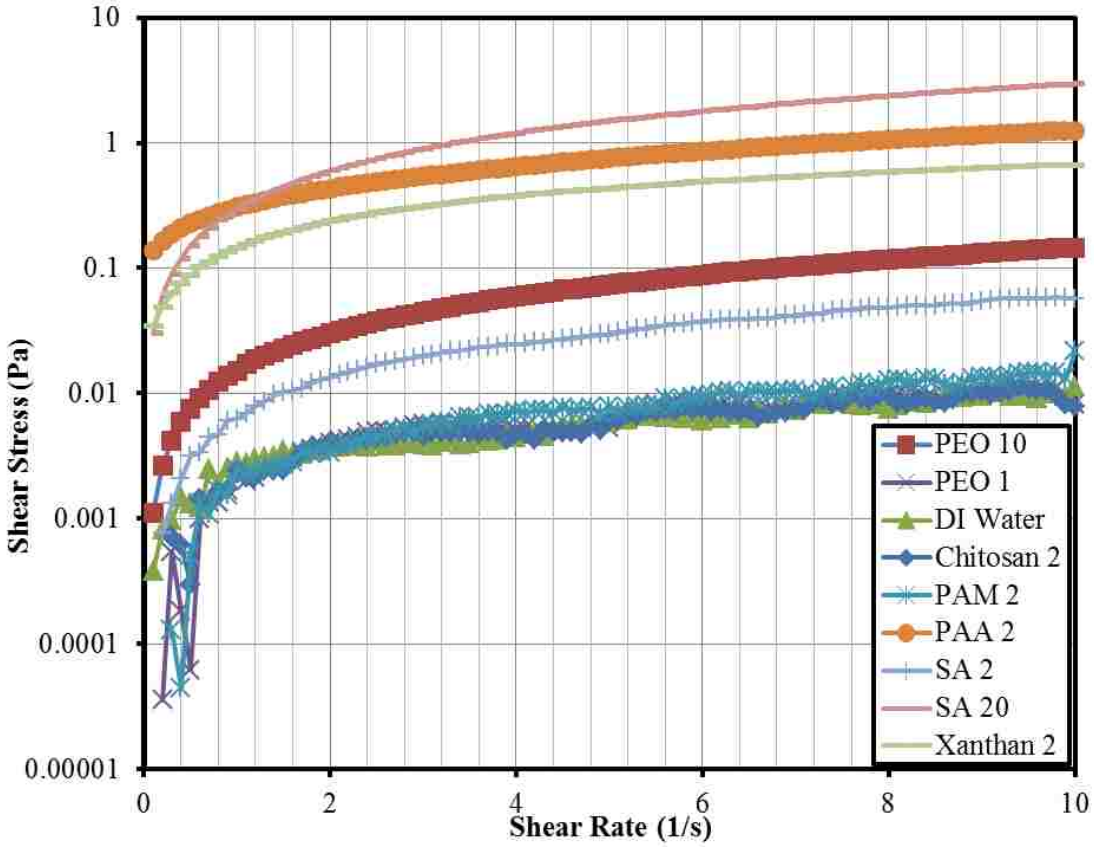

Figure 3.6 Relationship between Shear rate and Shear stress

According to Figure 3.6, 2 g/L PAA solution has shear thinning phenomenon. It means the viscosity of this fluid is variable corresponds to shear rate. Figure 3.7 provide the information of Viscosity – Shear rate relationship.

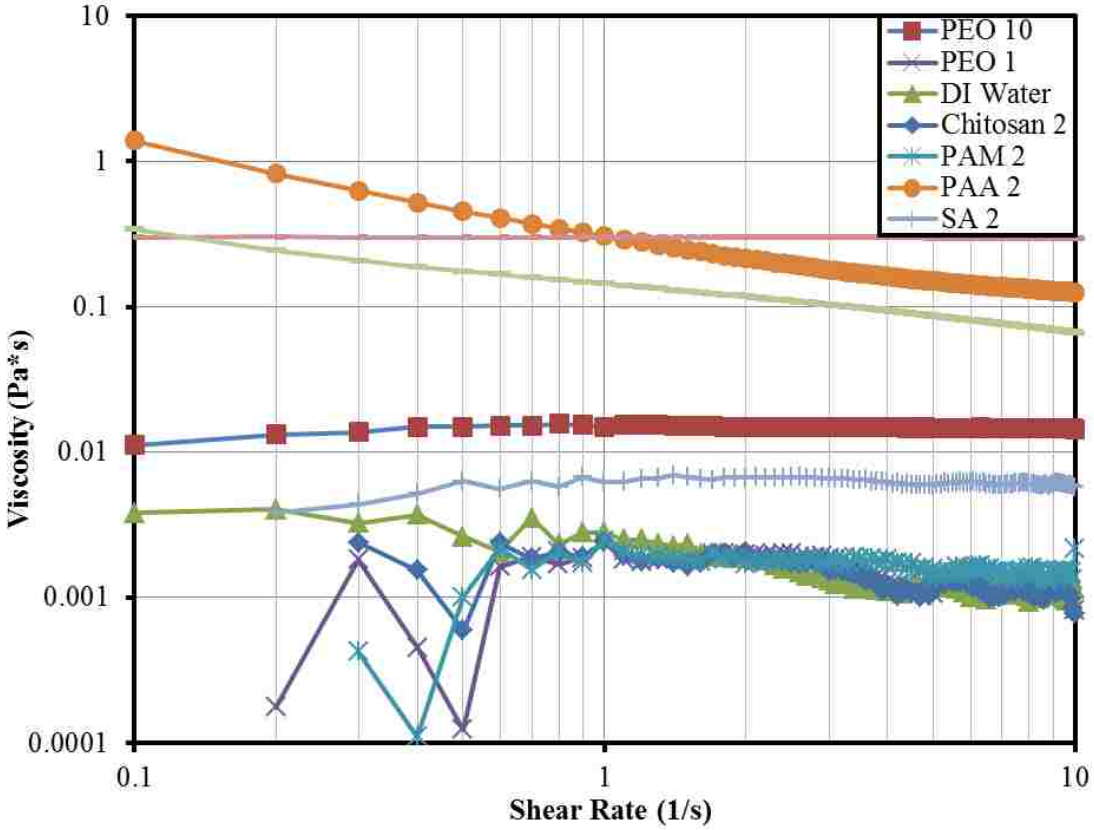

Figure 3.7 Relationship between Shear rate and Viscosity

According to Figure 3.7, PAA and Xanthan solution belong to shear thinning solution and the others are Newtonian Solution.

3.3.4. Determination of Viscosity Value. Through the viscosity measurement, a series of viscosity data is obtained under different shear rate. For each individual SWCC test, the viscosity value should be in a small range which is variable with degree of saturation. The appropriate value of viscosity should be used for future analysis.

3.3.4.1 Shear rate conversion method. Shear rate can be approximately estimated through Outflow – Time relationship. Table 3.11 exhibits the shear rate conversion process. The approximate equation for shear rate (SR) calculation is:

$$SR = \frac{Q \cdot V}{A \cdot t \cdot r} \qquad \text{Eq. 3.1}$$

$$r \approx \frac{D_{50}}{10} \qquad \text{Eq. 3.2}$$

Where,

Q is flow rate (ml/s).

V is volume of solution (ml).

A is cross-section area (cm^2).

t is time (s).

r is pore size (mm).

D_{50} is the average of grain size (mm).

Table 3.11 Shear rate conversion results

	grain size (cm)	**pore size (cm)**	**Area (cm^2)**	**Time (s)**	
	0.06	0.006	22.79666667	30	
	Concentration (g/L)	**Suction (kPa)**	**Volume (ml)**	**Q (ml/s)**	**SR (1/s)**
Water		1.000	0.167	0.00556667	0.092249
SA 20	20	50.000	0.050	0.00166667	0.027619
PAA 2	2	6.890	0.340	0.01133333	0.187812
PAM 2	2	3.450	0.100	0.00333333	0.055239
Chitosan 2	2	2.000	0.083	0.00276667	0.045848
Agar 2	2	2.000	0.030	0.001	0.016572
SA 2	2	2.067	0.200	0.00666667	0.110477
PEO 1	1	1.000	0.012	0.0004	0.006629
PEO 10	10	1.000	0.012	0.0004	0.006629
Xanthan 2	2	2.000	0.030	0.001	0.016572

From Table 3.11, all the conversion of shear rate is range from 0.001 to 0.1 s^{-1}. The value is smaller than the accuracy of the test machine. The viscosity measurement result for low shear rate will become negative value. The torque measurement device is not sensitive enough to measure this low value.

3.3.4.2 Viscosity value for future test. Since the shear rate for SWCC test is really low and the lowest value can be got from the test machine is 0.1 s^{-1} .So the viscosity value for future test should be taken the lowest shear rate which maintain the viscosity in a positive value. Table 3.12 listed all the value for future test usage.

Table 3.12 Viscosity value for future test

Solution	**Concentration (g/L)**	**Viscosity (Pa*s)**
Xanthan	2	0.344
SA	20	0.3
SA	2	0.0039
PAA	2	1.39
PAM	2	0.00043
Chitosan	2	0.0024
PEO	1	0.00018
PEO	10	0.0112
Agar	2	0.00126
DI Water	0	0.001

4. FREDLUND SWCC METHOD AND PRECAUTIONS

4.1. MEASURING DEVICE FOR SWCC

Suction in soil can be measured through many techniques, such as WP4 tensiometer (Decagon Devices, Pullman, WA), filter paper method (Fredlund and Rahardjo, 1993), and ceramic disk-based method, such as Fredlund SWCC device (GCTS, Tempe, Arizona), pressure plate (Fredlund and Rahardjo, 1993), and Tempe cell (Soilmoisture, Santa Barbara, CA).

Ceramic disk-based method was used to determine the soil SWCC at suctions below the air entry value (the pressure for air to enter the ceramic disk and continue to the soil) of the ceramic disk, which is usually below 1,500 kPa (Fredlund and Rahardjo, 1993). Two devices were used in this study: One is the GCTS Fredlund SWCC device (GCTS, Tempe, Arizona), and the other is Tempe cell (Soilmoisture, Santa Barbara, CA). The air entry value of the ceramic disk in Fredlund SWCC device and Tempe cell are 1,500 kPa and 130 kPa, respectively. The positive airpressure applied to the soil sample will not be able to exceed the air entry value of the ceramic disks, exceeding which air will break through the disk and enter the pressurized water chamber.

The Fredlund cell is used to measure SWCC of fine-grained soils, such as clay and silt. Because fine-grained soils with high fines content tend to have higher air entry value, and require high matric suction to drain out the aqueous solutions, the ceramic disk of high air entry value, such as 1500 kPa, is often needed. On the contrary, tempe cell is usually used for coarse-grained soils, such as sand and sandy silt, which normally have low air entry value due to the larger pore size than fine-grained soils. So ceramic disks with an air entry value of 130 kPa were used.

4.2. PROCEDURES FOR SWCC TEST

The soil materials used in this study are Georgia kaolinite (RP-2, ActiveMinerals, Cockeysville, MD), mine tailing (Doe Run site, MO), and Ottawa 20-30, 50-70, and 125 sands (US Silica, Frederick, MD). Biopolymers used in this study are PEO, PAM, PAA, Agar, Xanthan, Chitosan, Sodium Alginate (SA). Detailed index properties of these materials were measured as shown in Section 3.

4.2.1. Sample Preparation of Fine-grained Soils. Biopolymer powder was dissolved in flask at prescribed concentrations (Table 4.1) before use.

Table 4.1 Concentration of biopolymer solution

Biopolymer	Concentration (g/L)
PAM	2
PAA	2
PEO	10
Xanthan	2
Chitosan	2
Agar	2
Sodium Alginate	2
Sodium Alginate	20

Some biopolymers with high molecular weight will take at least 24 hours to become a uniform solution, in which case, ultrasonic bath was used to facilitation dissolution. Soil samples were first mixed with biopolymer solution. The mixture was then mixed manually and soaked for at least overnight. After mixed for 30 minutes, the slurry was let stand overnight as suggested by Fam and Santamarina (1995) to ensure that all the kaolinite particles were allowed to hydrate. Then the slurry was poured into a stainless steel consolidation tube (Diameter 2.5 in., height 6 in., Figure 4.2) with the sample ring connect at the bottom of the tube. Care should be taken not to generate any air by pouring slurry on side of the tube. Before loading on the slurry, the tube is covered with filter paper on top and bottom to make the sample double drained. The slurry was one-dimensional consolidated with load increasing from 6 to 50 kPa and then unloading to 0 kPa. Load will be gradually put on to prevent the slurry from pressing out from the small gap between porous stone and steel tube. One dimensional odometer (Figure 4.1, Humboldt, IL) is used for sample preparation. By using LVDT (Figure 4.1, Humboldt, IL) to measure the vertical displacement and vertical load is controlled by air pressure. Consolidation curve is determined by square-root time method. Taylor's square root time fitting method is used to check if this sample is finished consolidation under load. It is followed by unloading process after the soil sample get to the pre-consolidation pressure

which is 50 kPa. If loading is completely removed from sample, it will tend to expand and suck water from the top and bottom in order to keep the sample fully saturated. So the unloading process will follow the reverse of loading sequence. The same like what had been done on slurry compressing. The total mass of ring and soil were weighed. Initial water content of the soil sample can be determined by oven drying method on the remaining soil mass.

Figure 4.1 Humboldt consolidation device and LVDT

Figure 4.2 stainless steel sample preparation tube

4.2.2. Sample Preparation of Sand. Comparing to soil sample preparation, sand does not require pre-consolidation pressure. Sand is added into tempe cell without any compaction. To ensure all sand samples are in same initial condition, the mass of sand for each sample is 109g (void ratio e=0.718). Tempe cell will be filled with this amount of sand. Then add the biopolymer solution through the surface of tempe cell until the sample in saturation condition. Since there is no compaction for sand sample, the sand is in loose condition.

4.3. SWCC TEST

Before setup SWCC test, a ceramic disk with appropriate air entry value (AEV) was selected based on the soil type. For fine-grained materials, such as kaolinite and tailings, higher suction is expected to reach the residual water content. Therefore, high air entry value disk of 1,500 kPa was used to allow a matric suction range of 0 to 1,500 kPa. The presence of air in the ceramic disk could significantly increase the volume reading of the outflow water due to the high compressibility of air. Therefore, ceramic disk must be de-aerated before usage. Based on the recommendation by the manufacturer, the disk was soaked in de-aerated water overnight to ensure saturation.

The soil sample in the steel ring was then placed on the ceramic disk. A good contact between the ceramic disk and the soil sample should be carefully guaranteed, so that there is no entrained air at the interface. The excess water that might remain on the surface of the ceramic disk was carefully removed with a lint free tissue (Kim-Wipe, AMTS Inc.). The stainless steel chamber was then sealed.

Loading shaft with a cap inside Fredlund cell is put in contact with the soil sample to measure the possible shrinkage deformation induced by the applied matric suction. A small dead weight (0.38 kg) was used to apply a seating load to measure possible shrinkage of high compressible geo-materials.

Air pressure (u_a) was then applied inside the sealed stainless steel chamber, while the water chamber underneath the ceramic disk was open to the atmospheric pressure (u_w = 0). Matric suction ψ was calculated by:

$$\psi = u_a - u_w \qquad \text{Eq. 3.1}$$

Matric suction was increased to further de-saturate the specimen. The steps of matric suctions experimental matrix for SWCC tests with Fredlund SWCC device is shown in Table 4.2.

Table 4.2 Step of matric suction

Suction Step	Air pressure/Matric Suction (kPa)
1	0.01
2	0.1
3	1
4	2
5	4
6	25
7	50
8	100
9	200
10	500
11	1000

The outflow volume readings from the two vertical burettes were monitored over time visually. These two burettes were calibrated with a beaker (Fisher Scientific) and a balance (Ohaus) before usage. The cross section area of these two glass burettes were determined to be 0.119 cm^2 and 0.74 cm^2, respectively.

4.3.1. SWCC Measurement under Low Matric Suction. The accuracy of the Fredlund SWCC device is +/- 1 kPa. However, the air entry value for coarse grained soils, such as sands, is often below 1 kPa. This requires accurate matric suction as low as 0.05 kPa to delineate the low suction range. In order to measure the accurate water outflow at lower suction, Li and Zhang (2009) proposed a new design meet such requirement. The key of their design is to lower the outflow water level to create low suction (0.05 – 5 kPa). Atmospheric pressure was maintained at both inside the stainless steel chamber and the open end of the outflow tube. So the matric suction equals to the negative pore water pressure created by the lowered water column. This design was revised for this study (Figure 4.3). The outflow volume reading is through a long glass tube (cross-section area 0.119 cm^2).

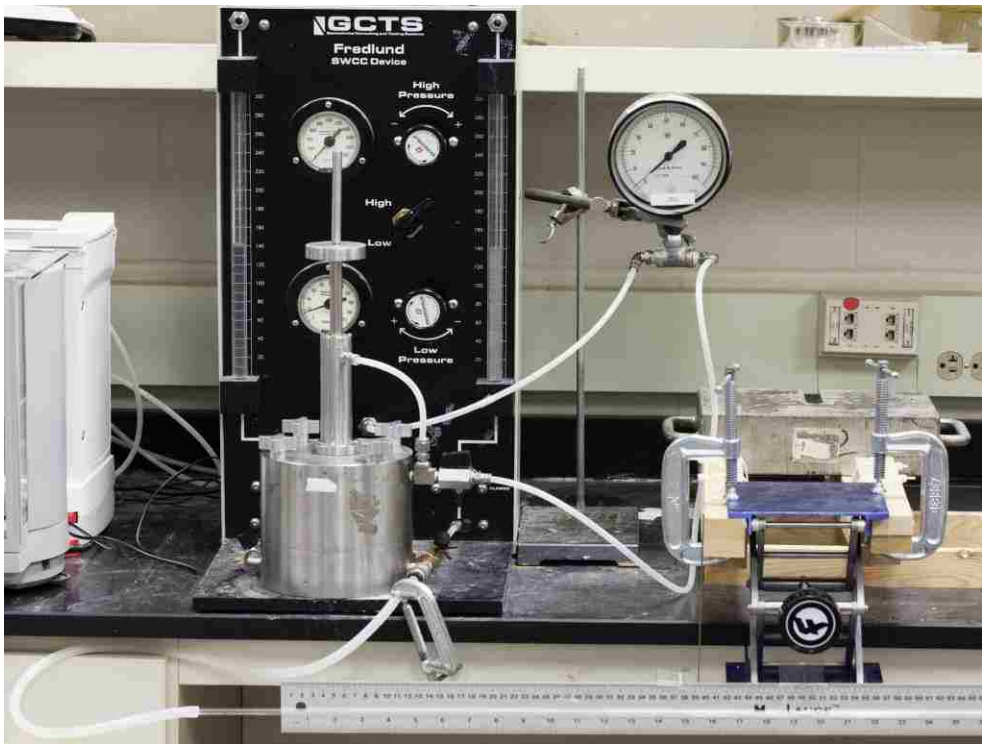

Figure 4.3 Schematic setup of low suction device for SWCC measurement

As shown in the photo, the elevation of tube is adjusted by the regulator of lab jack. On the left side of the lab jack, there is a ruler attached to the system and it is used

for locating the horizontal tube in accurate elevation. The horizontal tube is fixed with the ruler behind it which will provide the water flowing rate and volume.

4.3.2. Air Diffusion Correction. According to Henry's Law, air can dissolve in water. Since air pressure is applied to the sample, readings from vertical tube showing the volume of water. While water keep passing the ceramic disk, air diffused in water is also expelled. So every 4-6 hours, flush will be needed to flow away those air bubbles. Because accumulated air bubbles will affect the water expelling rate and volume measurement.

4.3.2.1 Fredlund cell flush. Since air bubbles are accumulated underneath the ceramic disk, the volume of water will be overestimated. To fix this problem, flushing is being used to decrease the effect of air bubbles. An empty water bottle is enough to flush the ceramic disk. First, connect the outlet of water bottle with one of the vertical burette. Second, compressing the empty bottle to make the water column inside vertical tube flowing back and forth through the water tank beneath ceramic disk. Repeating this process several times and the air bubbles will be pressed out. It was recommended by Manual that flushing will be needed every 4-6 hours.

4.3.2.2 Horizontal tube flush. The flushing process for horizontal tube is almost the same with Fredlund cell. The only difference between these two devices is that horizontal tube connects with water tank through a Swagelok. Before flushing, the horizontal tube should be sealed first and then open the two vertical burettes. The remaining procedures are the same with Fredlund cell. After flushing, close two vertical burettes and reopen the sealed horizontal tube.

4.3.3. Outflow for Each Matric Suction. The outflow versus time curve for every matric suctions are plotted. When a plateau in outflow volume was reached, the degree of saturation was considered reached at the specific matric suction condition. Then the next matric suction was applied. Before increasing air pressure and measure next data point, the height change of the sample was measured. The volume change during SWCC test for mine tailing is shown in Table 4.3.

Table 4.3 Sample volume change measurement

Matric Suction (kPa)	Height of sample (cm)
0.01	2.54
0.1	2.54
1	2.54
2	2.54
4	2.54
17.6289	2.54
45.39491	2.54
97.47883	2.49
197.787845	2.49
497.72408	2.49
997.6456	2.49

Since the change of sample height is only 0.5 mm which can be neglected. But if the volume of test sample changes a lot, the volumetric water content will be recalculated by using the new sample volume.

Above procedure was repeated for each matric suction value until the maximum applied matric suction, i.e., 1000 kPa.

After the completion of the last matric suction value, total mass of the ring and the soil was measured. Then the dry weight of the soil was measured by oven-drying method. As a result, the water content at the end of the last matric suction can be calculated. The summation of the total water outflow volume and the total water volume remained in the soil sample at 1000 kPa should be equal to the initial water volume. The difference, if any, was calculated to double-check the quality of the results. Table 4.4 shows the example calculation of mine tailing water remaining back calculation result. The difference between the initial total water volume and the summation of expelled water and residual water in the soil sample is 1.03 g (Table 4.4). This is less than 3% of the initial total water volume, and the difference is considered negligible. The difference was attributed to the slight water expelling from the ceramic disk.

Table 4.4 Sample back calculation

Matric Suction (kPa)	volume of water (ml)
0.01	0.01785
0.1	0.02142
1	0.0119
2	0.6069
4	0.55454
17.6289	3.33
45.39491	10.064
97.47883	5.994
197.787845	2.516
497.72408	0.962
997.6456	0.888
Total expelling Water (ml)	24.96661
Total water in sample (ml)	35.06
Calculated water remained in sample (ml)	10.09339
Measured water remained in sample from oven drying (g) Difference (g) Difference (%)	11.12 1.03 2.9%

4.3.4. Calibration of Cross-section Area. To accurately measure the outflow water volume, the inner cross-section areas of all the tubes and burettes need to be calibrated. The tube or the burette was first filled with de-aerated water. Then a significant amount of water was drained out into a beaker with known weight. This test was repeated three times, and the average value of inner cross-section area was used. The weight of the water and the beaker was measured with an accurate balance (Ohaus). Then the weight and the volume of drained water can be calculated. The expelling water length before and after the water drainage was measured by a ruler. The cross-section areas of the vertical burette in the Fredlund SWCC device and the horizontal tube in the elevation-controlled low suction device were calculated to be 0.119 cm^2 and 0.74 cm^2, respectively. The results and the calculation were tabulated in Tables 4.5 and 4.6.

Table 4.5 Horizontal Tube Calibration

Initial water length (cm)	**Final water length (cm)**	**mass of releasing water (g)**	**inner area (cm^2)**
96	71.4	2.8989	0.118
71.4	33.3	4.5331	0.119
33.3	1.7	3.7939	0.120
		avg	0.119
98.95	63.72	4.2312	0.120
63.72	25.25	4.6109	0.120
25.25	0.88	2.8685	0.118
		avg	0.119
99.48	78.77	2.4734	0.119
78.77	49.68	3.4764	0.120
49.68	1.2	5.7345	0.118
		avg	0.119
		Final Average Value	0.119

Table 4.6 Vertical Tube Calibration

Left Tube	**Initial water length (mm)**	**Final Water length (mm)**	**mass of water (g)**	**inner area (cm^2)**
1	28.4500	15.6000	9.152	0.71
2	15.6000	7.0500	5.897	0.69
3	7.0500	.3000	4.920	0.73
Right Tube	**Initial water length (mm)**	**Final Water length (mm)**	**mass of water (g)**	**inner area (cm^2)**
1	25.9500	18.2500	6.673	0.87
2	18.2500	10.0000	5.845	0.71
3	10.0000	1.2500	6.231	0.71
			Final Value	1.47

4.3.5. Evaporation Calibration. Water will evaporate if exposed to the atmosphere. As a result, the measurement of water volume will decrease. The rate of evaporation is affected by three conditions: temperature, water surface area and the flow rate of air. Because the test is performed in laboratory, temperature is relatively stable (22 - 24 oC). The surface areas of water column in vertical burettes and horizontal tube are 0.74 and 0.119 cm2, respectively. The air flow in this room can be treated as a steady state flow. So the flow rate is constant. It can then be concluded that the rate of evaporation is constant.

The evaporation of the horizontal tube in low-suction SWCC setup can be estimated as follows. Fill in water and mark the beginning reading of horizontal tube. Then take readings from the tube every 2-3 hours up to a total time of 20 hours. The average value of evaporation correction is 0.10 cm/hour (Table 4.7), which corresponding to a 0.286 cm^3/day. The standard deviation is 0.99% (Table 4.7).

Table 4.7 Evaporation rate results

Time (h)	**tube reading (cm)**	**Evaporation Rate (cm/h)**
0	57.45	
3.3	57.11	0.103030303
5	56.92	0.111764706
8	56.59	0.11
20	55.51	0.09
	Average	0.103698752

For Fredlund SWCC device, the openings of the two burettes are essentially closed to the air. Therefore the evaporation is negligible.

5. EXPERIMENTAL RESULT OF SWCC

In this section, SWCC results from both GCTS Fredlund SWCC device and Tempe cell were presented. In addition, Fredlund and Xing (1994) and van Genutchen (1980) SWCC equations were used to fit these laboratory measured SWCC results. Least square method was applied by the SOLVER function in Microsoft EXCEL. The 3 fitting parameters in both Fredlund and Xing (1994) model (*a*, *m*, *n*) and van Genutchen (1980) model (δ , λ , η) were independently fitted. The results were divided into five groups, namely:

i). Uniform sand with water (Ottawa 20-30, 50-70, 125 sands)

ii). Uniform sand with biopolymer solutions (Ottawa 20-30 sand)

iii). Uniform sand mixture with biopolymer solutions (Ottawa 20-30 and 57-70 sands, weight ratio 1:1)

iv). Kaolinite with both water and PEO solutions

v). Mine tailing with water

Each group contains SWCC result, curve fitting parameters for two models and pore size distribution. The lines inside SWCC figure is not fitted results, they are for visual illustration purpose only. All the curve fitting lines are included in Appendix A.

5.1. CAPILLARY PORE SIZE DISTRIBUTION

Capillarity is the main reason caused water sneak inside the pore space between each grain. Pore size can be calculated through this equation below,

$$r = \frac{2 \cdot T_s \cdot \cos\beta}{\psi} \qquad \text{Eq. 5.1}$$

Where,

r, pore size;

T_s, surface tension;

β, contact angle;

ψ, matric suction.

From SWCC result, the amount of water stored inside of pore can be quantified. The volume of water expelled under each matric suction step equals to the total volume

of pore space. The radius of pore size can be calculated through Eq. 5.1 (Lu and Likos, 2006). Total volume of a specific pore size under matric suction will be divided by total expelling water which will be normalized into weight fraction. So each matric suction correlate to a specific pore size and the normalized weight fraction can be determined which indicate the pore size distribution of soil sample. This method is used to analyse the effect of biopolymer modification.

5.2. SWCC RESULTS OF GRADED SAND WITH WATER

SWCCs and pore size distribution of three uniform sands, i.e., Ottawa 20-30, 50-70 and 125 sands, were shown in Figure 5.1 and 5.2. The D_{50} of each sand was listed in Table 5.1. It was found that as the D_{50} decreased, air entry value increased and the residual metric suction increased. This is because smaller particle size leads to smaller pore size, which requires higher matric suction to move the water in the soils (Eq. 2.1). This observation was further validated by the fitted a and n values in Fredlund and Xing (1994) SWCC model (Table 5.2 and Figure 2.4 and 2.5). In addition, δ parameters, which is approximately equal to the inverse of AEV, in van Genutchen (1980) model also decreased as D_{50} decreased.

Table 5.1 D_{50} of graded Ottawa sands

Sand	$\boldsymbol{D_{50}}$ **(mm)**
Ottawa 20-30 sand	0.7
Ottawa 50-70 sand	0.23
Ottawa 125 sand	0.05

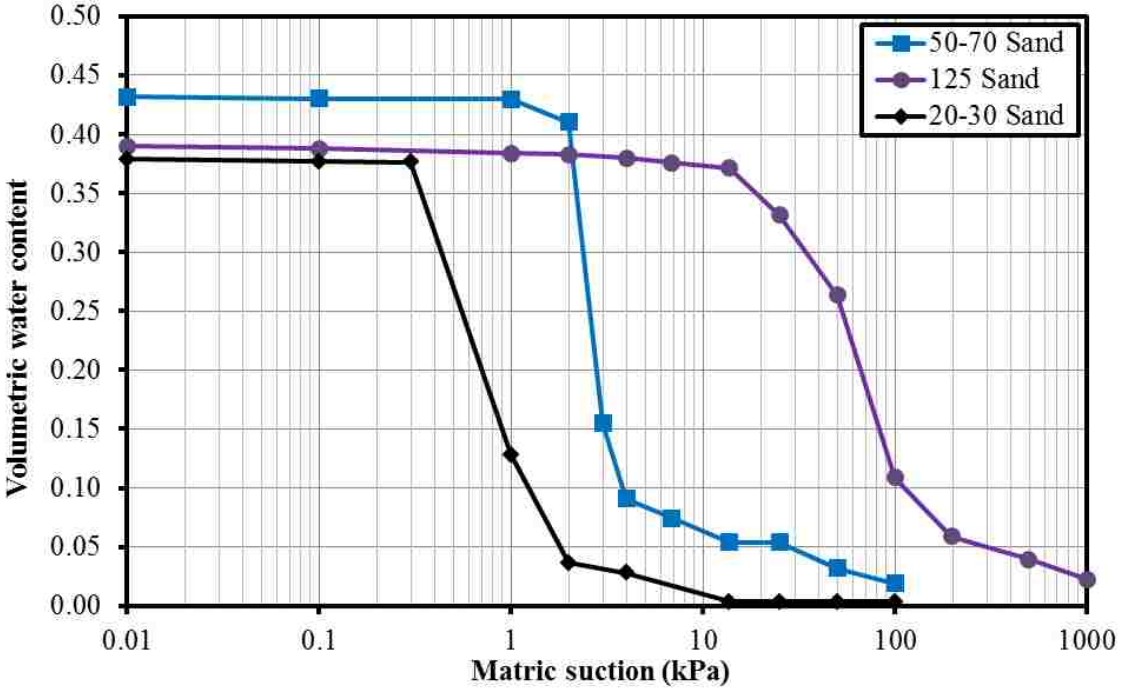

Figure 5.1 SWCC for different gap graded Ottawa Sand with water

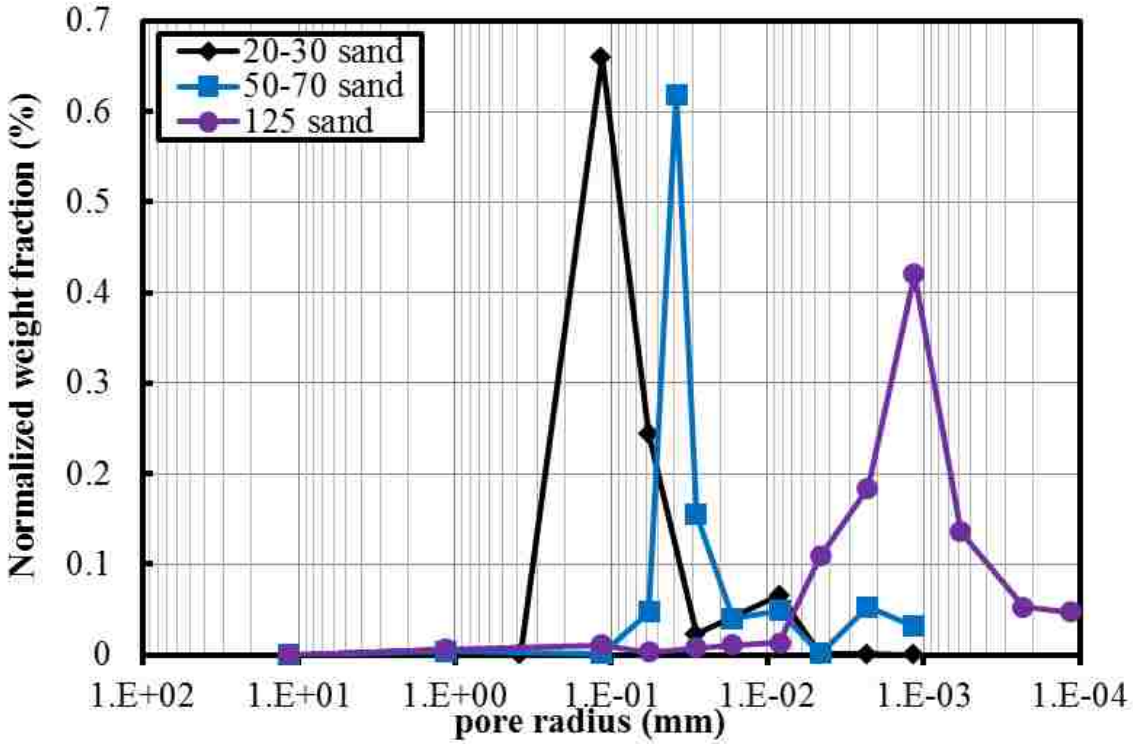

Figure 5.2 pore size distribution of sand with water

Table 5.2 fitting parameter for different uniform sand

Fredlund and Xing	***a***	***m***	***n***	**Van Genutchen**	***δ***	***λ***	***η***
Ottawa Sand 20-30	0.69	1.39	4.90	Ottawa Sand 20-30	1.98	0.23	7.16
Ottawa Sand 50-70	2.18	0.63	16.39	Ottawa Sand 50-70	0.51	0.02	152.73
Ottawa Sand 125	34.16	0.90	2.75	Ottawa Sand 125	6.30E-04	218.40	0.73

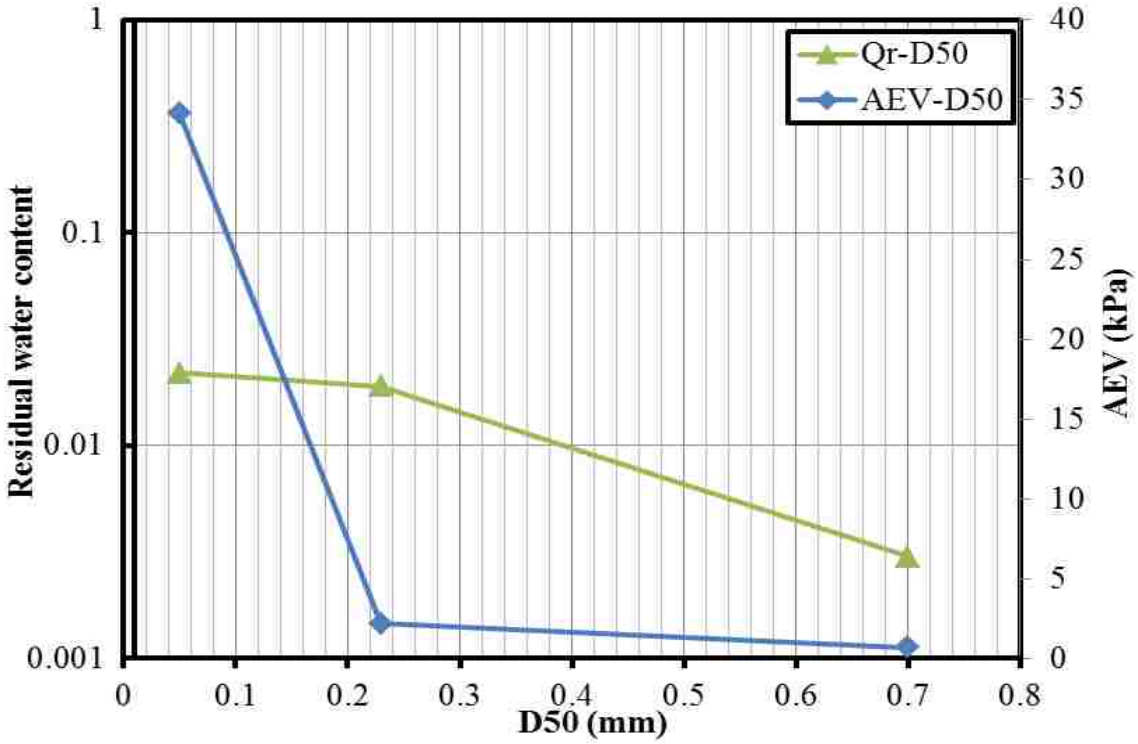

Figure 5.3 fitted parameter AEV and residual water content

5.3. SWCC RESULT OF GRADED SAND WITH BIOPOLYMER

5.3.1. Unimodel SWCC Result. Unimodel SWCC curves for Ottawa 20-30 sand with five different types and concentrations of biopolymers (PAA 2g/l, SA 2g/l, SA 20 g/l, xanthan gum 2 g/l, and PEO 10 g/l) were observed and plotted in Figure 5.4.

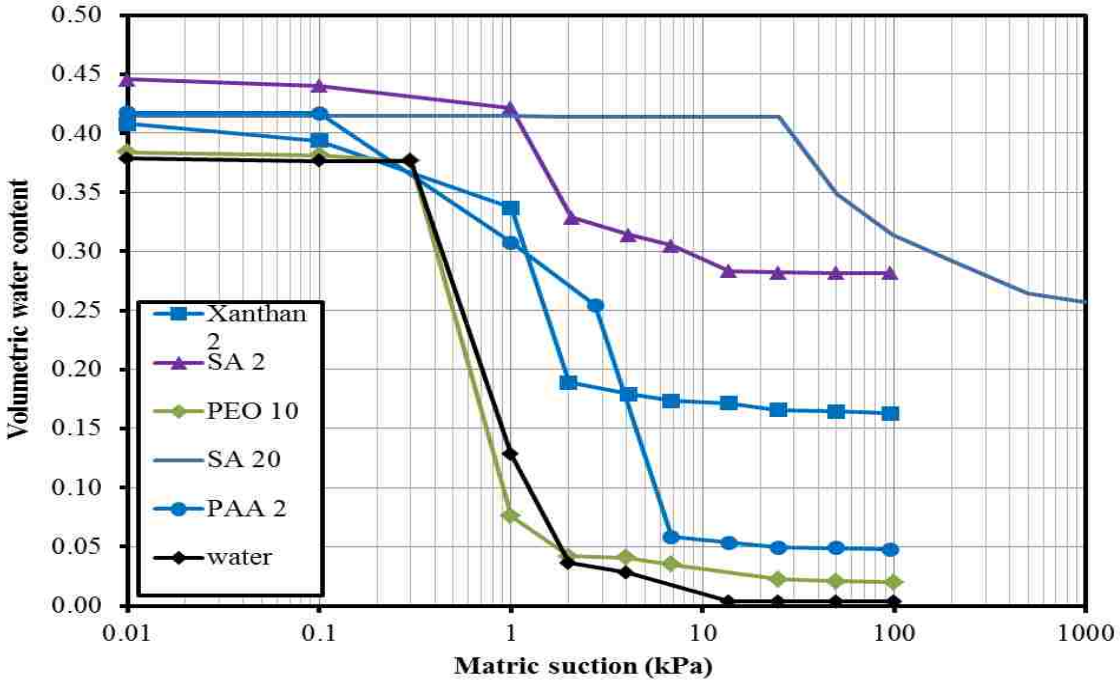

Figure 5.4 SWCC result for uniform sand with biopolymers

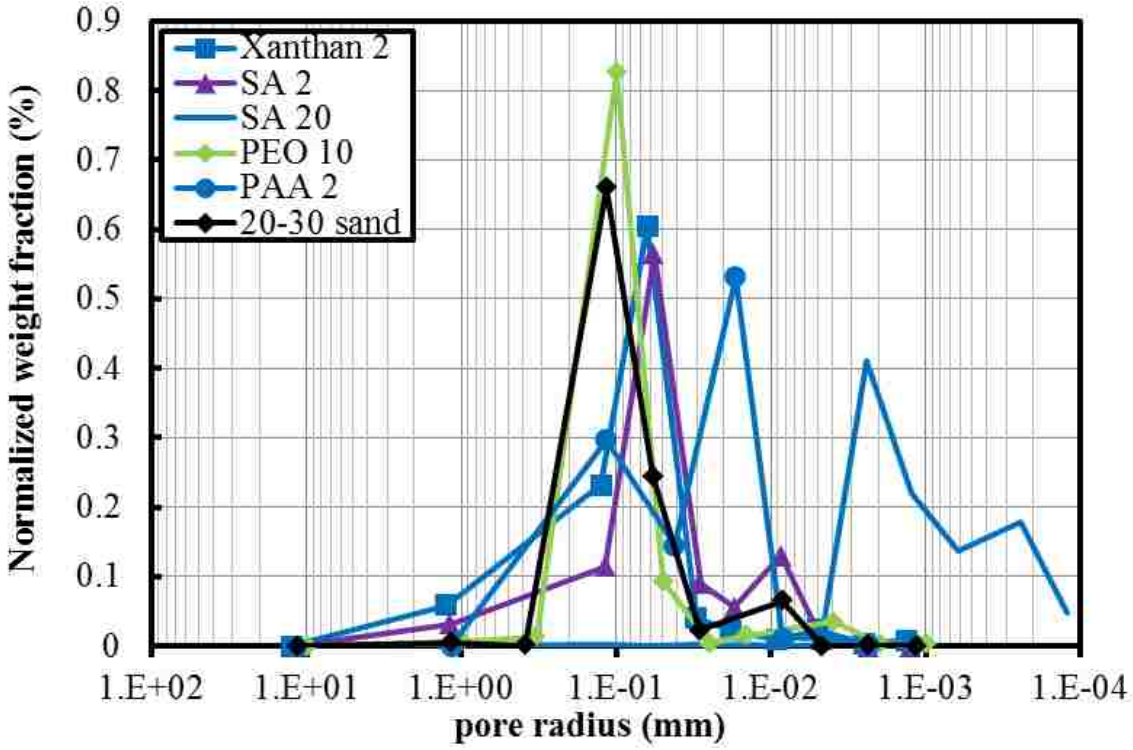

Figure 5.5 pore size distribution of uniform sand with biopolymers

Table 5.3 exhibits all the curve fitting parameters. From Figure 5.4, AEV was increased by all biopolymers except for 10 g/l of PEO solutions. This trend agrees with the fitted *a* parameter from Fredlund and Xing (1994) model. The reason is attributed to the reduced pore throat size by the attachment of biopolymers on the sand surface. This "clogging effect" can be illustrated in Figure 5.6 and 5.7 (SEM).

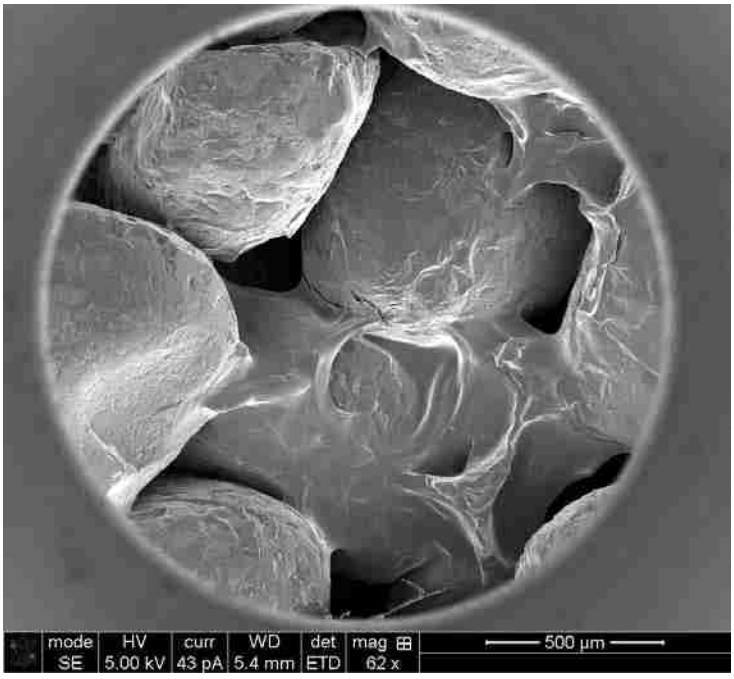

Figure 5.6 SEM image of Ottawa 20-30 sand with 2 g/l of xanthan gum

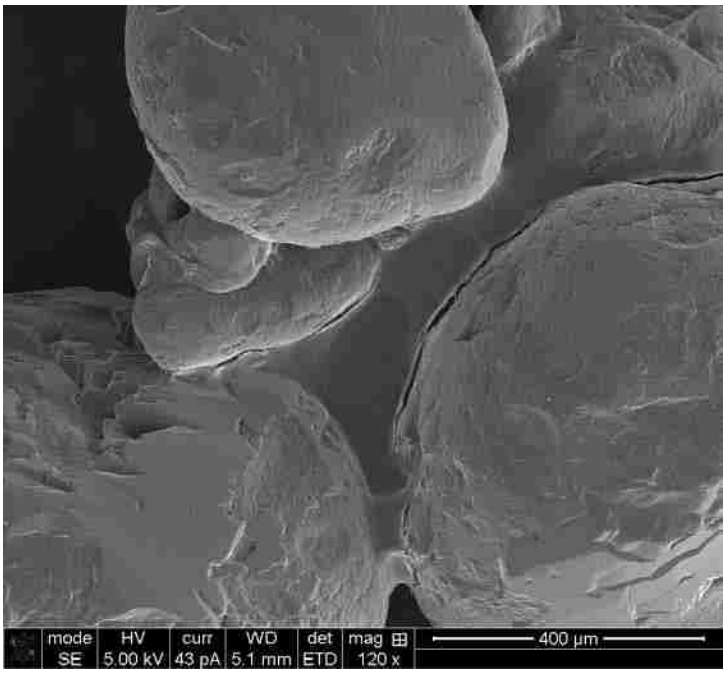

Figure 5.7 SEM image of Ottawa 20-30 sand with 20 g/l of SA

From these two figures above, the pore size generated from sand particle is decreased. It is caused by the coating effect of biopolymers. Biopolymers attached on the surface of sand particles, it will decrease or block the pore which lead to a higher AEV and residual water content. The surface-attached biopolymers can also increase the residual matric suction by clogging the smaller pores of the soils. It was also observed that large biopolymers, such as xanthan gum and sodium alginate (SA), had higher residual volumetric water content.

SA passing ceramic disk test was performed. 30 g of SA 20g/L was added into tempe cell and applied air pressure on top of the surface. The mass of SA passing through disk will be measured by a weight balance below the cell. Part of these large biopolymers might not be able to pass the small pore channel in the ceramic disk. Figure 5.8 shows the amount of SA 20g/l solution passing through ceramic disk at different matric suctions (total mass of the solution was 30 g).

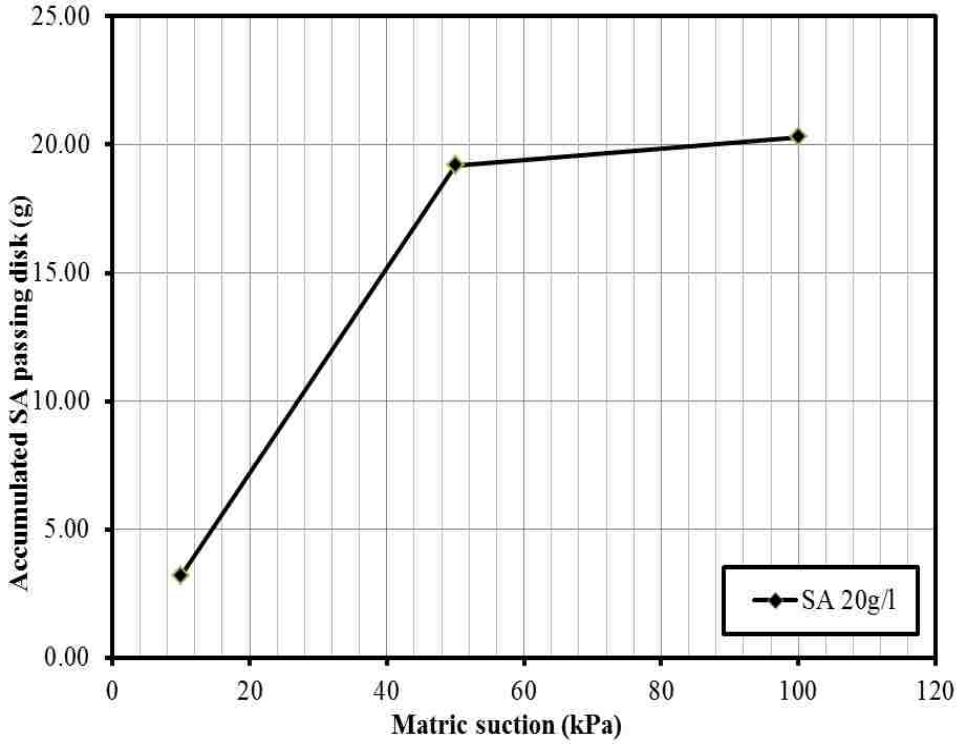

Figure 5.8 Amount of SA passing through ceramic disk at different matric suctions

Table 5.3 Curve fitting parameters for unimodel SWCC results

Fredlund and Xing	***a***	***m***	***n***	**Van Genutchen**	***δ***	***λ***	***η***
PEO 10	0.398	0.757	9.486	PEO 10	3.380	0.012	120.000
Xanthan 2	0.974	0.147	154.889	Xanthan 2	1.149	0.102	24.151
SA 20	31.507	0.122	8.390	SA 20	0.035	0.067	14.952
SA 2	0.960	0.097	28.356	SA 2	1.156	0.044	27.411
PAA 2	1.772	1.626	1.475	PAA 2	0.002	276.630	1.179
water	0.691	1.391	4.897	water	1.983	0.226	7.166

5.3.2. Bi-model SWCC Results. Bimodal SWCC results were observed with 2 g/l solutions of Agar, chitosan, and PAM (Figure 5.7). Zhang and Chen (2005) used the bimodal form of Fredlund and Xing (1994) SWCC curves to fit gap-graded coarse grained soils. Similar method was used in this study. The weight, *p*, of each SWCC model was the relative volumetric water content. *n* represents porosity of each material. ψ_r equals to 1500 kPa. ψ is matric suction. The equation is:

$$\theta(\psi) = p_l n_{pl}\left[1-\frac{\ln\left(1+\frac{\psi}{\psi_r}\right)}{\ln\left(1+\frac{10^6}{\psi_{rl}}\right)}\right]\left\{\frac{1}{\ln\left[e+\left(\frac{\psi}{a_l}\right)^{nl}\right]}\right\}^{ml} + p_s n_{ps}\left[1-\frac{\ln\left(1+\frac{\psi}{\psi_{rs}}\right)}{\ln\left(1+\frac{10^6}{\psi_{rs}}\right)}\right]\left\{\frac{1}{\ln\left[e+\left(\frac{\psi}{a_s}\right)^{ns}\right]}\right\}^{ms}$$

Eq. 5.1

Where,

θ_ψ : water content under different matric suction.

The fitting results were shown in Table 5.3. The gap in matric suction, ranging from 2 to 25 kPa, suggested that morphology of the original Ottawa 20-30 sand was changed. This can also be related to the surface tension and contact angle changes due to biopolymer.

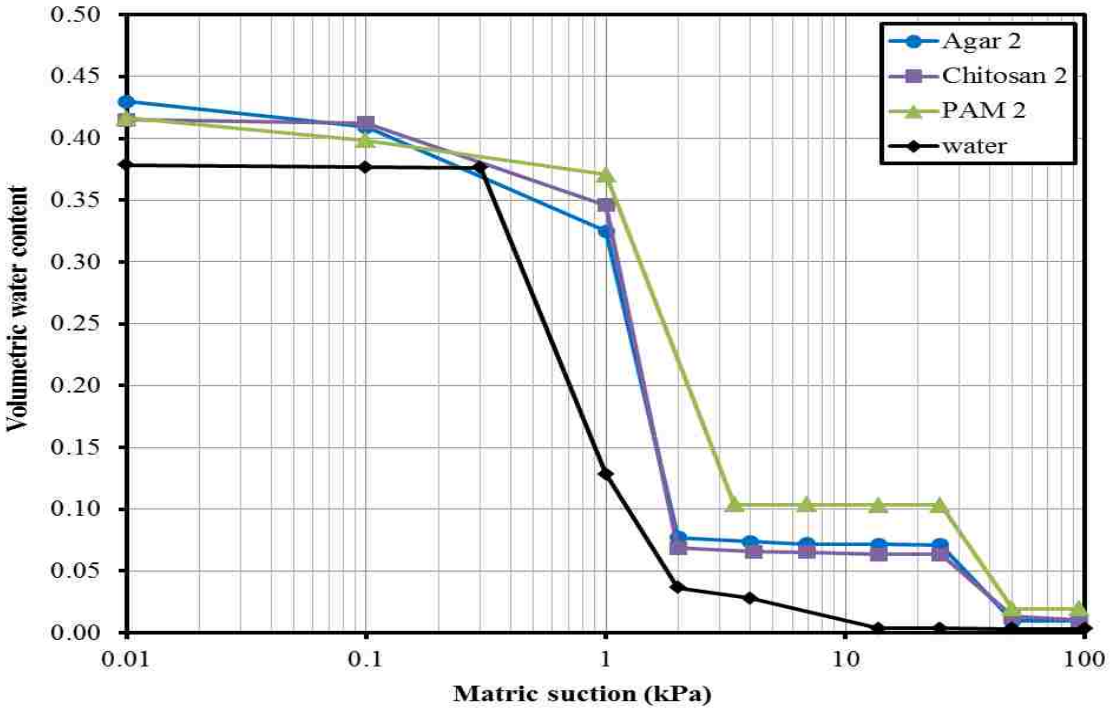

Figure 5.9 Bimodel result of Ottawa sand 20-30 with biopolymer

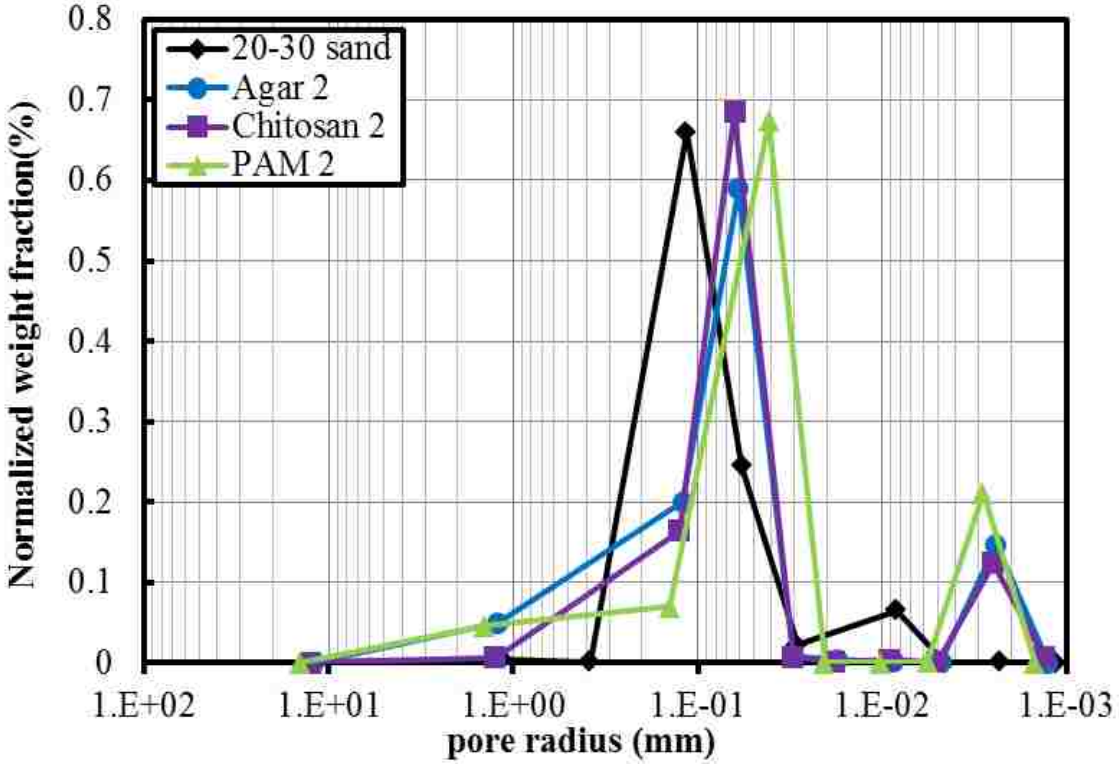

Figure 5.10 pore size distribution of bimodel result

Table 5.4 Bimodel fitting parameters

Fredlund and Xing	a_l	m_l	n_l	a_s	m_s	n_s
Agar 2	0.994	0.800	104.149	25.197	0.314	500.000
Chitosan 2	1.000	0.800	104.149	25.197	0.314	500.000
PAM 2	1.015	1.768	104.150	25.345	0.263	500.002
water	0.691	1.391	4.896			
Van Genutchen	δ_l	λ_l	η_l	δ_s	λ_s	η_s
Agar 2	0.719	2.185	5.317	0.020	2.438	14.712
Chitosan 2	1.034	0.090	70.345	0.020	3.151	20.751
PAM 2	1.020	0.096	73.100	0.020	3.165	10.000
water	1.983	0.225	7.165			

5.4. SWCC RESULT OF GRADED SAND MIXTURE WITH BIOPOLYMER

The first major desaturation occurs at matric suction of about 1 kPa for sand mixtures with either water or biopolymer solutions. However, the rate of the first desaturation for sand mixture with biopolymers is lower than that for sand mixture with water. This is an indication of wider pore size distribution for sand mixture with biopolymer solutions. The presence of residual volumetric water content indicates either the presence of smaller flow channels (pores) or higher viscosity induced by biopolymer solutions.

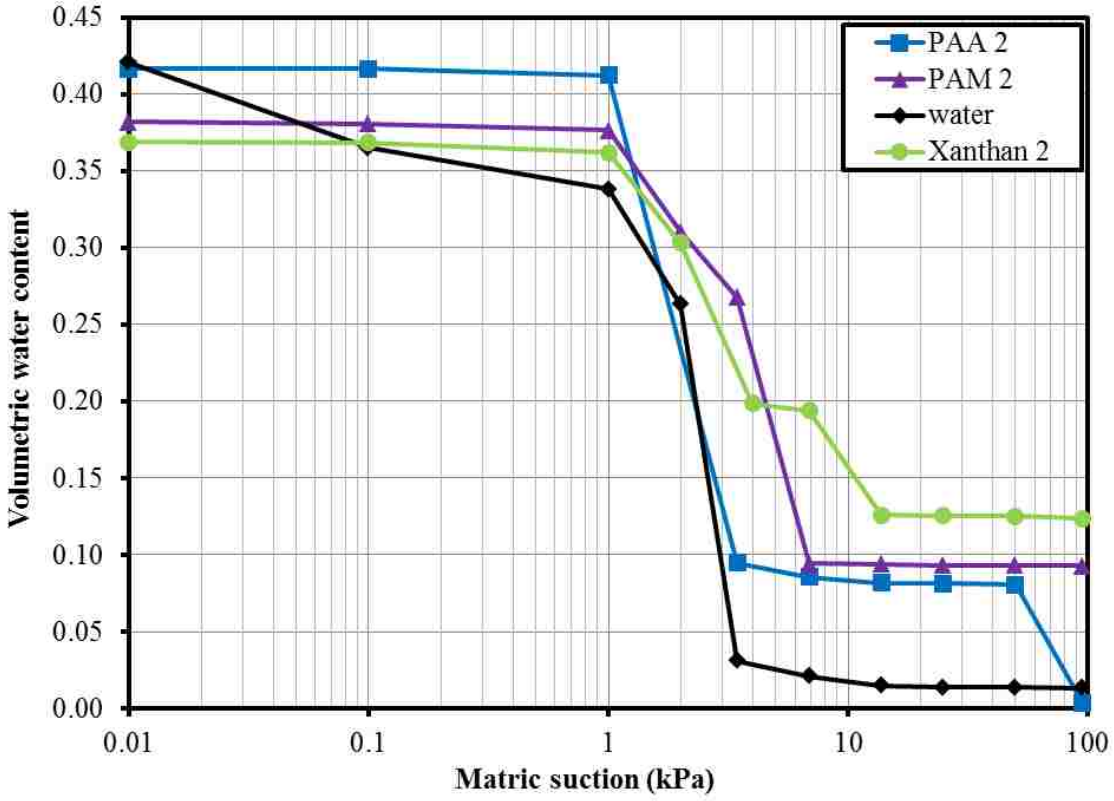

Figure 5.11 SWCC result of sand mixture with biopolymer

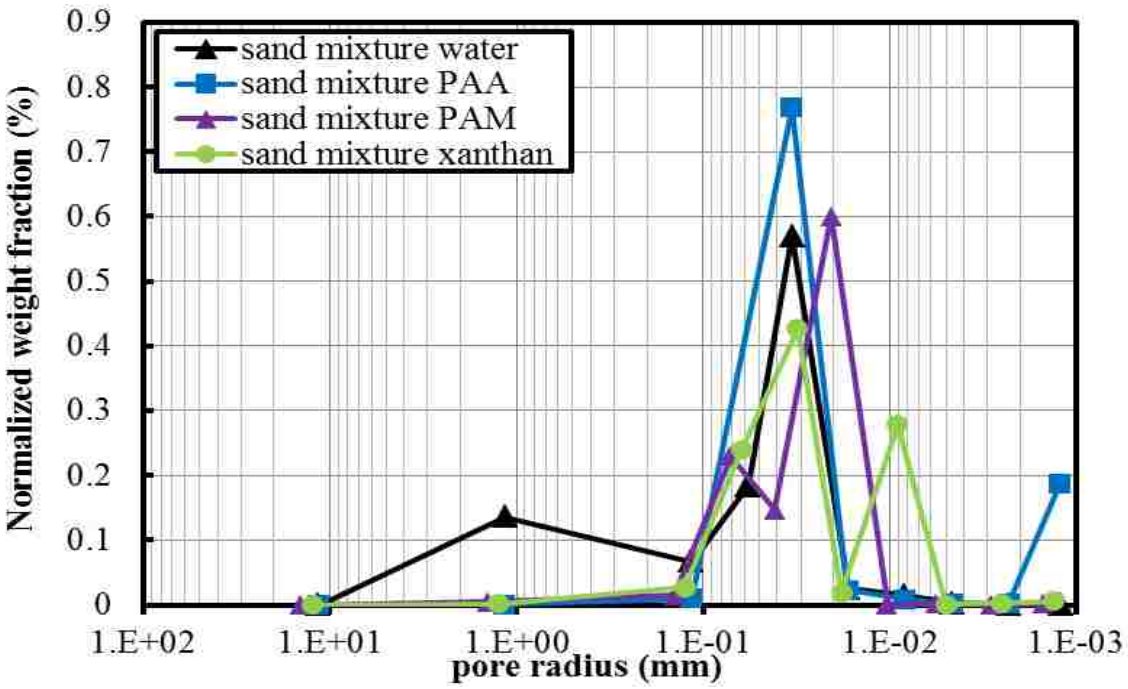

Figure 5.12 pore size distribution of sand mixture with biopolymer

Table 5.5 Sand mixture fitting parameters

Fredlund and Xing	a_l	m_l	n_l	a_s	m_s	n_s
PAA 2	3.400	10.000	100.000	64.280	2.336	10.270
PAM 2	2.141	0.654	3.736			
Xanthan 2	1.825	0.454	4.333	7.000	0.055	250.000
water	17.688	289.936	2.394			
Van Genutchen	δ_l	λ_l	η_l	δ_s	λ_s	η_s
PAA 2	0.320	2.100	22.000	0.017	2.500	19.230
PAM 2	0.042	47.019	2.253			
Xanthan 2	0.577	0.281	5.048	0.158	0.014	65.279
water	0.055	143.898	2.475			

5.5. SWCC RESULT OF FINE-GRAINED MATERIALS

SWCCs of kaolinite, kaolinite with 0.1g/l PEO and mine tailing are shown in Figure 5.9. Fitting parameters are listed in Table5.5. Mine tailing has less AEV than kaolinite does, because its grain size is larger than that of kaolinite (Figure 3.2). Addition of PEO to kaolinite reduced the AEV, this is due to the enhanced aggregation/agglomeration effects of PEO, which is a good dewatering agent used in

mining industry (Mpofu et al., 2004). Due to the AEV limitation of the available ceramic disk (maximum at 1500 kPa), SWCCs of kaolinite and kaolinite with PEO were not fully inspected. On the other hand, mine tailing seems to reach its residual state (Figure 5.9). As a result, mine tailing was used as an example in inverse numerical simulation as shown in Section 6.

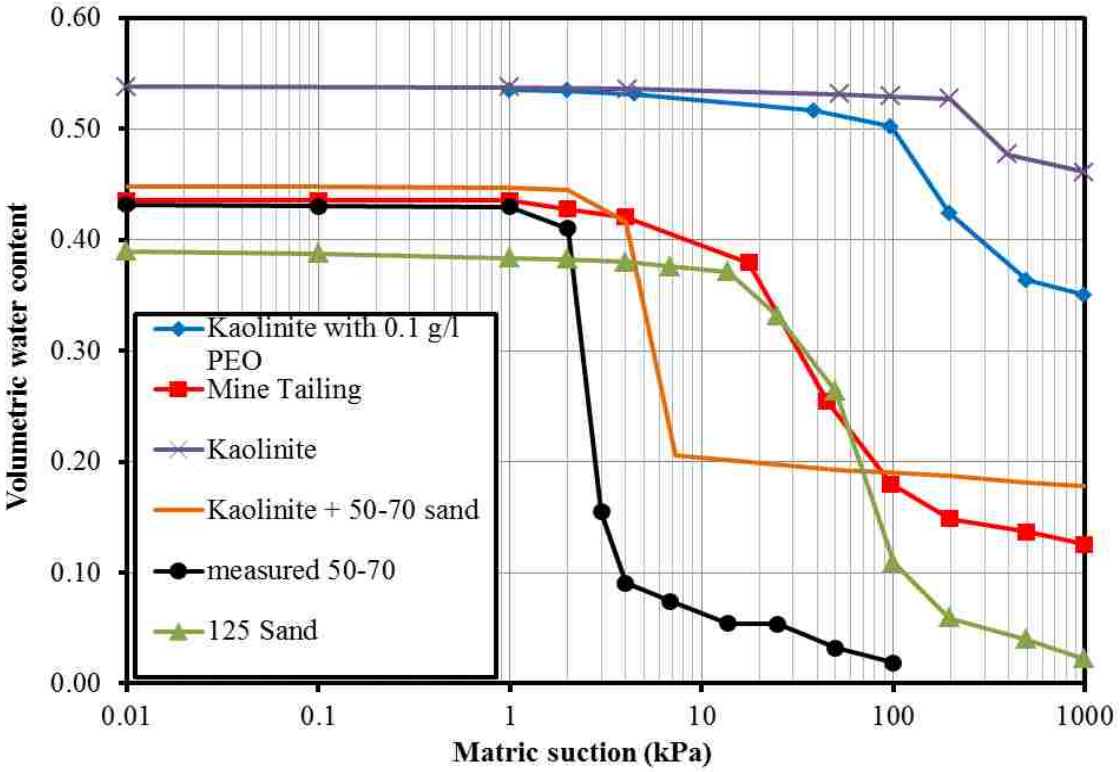

Figure 5.13 SWCC result of fine-grained material

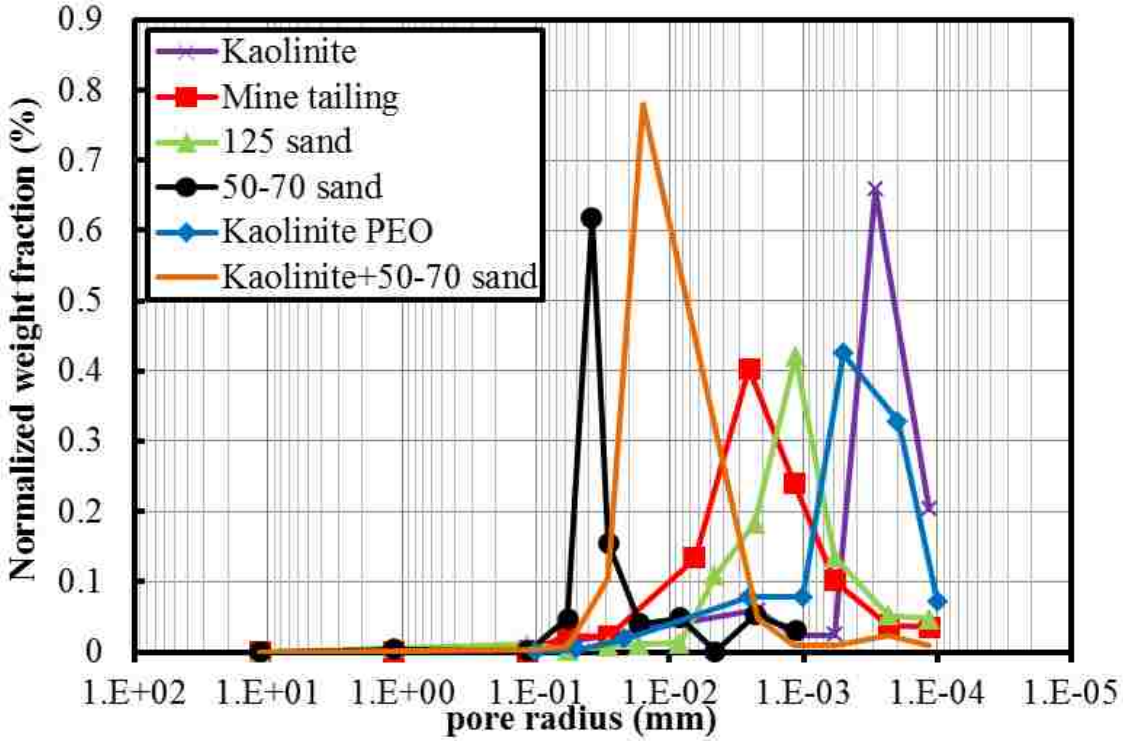

Figure 5.14 pore size distribution of fine-grained material

Table 5.6 Fitted parameters of Kaolinite, 125 sand and mine tailing

Fredlund and Xing	***a***	***m***	***n***	**Van Genutchen**	***δ***	***λ***	***η***
Kaolinite	199.061	0.013	440.000	Kaolin	0.008	0.023	3.408
Kaolinite PEO	90.48	0.019	51.27	Kaolinite PEO	0.0062	10.49	1.23
Kaolinite 50-70 sand	3.97	0.15	120	Kaolinite 50-70 sand	0.99	13.23	4.99
50-70 sand	2.18	0.63	16.39	50-70 sand	5.21	0.015	151.73
125 sand	34.16	0.903	2.75	125 sand	0.0064	218.4	1.73
Mine Tailing	18.019	0.526	2.894	Mine Tailing	0.037	0.623	2.105

6. NUMERICAL PREDICTION OF SWCC

6.1. FINITE ELEMENT METHOD (FEM) PREDICTION WITH HYDRUS 1D

6.1.1. Fundamental Theory. Hydrus 1D, a finite element code developed by Simunek and van Genuchten in 1980s, was used to numerically simulate the measured soil water characteristic curve (SWCC) results of selected geomaterials as used in this study. Hydrus 1D is powerful in solving a variety cases of two-phase flow and chemical transportation in porous media. Wayllace and Lu (2012) used it for estimating SWCC with a transient water release and imbitions method (TRIM) for rapidly measuring wetting and drying SWCC and hydraulic conductivity functions. The input is the outflow vs. time curves at only two suction values, one near air entry value (AEV) and one that can induce significant volumetric water content change. Then the SWCC were inversely solved by Hydrus 1D. Hopmans et al. (2002) and Figueras (2009) also stated that multistep outflow method (MOM) could be used to estimation hydraulic conductivity.

The theoretical foundation of Hydrus 1D simulation is Richards' equation:

$$\frac{\partial \theta}{\partial t} = \frac{\partial}{\partial z}\left[K(\theta)\left(\frac{\partial \psi}{\partial z} + 1 \right) \right] \qquad \text{Eq. 6.1}$$

Where,

K is hydraulic conductivity

h is the pressure head, or matric suction

z is the elevation above vertical datum

θ is water content

t is time

Richards' equation (Richards, 1931) describes the movement of water flow in unsaturated soils. Compared to Darcy's Law, Richards' equation is a transient state form of flow equation.

Mass balance, which dictates that the changing rate of saturation is equal to changing rate of total fluxes in and out of porous media, is satisfied. SWCC models are required to solve Richards' equation.

There are several available SWCC models in Hydrus 1D simulation. Van Genuchten model (1980) was used in this study. The equation was shown in Eq. 6.2, and was repeated below for clarity:

$$\theta = \theta_r + \frac{\theta_s - \theta_r}{\left[1+(\alpha h)^n\right]^m} \quad \text{Eq.6.2}$$

Van Genuchten (1980) proposed a relative hydraulic conductivity function for unsaturated soils:

$$K(h) = K_s S_e^l \left[1-\left(1-S_e^{1/m}\right)^m\right]^2 \quad \text{Eq.6.3}$$

With given initial and boundary conditions, SWCC can be inversely solved with known outflow rate vs. time results.

6.1.2. Hydrus 1D. Hydrus 1D is one-dimentional finite element software designed by Jikra Simunek and van Genutchen (1991). Since it is one dimentional, the element is just on node. The simulated soil sample is discrete into one hundred nodes with uniform vertical distance.

6.1.3. Procedure of Prediction. SWCC results for mine tailing were used as an example to illustrate the procedures to predict SWCC curves.

6.1.3.1 Initial estimation of parameters. Hydrus 1D requires five parameters to inversely calculating SWCC, i.e., θ_s, θ_r, a, n, and K_s:

Where,

θ_s is the saturated volumetric water content of soil;

θ_r is the residual volumetric water content after SWCC test;

a is the parameter for SWCC model which represents the inverse of air-entry value (AEV);

n is the other parameter for SWCC model, it controls the slope of major desorption curve which is the middle dramatically changing part of SWCC;

K_s is the saturated hydraulic conductivity.

Hydrus 1D allows assigning initial estimated values, as well as confining the range of variation for above parameters. Those input information are based on

experimental results and previous studies in the literature. θ_s can be determined from phase relationship before testing. Through applying small suction values to soil sample with the elevation-controlled low suction measurement, the air entry value can be estimated by observing the initiation of desaturation. Residual volumetric water content (θ_r) of soil can be estimated from previous results in the literature. For example, θ_r of sand is between 0.01 and 0.1 (Fredlund et al. 1997 & Imre 2008). Mine tailings could be higher since the particle size is smaller than sands, which will give the soil more water hold capacity. The range of residual volumetric water content of mine tailing is between 0.1 and 0.2 (Swanson, 1999). Kaolinite is a fine-grained soils, whose residual water content usually ranges from 0.4-0.5 (Anandarajah, 2011). *n* is related to the type of soil and its grain size distribution (van Genutchen, 1980). For gap graded sand, *n* could be as high as 15 (Imre, 2008). Since clay has the highest water hold capacity, the major desaturation curve is really flat, which leads to the range of *n* values from 1.001 to 5. *n* value of mine tailings and silts are between sand and clay. Saturated hydraulic conductivity of sand can be measured through constant water head test. It is more difficult and time consuming to measure the saturated hydraulic conductivity (K_s) of clay due to its low hydraulic conductivity. A reasonable range of initial K_s values was assumed based on literature review. Table 6.1 summarized the initial parameters for different materials used in this study.

Table 6.1 Estimated initial values and ranges for SWCC coefficients

	a		***n***		***r***		***Ks* (cm/h)**	
	Min	Max	Min	max	Min	Max	Min	Max
Uniform Sand	0.5	1	3	20	0.01	0.1	1	60
Fine Sand	0.001	0.01	1.001	5	0.01	0.1	0.01	10
Mine Tailing	0.01	0.1	1.001	5	0.1	0.2	3.60E-03	3.60E-05
Kaolinite	0.0001	0.001	1.001	5	0.4	0.5	3.60E-04	3.60E-06

6.1.3.2 Initial and boundary conditions. Hydrus 1D model is composed of two materials, one is the soil specimen and the other is high air entry value ceramic disk

(Figure 6.1). The water flow through soil sample is from top to bottom. The initial condition and boundary conditions for Hydrus 1D simulation is plotted in Figure 6.1.

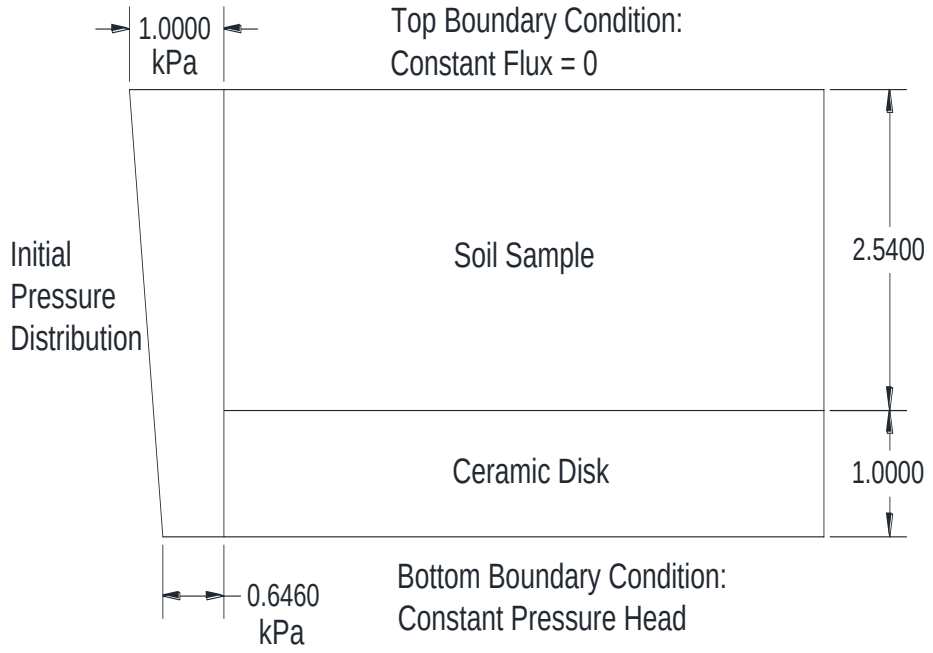

Figure 6.1 Initial condition and Boundary condition of Simulation

It should be noted that a non-uniform initial matric suction distribution is required for using inverse modeling for multistep simulation (van Dam, 1992). Toorman et al. (1992) designed a device to measure matric suction inside the soil sample during testing. In this study, these values were not measured. Instead, on top of the applied single matric suction value, hydrostatic matric suction distribution with respect to the middle height of the specimen was assumed (Figure 6.1).

6.1.3.3 Fluxes verse time curve. The numerically simulated flux vs. time results should agree with the measured ones. Figure 6.2 shows the typical measured flux vs. time curve for each suction step. Each curve represents the outflow distance under different suction. At each applied matric suction value, the observed curve will be linear initially, and then the slope will decrease until reaching a plateau value. Outflow vs. time relationship is the objective for Hydrus 1D's inverse problem-solving.

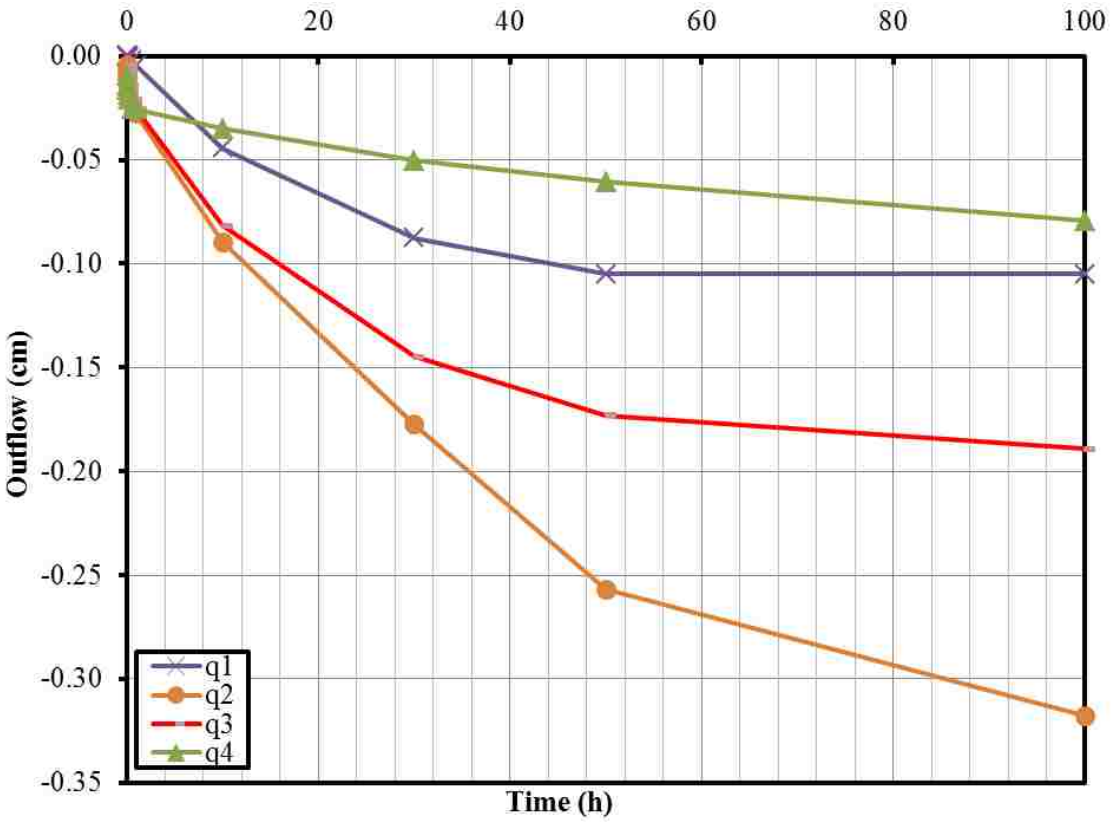

Figure 6.2 Fluxes – Time relationship

It is shown in Figure 6.2 that water will come out of sample under each suction step. When air pressure gets to AEV, volume of water will increase quickly until soil sample reached residual condition.

6.1.4. Hydrus Inverse Solution Method. One-step Outflow Method (OOM), Multiple Single Step Outflow Method (MSOM), and Multistep Outflow Methods (MOM) were exercised to determine SWCC. Each of them was elaborated below.

6.1.4.1 Multiple single-step outflow method (MSOM). Multiple single-step outflow method (MSOM) is a method by simulating the observed outflow – time relationship for each matric suction with inversely solved SWCC functions. MSOM simulates exactly the same process as the actual SWCC measurement. Desaturation of the sample takes for about 100 hours for mine tailing under each matric suction step. Four matric suction values, 18 kPa, 45 kPa, 97 kPa and 197 kPa, which account for the

majority of the water content changes, were chosen for the simulation. Figure 6.3 exhibits the Outflow – Time relationship under these matric suctions.

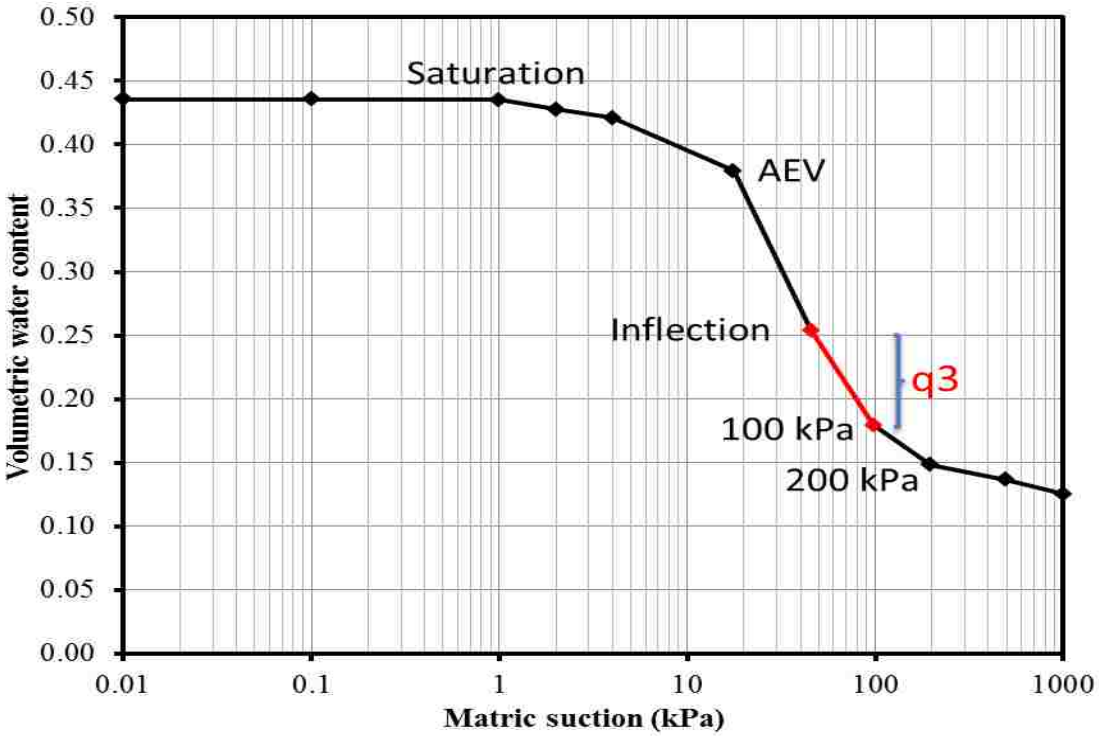

Figure 6.3 MSOM method

Figure 6.2 shows the same information with Figure 6.3. The differences between these two are the vertical axis. Figure 6.2 demonstrates the reading change of water volume measurement as obtained from laboratory tests. Figure 6.3 changes the volume of water into outflow distance by dividing the surface area of sample as used in Hydrus 1D. Since water is flow out of sample, the outflow is negative.

MSOM was simulated at four matric suction values were AEV (18 kPa), inflection point (45.3 kPa), 100 kPa and 200 kPa. Figures 6.4 and 6.5 show simulated SWCC and Q-T results at these four matric suction values. The simulated a, n, θ_r and K_s are listed in Table 6.2. In addition, the differences between the measured and simulated SWCC or Q-T curves, in terms of coefficient of determination (R^2), were also calculated (Table 6.2).

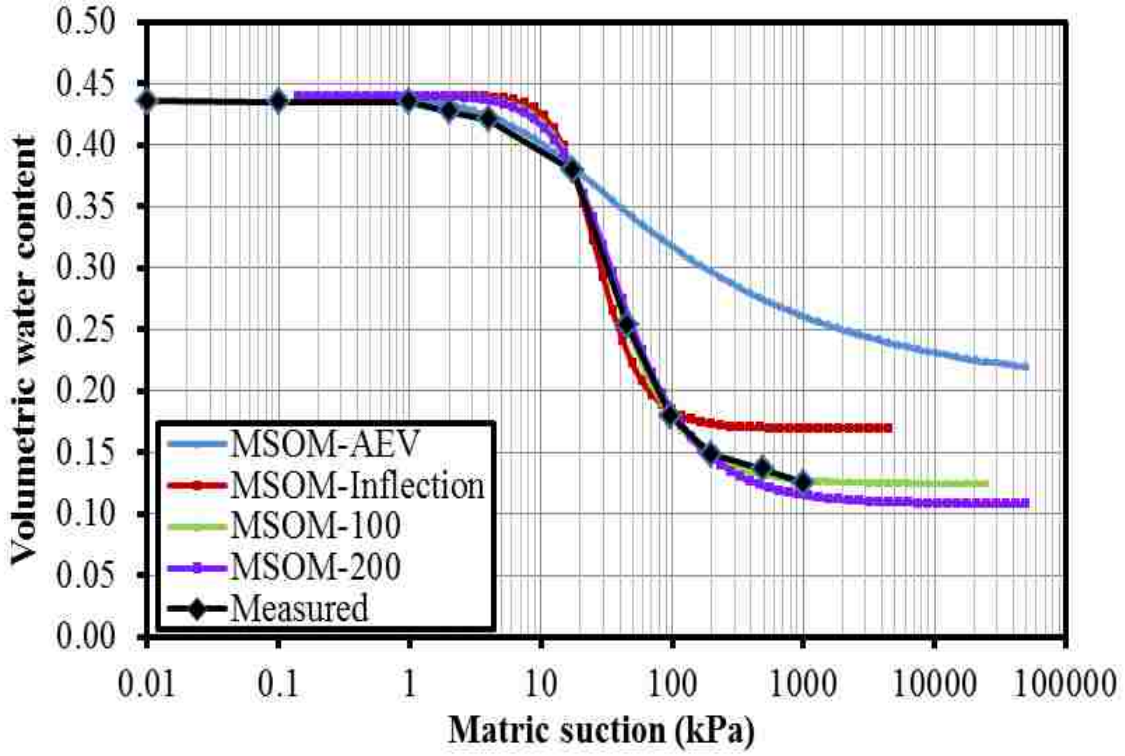

Figure 6.4 MSOM Simulation Results

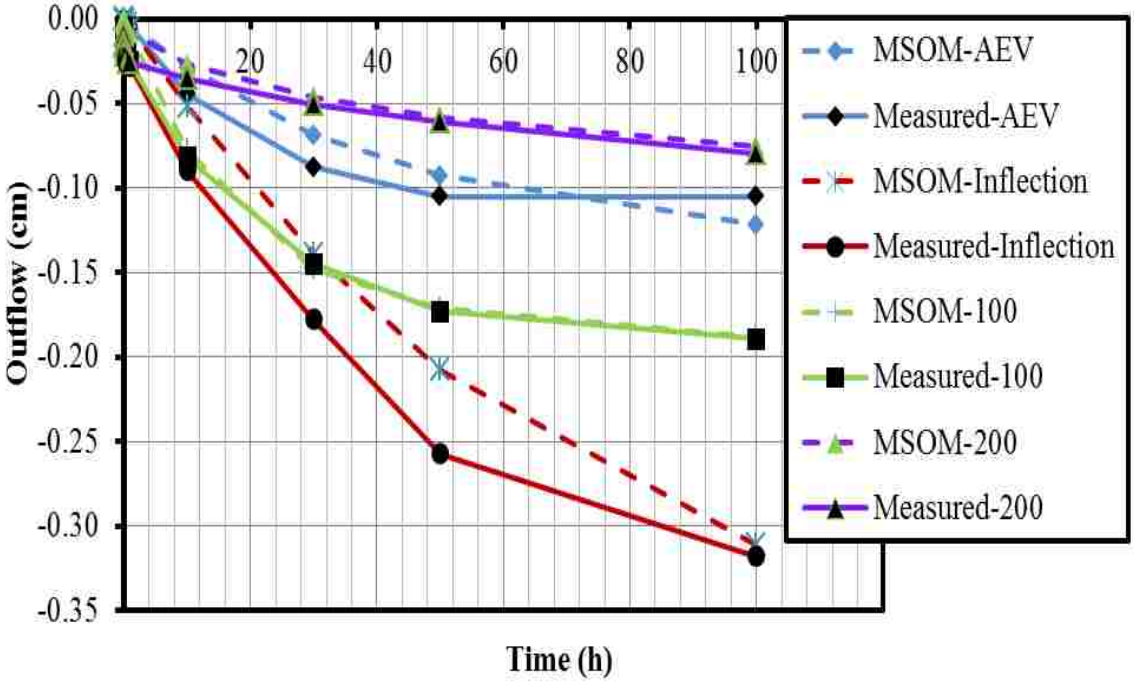

Figure 6.5 MSOM Flux – Time

Table 6.2 Summary of simulation results

		a	n	θr	K_s	R^2 for Q-T	R^2 for SWCC
	AEV	0.0113	1.29	0.26	0.00313	0.99670	0.87267
	Inflection	0.00439	3	0.17	0.0231	0.99000	0.95034
	100 kPa	0.004	2.27	0.13	0.0282	0.99800	0.98290
MSOM	200 kPa	0.004	2.04	0.12	0.0143	0.96400	0.92528
	AEV	0.0138	1.36	0.24	0.00463	0.99810	0.86380
	Inflection	0.08	1.73	0.11	0.0151	0.98980	0.96384
	100 kPa	0.00616	1.66	0.08	0.0141	0.98270	0.97578
OOM	200 kPa	0.00729	1.51	0.1	0.0144	0.97560	0.96791
MOM	All	0.0095	1.44	0.11	0.0114	0.96350	0.99613
Measured		0.0370	2.10	0.125			

Among these four simulated curves, the best one is inverse calculation from 100 kPa ($R^2 = 0.998$).

It is observed that simulated SWCC based on Q-T curve at AEV matches with the measured SWCC only at suctions no higher than AEV. This is because no information on matric suctions or pore sizes was given by Q-T curves at AEV, and because the outflow at AEV only accounts for a small portion of the overall outflow. On the other hand, it is observed that simulated SWCC based on Q-T curve at the 100 kPa best represents the measured SWCC, especially before 250 kPa (near residual condition). This is because the outflow at 100 kPa accounts for the major portion of the overall outflow. This is also because expelled water (Q-T) at 100 kPa, corresponding to the matric suction range from 45 kPa and 100 kPa, passes through the major range of the pore sizes of this soil. Similar trends can also be observed for simulated SWCCs from Q-T curves at inflection (45 kPa) and 200 kPa that, in general, the most accurate estimations of SWCC were obtained near the matric suction values at which the actual Q-T curves were used as the input. This observation was further validated by the simulated SWCCs from Q-T at 200 kPa, where accurate SWCC estimation was observed only from 110 to 1000 kPa.

Inverse modeling of Hydrus 1D used van Genutchen (1980) hydraulic conductivity function (Eq. 6.3). It was noted that van Genutchen's (1980) hydraulic conductivity function shares the same parameter, *m*, as van Genutchen's SWCC model (Eq. 6.2). This exerts an additional restriction to hydraulic conductivity function, which

might lead to larger difference between the simulated and measured Q-T curves. Unfortunately, there is no alternative hydraulic conductivity functions in Hydrus 1D, which allows different *m* parameters from van Genutchen's SWCC model. Hydrus 1D can simulate both SWCC and hydraulic conductivity, the result of Hydraulic conductivity is shown in Figure 6.6.

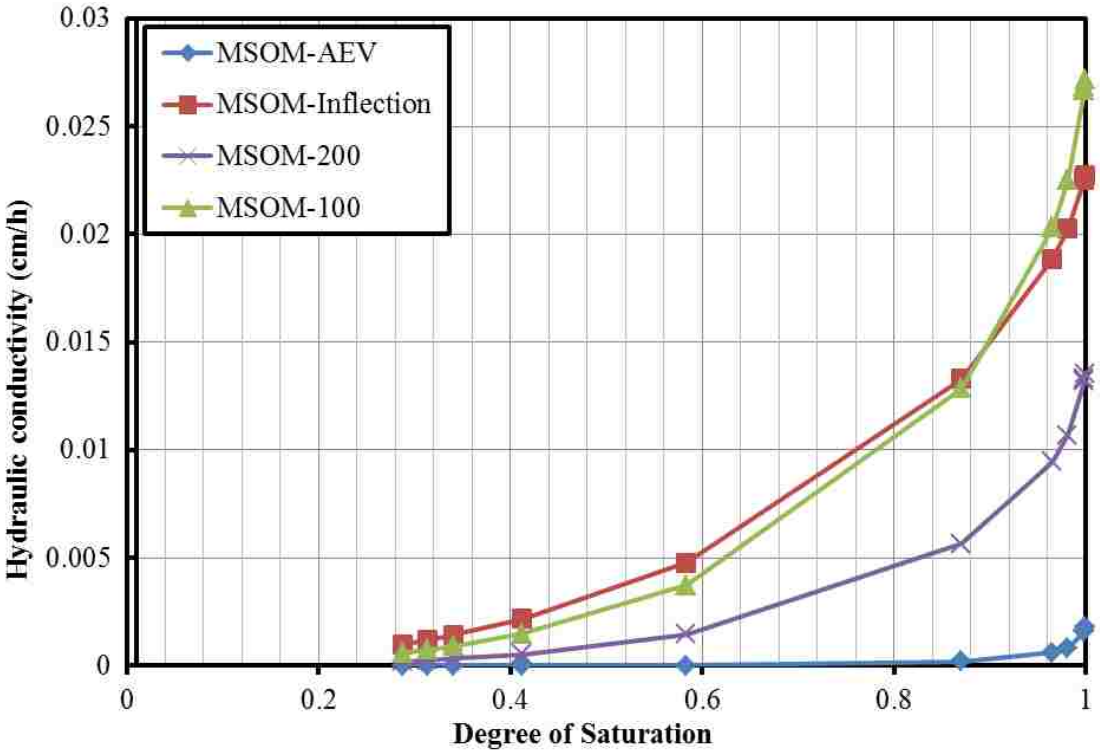

Figure 6.6 MSOM simulation result of unsaturated hydraulic conductivity

According to Figure 6.6, the hydraulic conductivity changed with degree of saturation which is related to matric suction.

6.1.4.2 One-step outflow method (OOM). Gardner (1958) applied a series of matric suctions on the saturated soil sample, and the outflow was recorded at each matric suction step. From Gardner's method, Doering (1965) proposed a one-step experiment to avoid the traditional time consuming SWCC test and achieve a precise result. Whisler and Watson (1968) further stated that the drainage over time measurement and one-step SWCC can be used to predict the unsaturated hydraulic conductivity curve by matching observed outflow and simulated results. Russo (1988) found that the soil hydraulic

conductivity function could be optimized through one-step method. Also, Simunek and Hopmans (2002) discussed the parameter optimization and uniqueness of inverse modeling. Their approach assumed the initial input parameters are the true description of SWCC. Through iterations on the parameters, final input parameters were obtained by matching the simulated flux with measurement outflow.

The input data of one-step outflow method are soil geometry, fitting parameters, initial and boundary conditions, and Q-T data. Soil geometry, boundary conditions, and fitting parameters (initial and range) were the same as those in multiple single-step outflow method (MSOM). Initial matric suction values were hydrostatic as shown in Figure 6.1, with no additional initial uniform matric suction (start from saturation).

The major difference between MSOM and OOM is the input Q-T data. As suggested by Wayllace and Lu (2012) the Q-T in OOM should be cover a large suction range, or a significant amount of water content change. In this study, however, the outflow was measured at small increment of matric suction. To simulate One-step Outflow case, the Q-T curves at subsequent matric suction values from 1 kPa to a larger value (AEV, 45 kPa, 100 kPa, and 200 kPa in this study) were superposed to yield a pseudo One-step Outflow versus time curve (Figure 6.8). This pseudo One-step Outflow vs. time curve will be used as input in Hydrus 1D inverse modeling.

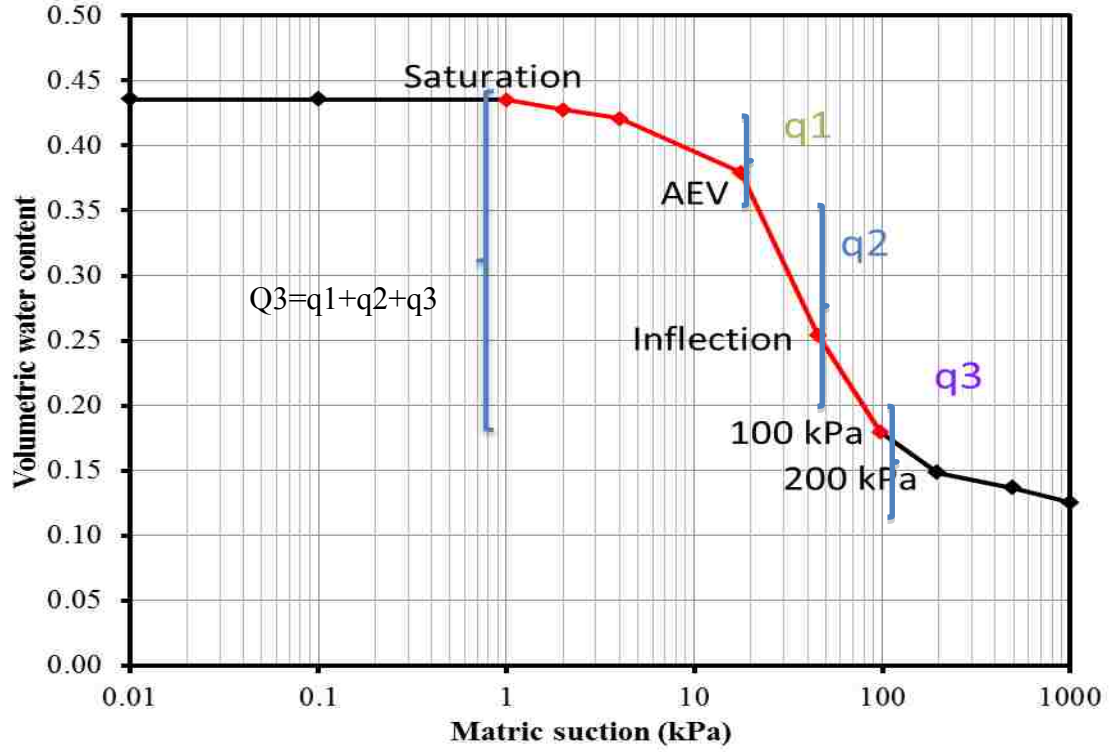

Figure 6.7 OOM simulation

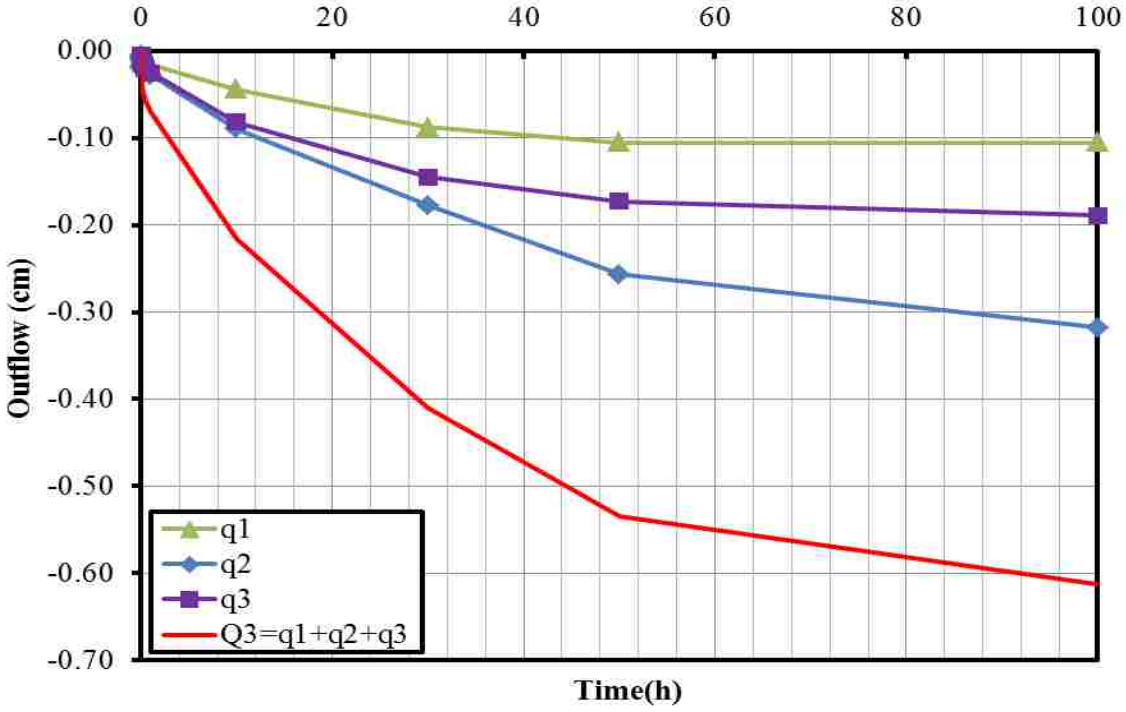

Figure 6.8 Superposition of MSOM outflow (q) to OOM outflow (Q)

The typical SWCC prediction result of mine tailing is shown on Figure 6.7 and Fluxes – Time relationship (Q-T) is in Figure 6.8. The simulated parameters θ_s, θ_r, a, n are listed in Table 6.2.

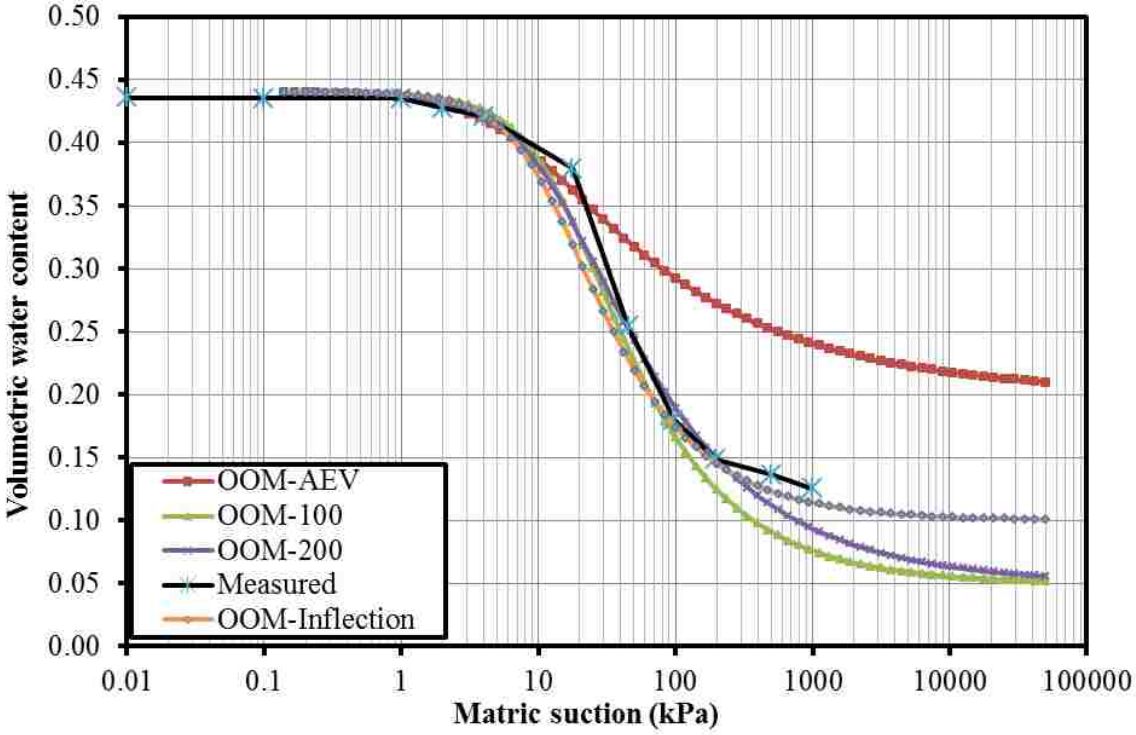

Figure 6.9 OOM simulation result

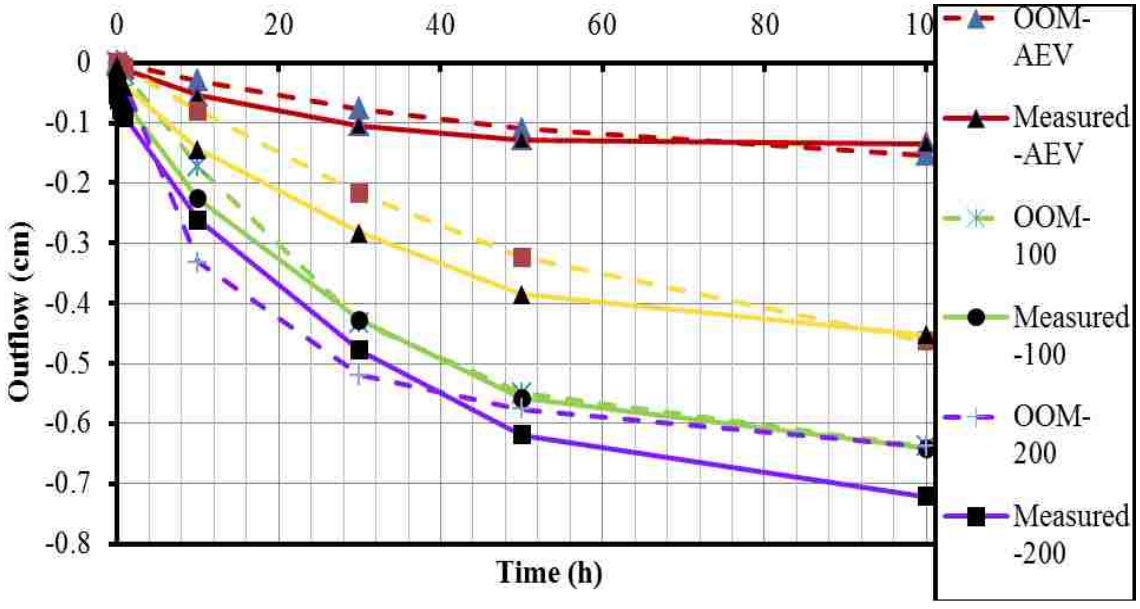

Figure 6.10 OOM Fluxes - Time

It is observed that simulated SWCC based on cumulative Q-T curve at 200 kPa best represents the measured SWCC, especially before 100 kPa (Figure 6.8). Simulated SWCC based on cumulative Q-T curve at AEV (18 kPa) yielded good estimation only before 20 kPa (Figure 6.8). Similar to MSOM, it was observed that cumulative Q-T curve with larger amount of outflow volume, containing more information of the matric suction and inherent pore size distribution, yielded better prediction of SWCC.

It is also observed a gradual increase in K_s value as final matric suction increased (Table 6.2), which is necessary to accommodate the superposed flow rate, especially at near saturation state. Figure 6.11 exhibits the simulation result of unsaturated hydraulic conductivity verses matric suction.

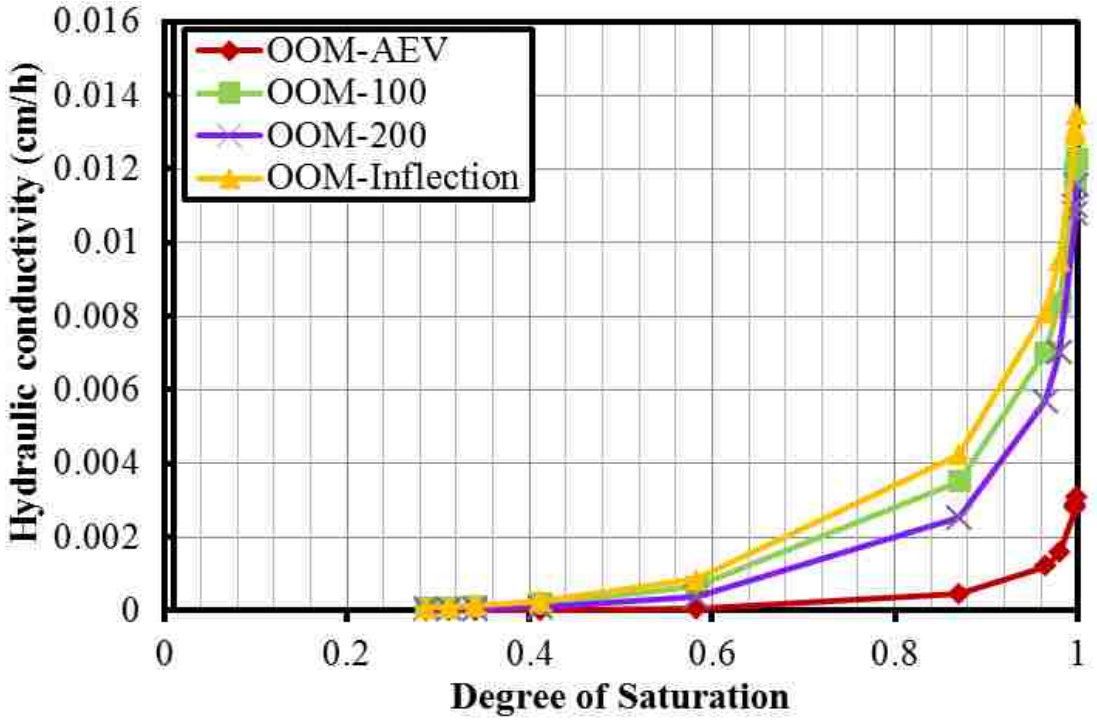

Figure 6.11 Degree of saturation verses unsaturated hydraulic conductivity

6.1.4.3 Multi-step outflow method (MOM). Multi-step outflow method (MOM) shared the same soil geometry, fitting parameters (initial and range), and initial conditions with one-step outflow method (OOM). However, the boundary condition and Q-T curve were different. A stepwise increment of matric suction, namely 18, 45, 100,

and 200 kPa, was applied at the bottom of the ceramic disk. The corresponding Q-T curve under each of the four matric suctions was used directly as the input.

Figure 6.12 and Figure 6.13 exhibit the inversely calculated Q-T curve and SWCC results. Table 6.2 lists the simulated parameter.

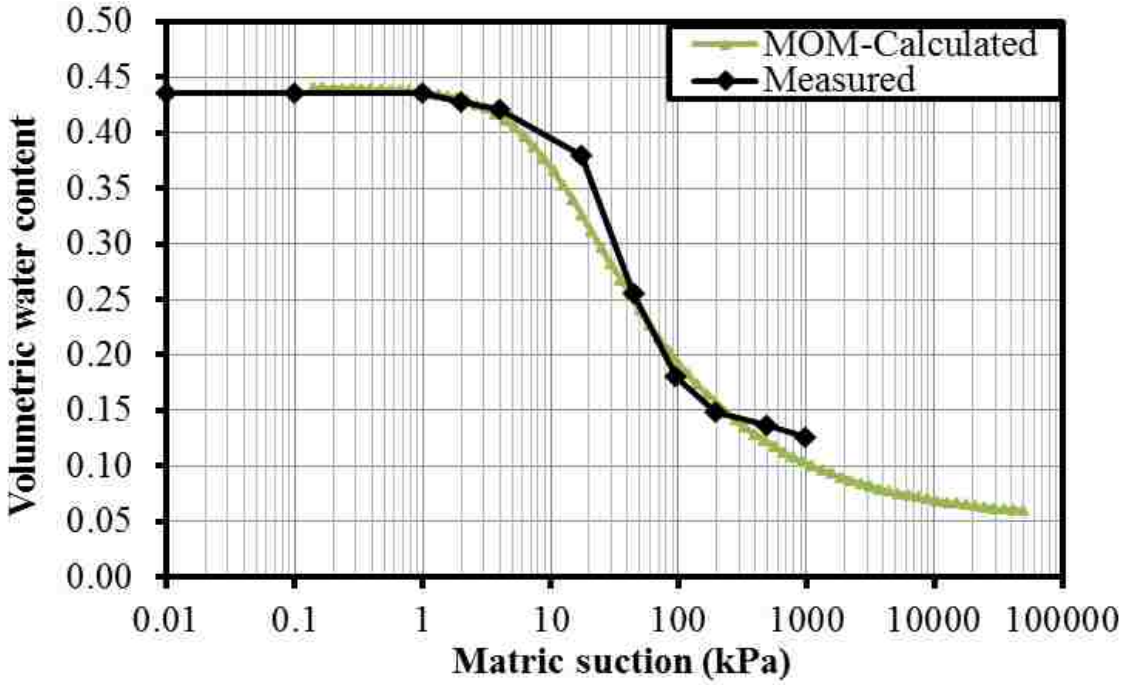

Figure 6.12 MOM prediction result of mine tailing

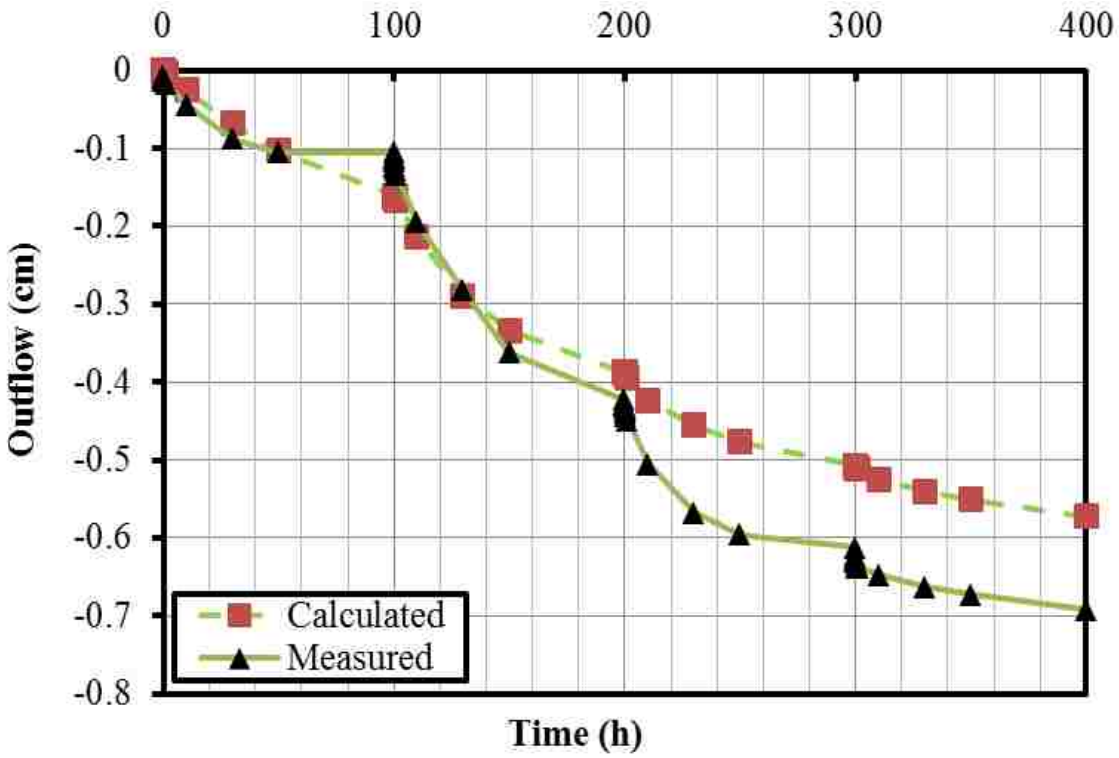

Figure 6.13 Simulated Outflow - Time curve for MOM

From Figure 6.13, MOM simulated SWCC curve had higher R^2 value (0.996) than OOM or MSOM did. This is reasonable because MOM has four points in SWCC, while OOM or MSOM only has two points in SWCC. However, the difference in R^2 is not so significant, and both OOM and MSOM can yield reasonable SWCC predictions.

Outflow vs. time curve from MOM, however, yields the least accurate Q-T results (Table 6.2). In first two matric suction steps (18 and 45 kPa) the outflow was overestimated, while in the last two matric suction steps (100 and 200 kPa) the outflow was underestimated. The high difference was the result of the compromise of K_s values for the four Q-T results under different matric suctions.

Figure 6.14 describes the simulated unsaturated hydraulic conductivity relationship with degree of saturation.

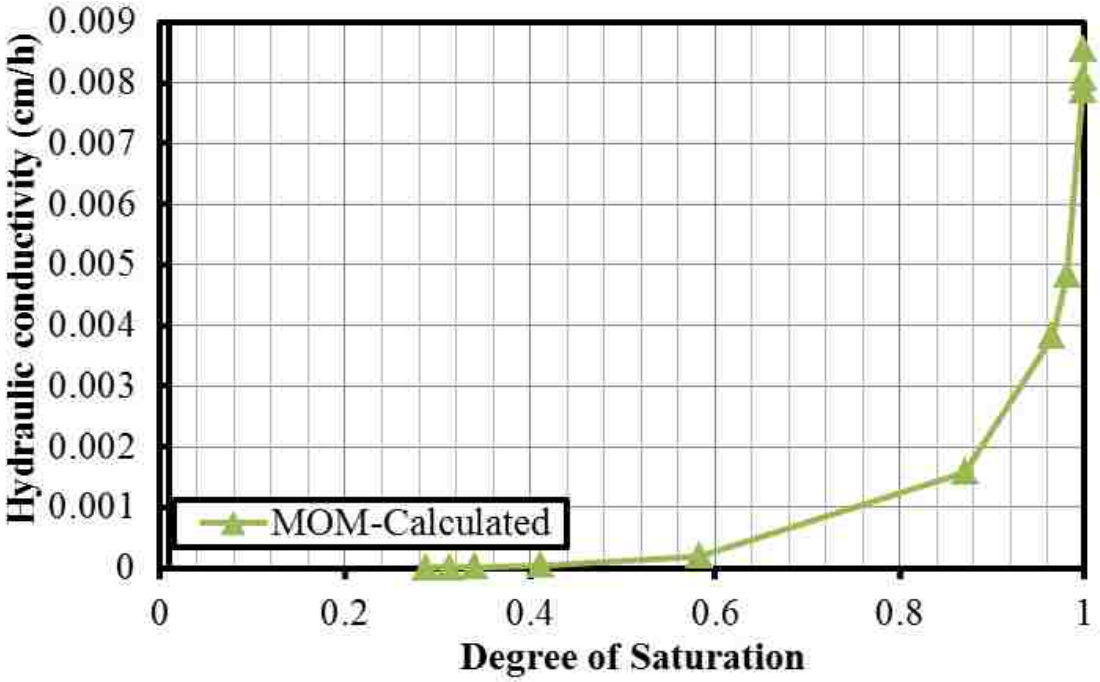

Figure 6.14 MOM simulated unsaturated hydraulic conductivity

6.2. SUMMARY

All the simulation result is shown in Table 6.2. Simulated parameters will be compared with measured value. Figure 6.13, 6.14 and 6.15 exhibit the simulated parameter verses different data point (AEV, inflection, 100 kPa, 200 kPa)

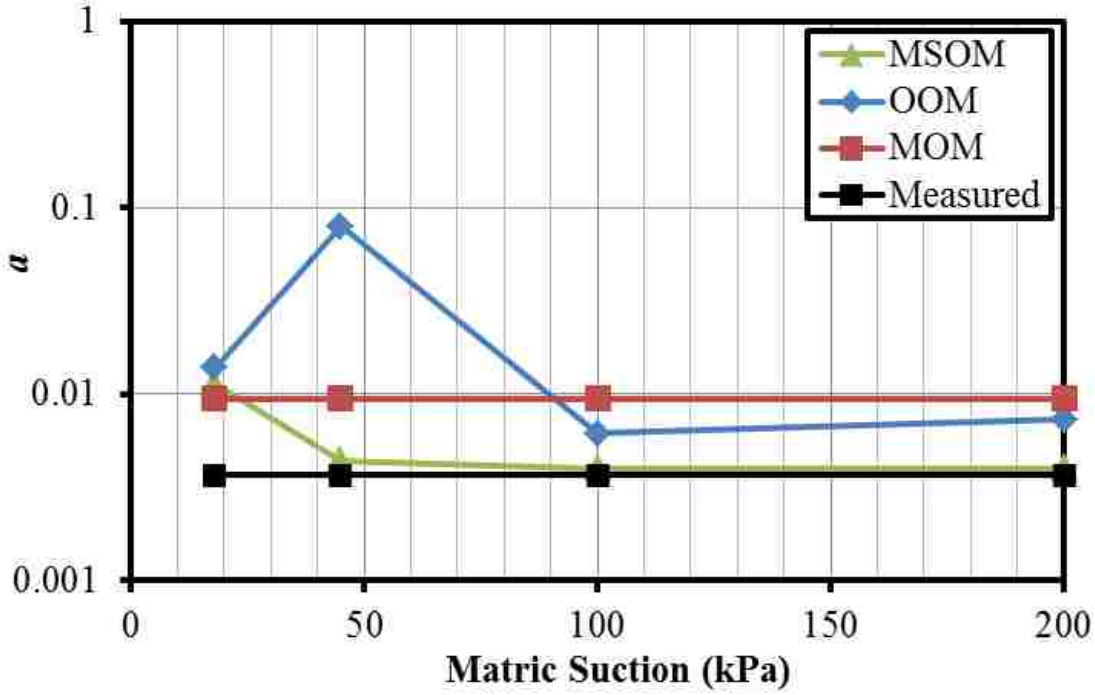

Figure 6.15 Simulated parameter a verses matric suction

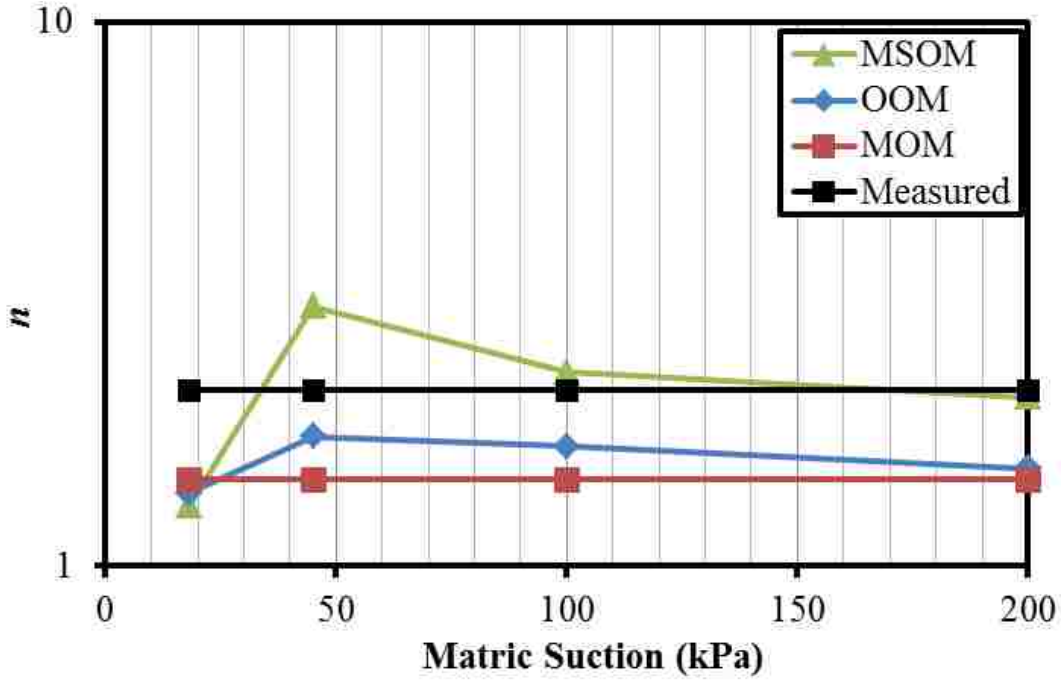

Figure 6.16 Simulated parameter n verses matric suction

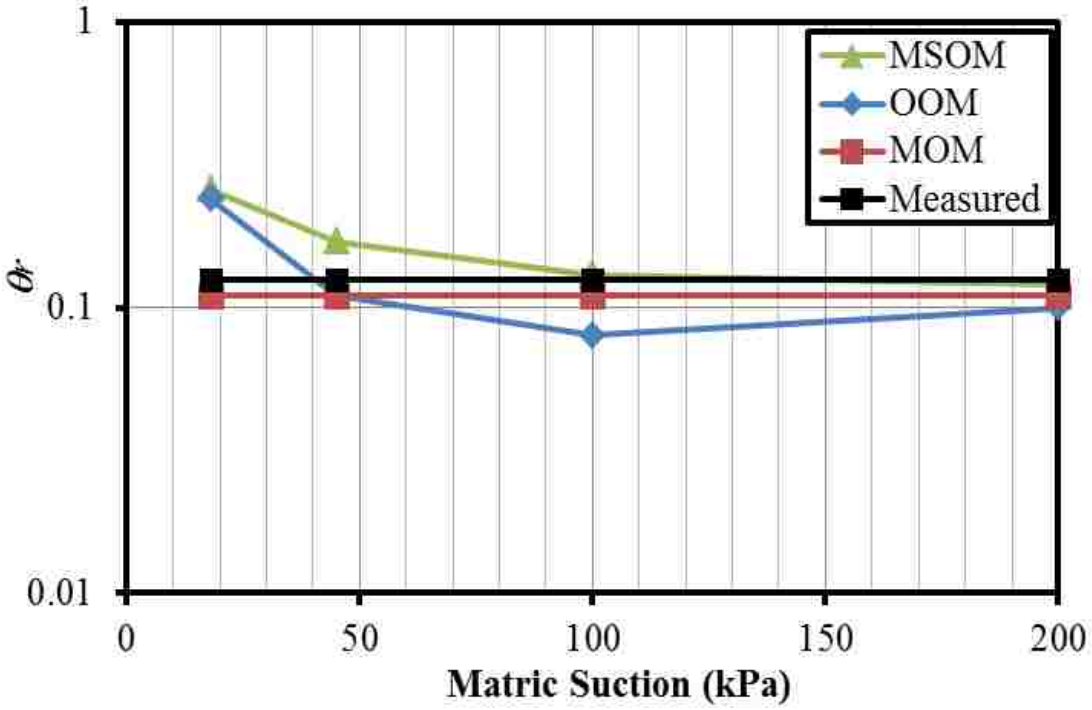

Figure 6.17 Simulated parameter θ_r verses matric suction

The observed Outflow – Time curve all fits well but SWCC does not. From the R Square value of SWCC, the best fitting curve is MOM simulation.

Value *a* ranges from 0.004-0.0049 which implies the AEV is between 20-25 kPa. Only MSOM-200 kPa gets the AEV equals to 0.009 which is not close to the measured data. The reason is the data provided to Hydrus is only in residual condition which will lead to the bias under lower suction. Fredlund and Xing model gives out the AEV around 18 kPa which is close to the simulation result.

Simulation parameter n is variable from 1.5-2.08, the two smallest value come from simulation of AEV, because data point AEV does not provide enough data for major desorption curve which is close related to parameter n. Residual water content θ_r does not have a good match with the measured data.

Since SWCC is directly related to unsaturated soil permeability, so any misinterpretation of permeability will cause the difference between measured and fitted SWCC. Hydrus is using van Genutchen (1980) unsaturated soil permeability function which is not appropriate for MT, especially under higher suction. If there is a permeability function can represent the real value of MT, the residual water content will

be calculated accurately. Ks describes the saturated permeability of MT which is variable through 0.00014 cm/h to 6.3 cm/h. The best fit curve is calculated from MOM so the Ks value 0.00453 cm/h should be close to the real condition.

7. CONCLUSION AND FUTURE WORK

7.1. SUMMARY OF WORK

In this study, soil-water characteristic curve (SWCC) of sands modified with different biopolymers were measured with both Tempe cell and Fredlund SWCC device. An elevation-controlled low suction (0.01 to 5 kPa) horizontal tube was developed to accurately measure SWCC of sands. Corrections for air diffusion and evaporation were performed. With above modifications, consistent SWCC results can be obtained for biopolymer modified sands. Inverse simulation of SWCC based on One-step or multistep measurement were carried out with Hydrus 1D. The measured SWCC results of mine tailing were used as an example.

7.2. CONCLUSION

1) The developed low suction horizontal tube are suitable for measuring SWCC of sands and indicate a good estimation of air-entry value (AEV). The AEV of Ottawa 20-30 sand is 0.5 kPa which is impossible to measure with regular device.
2) SWCC results were fitted by both Fredlund and Xing (1994) and van Genutchen (1980) equations. It was found that air entry value and residual matric suction increased with xanthan gum, polyacrylamide (PAM), and sodium alginate (SA). SA has the most huge impact on increase AEV and residual water content. The AEV was increased from 0.5 kPa to 25 kPa and the residual water content was increased from 3% to 20%.
3) By using Scanning Electron Microscope (SEM), Laplace equation and the measurement of contact angle, surface tension, viscosity. It is indicate that the addition of biopolymer will decrease the pore size and increase the water holding capacity.

4) SWCC prediction was performed by using Hydrus 1D. The three methods MSOM, OOM and MOM all provide good prediction with R^2 larger than 95% except for the AEV. Because AEV does not provide enough information. It was found that MOM provided the most accurate SWCC, while MSOM yielded the most accurate Q-T results.

7.3. FUTURE WORK

1) More SWCC tests on biopolymer modified fine-grained soils are suggested to expand current pool of SWCC database.
2) Although SA increased AEV and residual water content of sand however, mine tailing is not tested with biopolymers. Experimentally identify good biopolymer candidate to increase the water retention capacity of mine tailing.
3) Only drying curve was measured but hysteresis of SWCC, including both drying and wetting processes, is suggested to provide a complete SWCC behavior.
4) SWCC and relative hydraulic conductivity models with separate sets of parameters are suggested for better Hydrus 1D inverse simulation.

APPENDIX

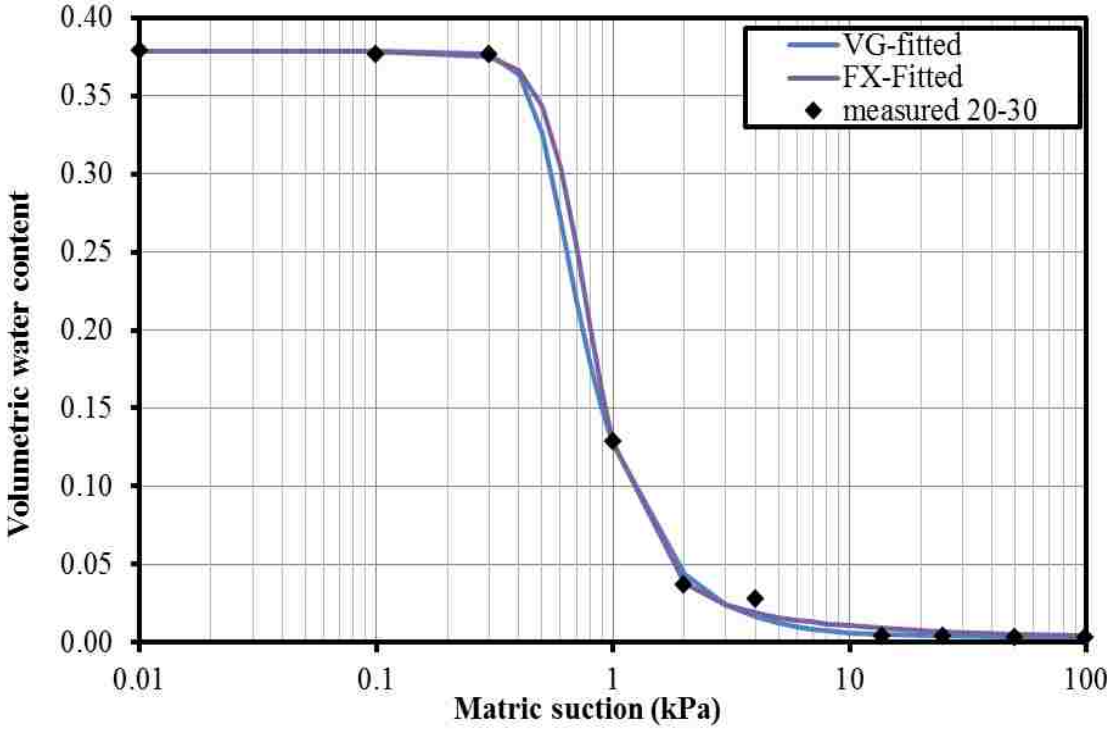

Figure A.1 SWCC and test result of Ottawa sand 20-30with water

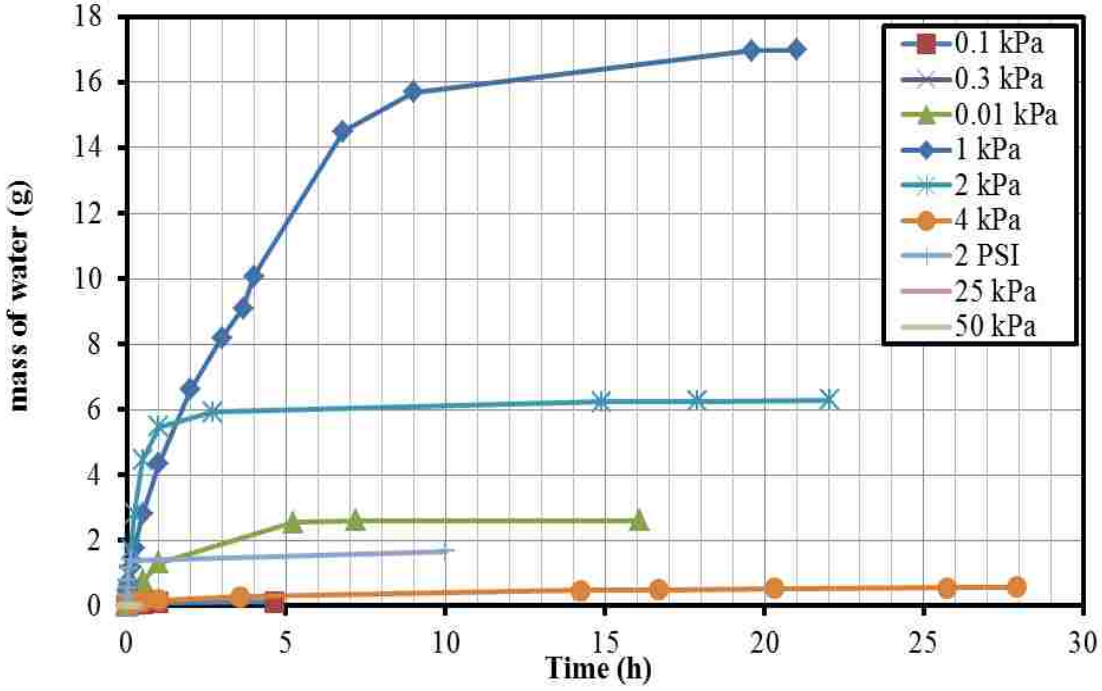

Figure A.2 Flux – Time for Ottawa sand 20-30 with water

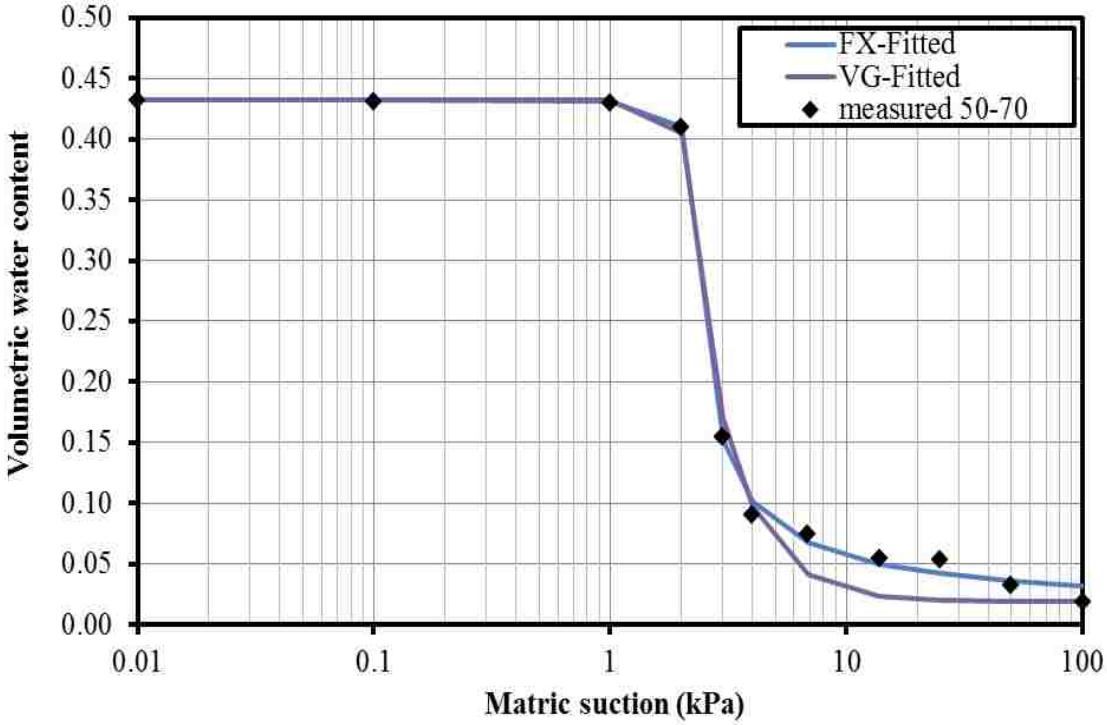

Figure A.3 SWCC for Ottawa Sand 50-70 with water

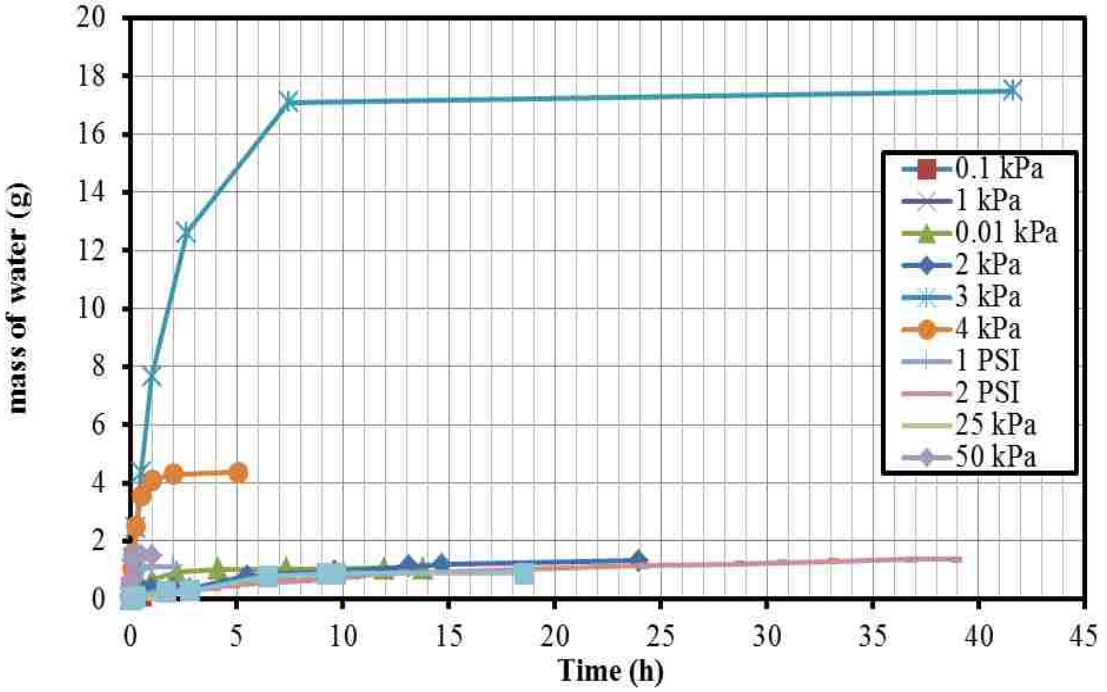

Figure A.4 Flux – Time relationship for Ottawa Sand 50-70 with water

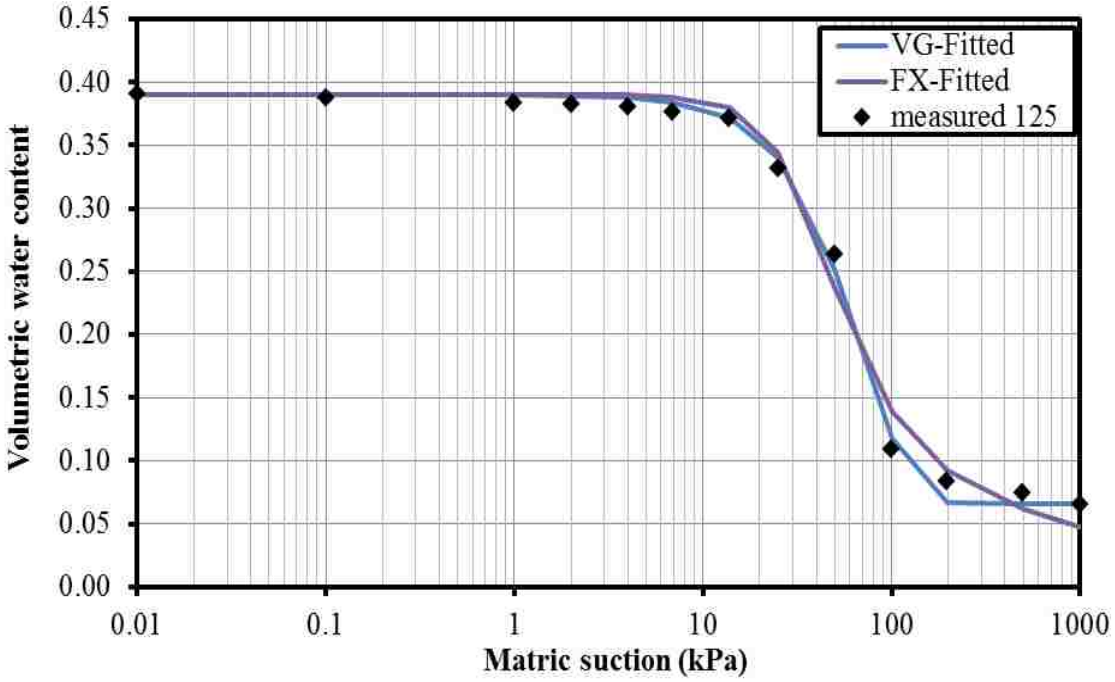

Figure A.5 SWCC result and curve fitting for Ottawa Sand 125 with water

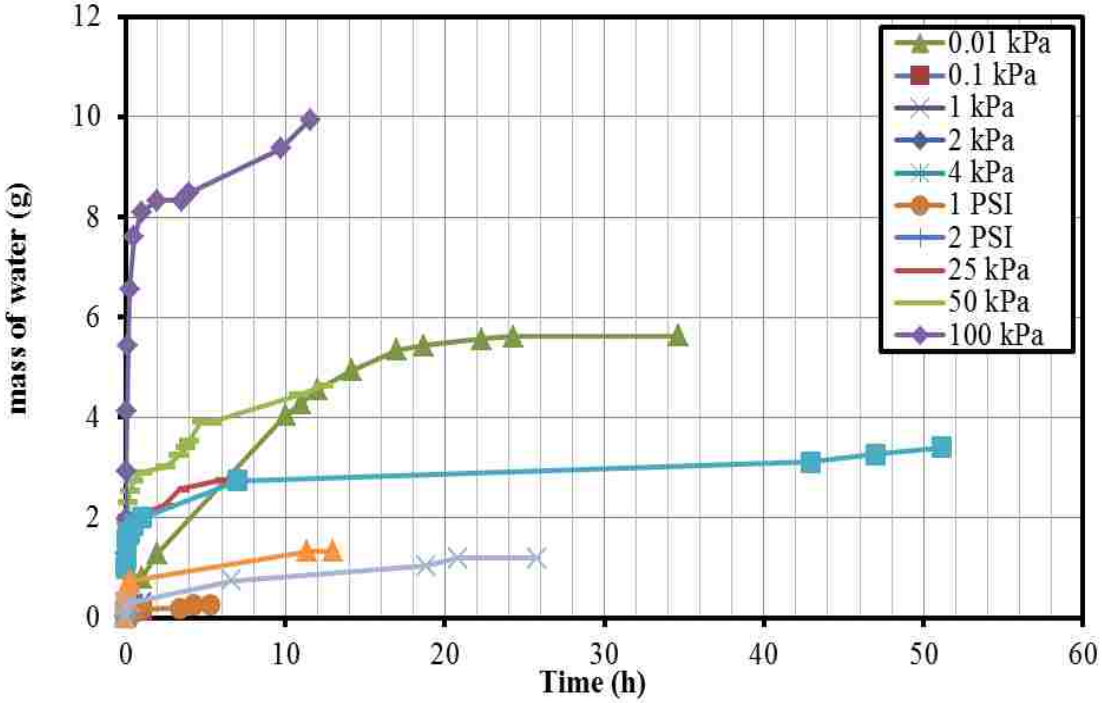

Figure A.6 Flux – Time curve for Ottawa Sand 125 with water

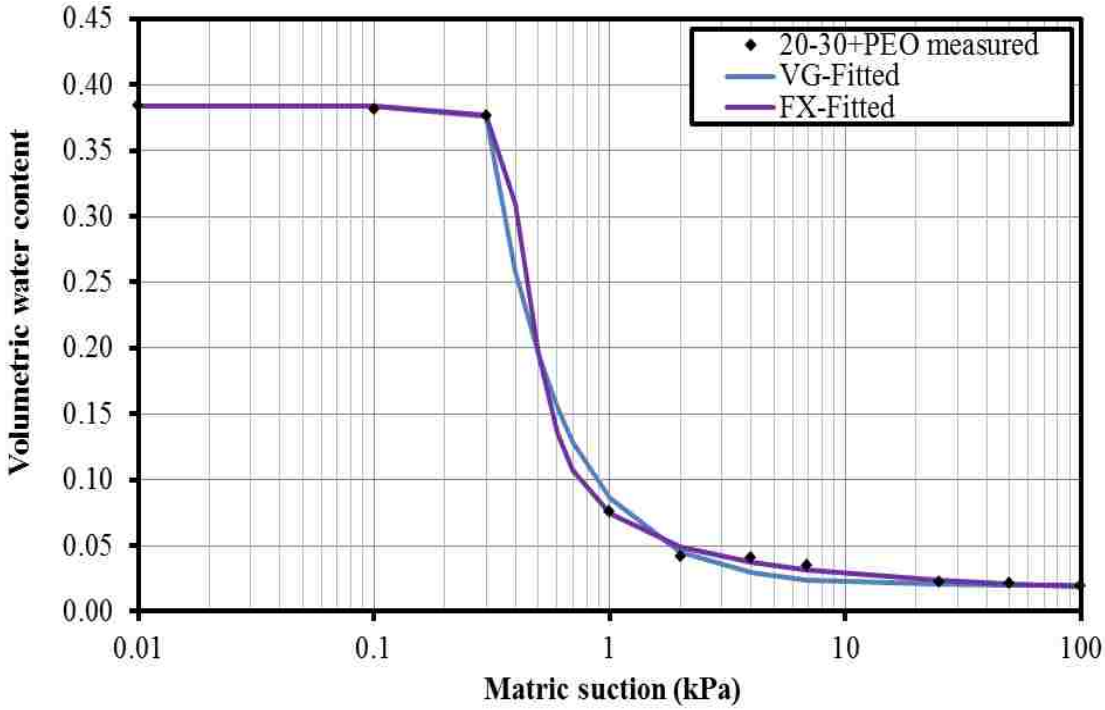

Figure A.7 SWCC result of sand with 10 g/L PEO

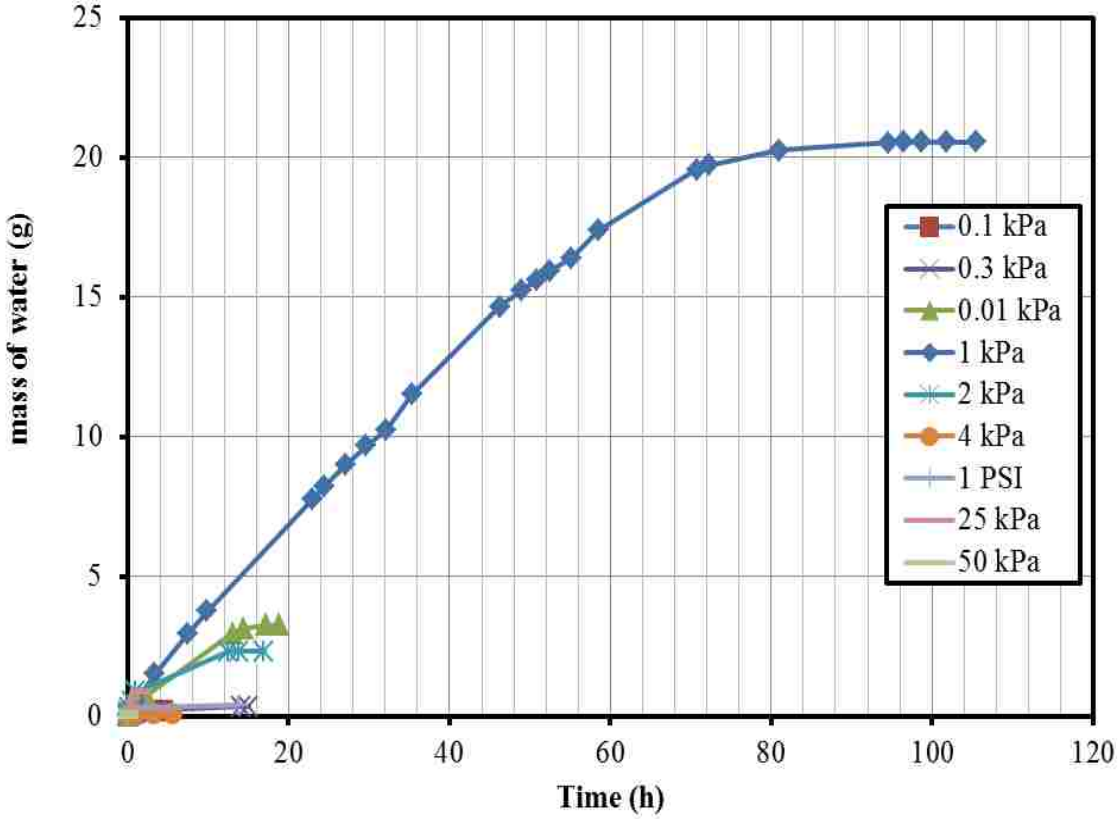

Figure A.8 Flux – Time relationship for 10 g/L PEO

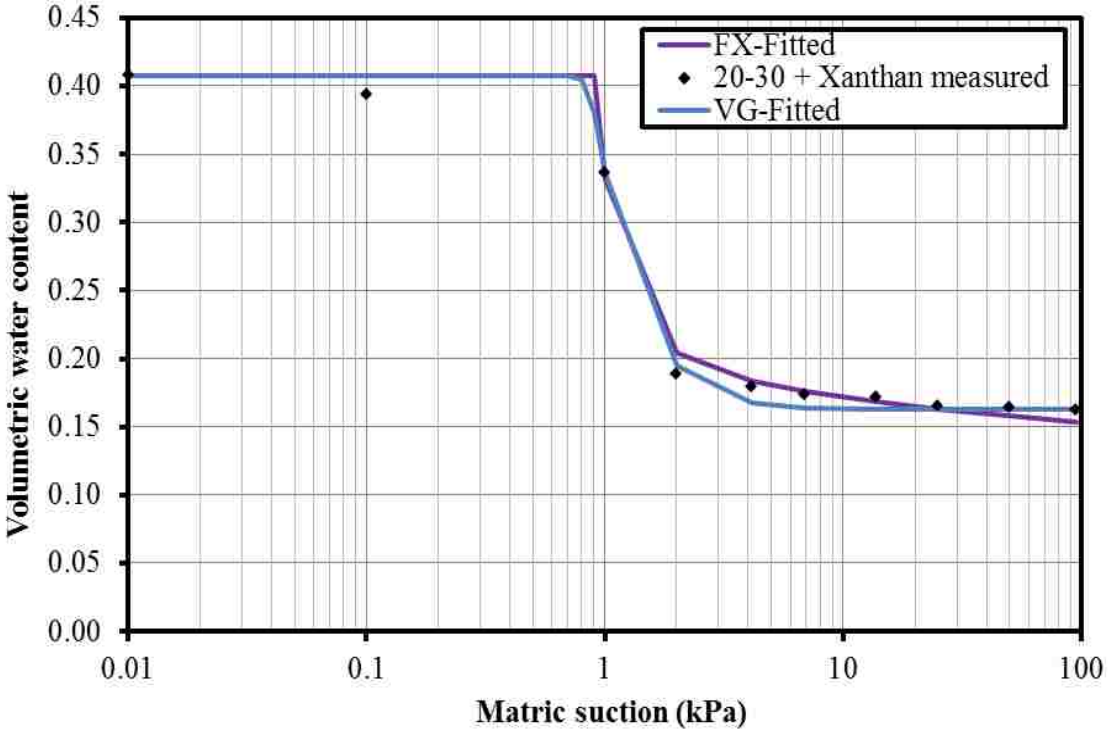

Figure A.9 SWCC result of sand with xanthan

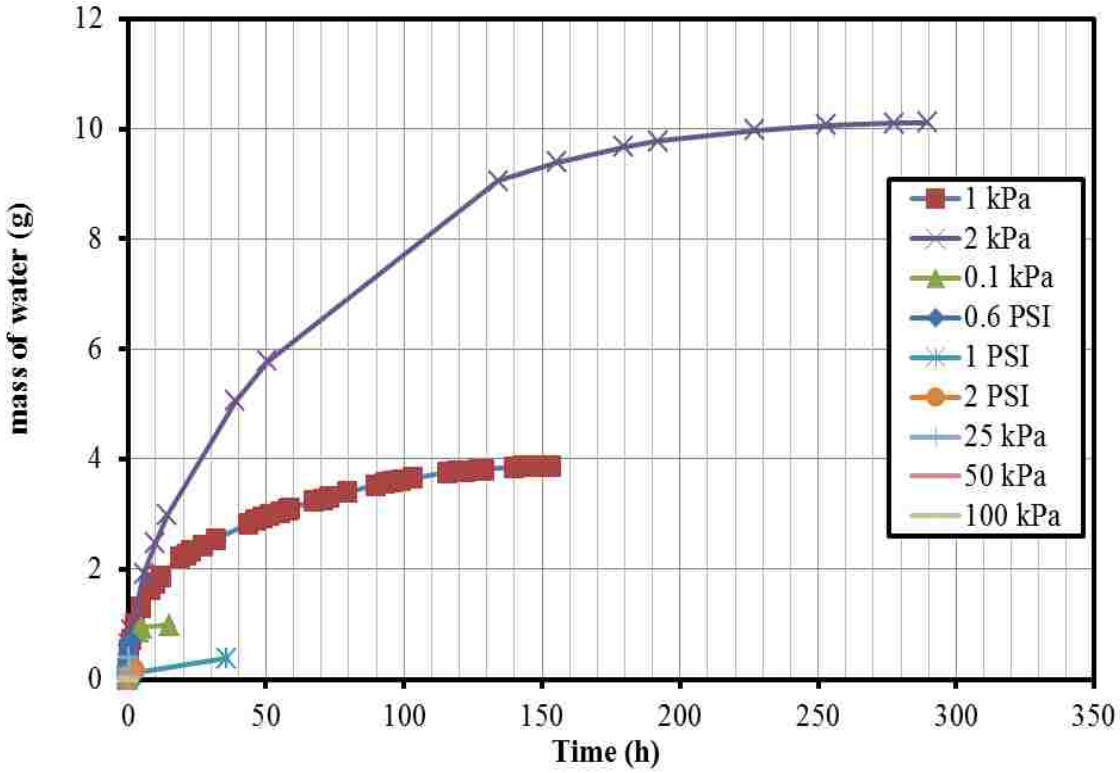

Figure A.10 mass of water expelling for sand with xanthan

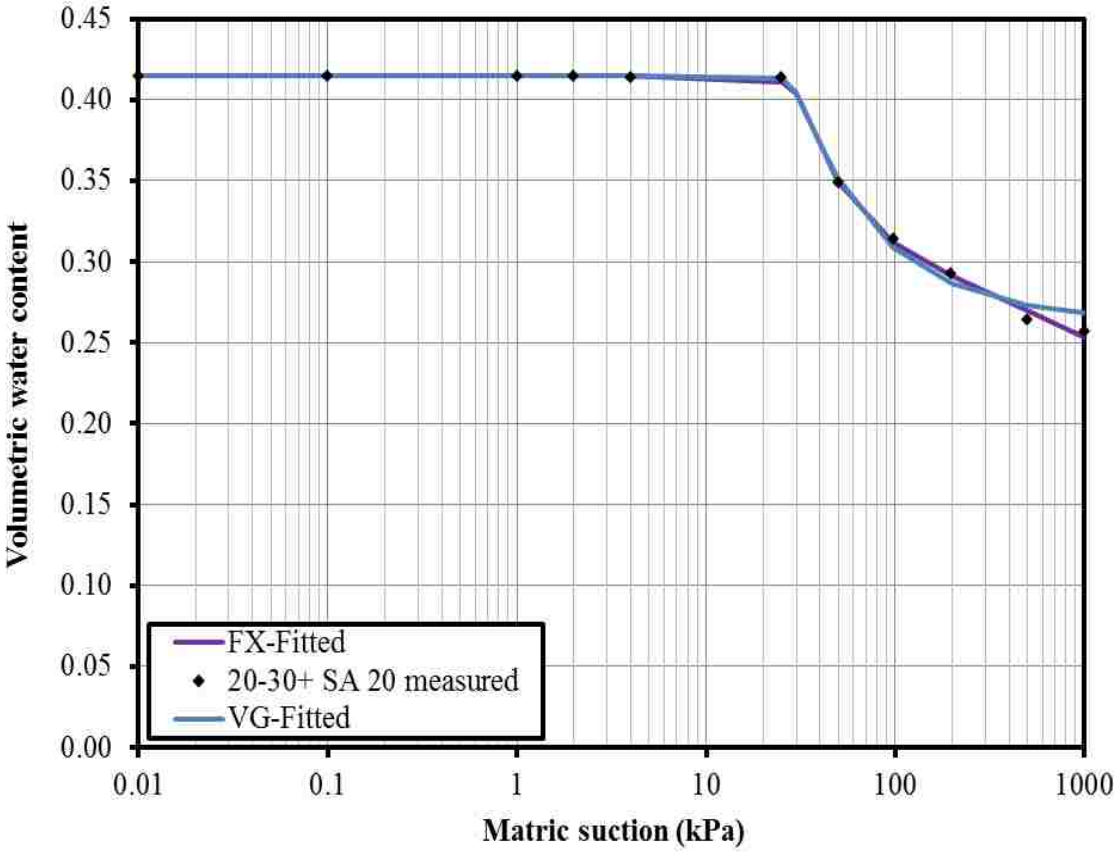

Figure A.11 SWCC result of 20g/L SA with sand

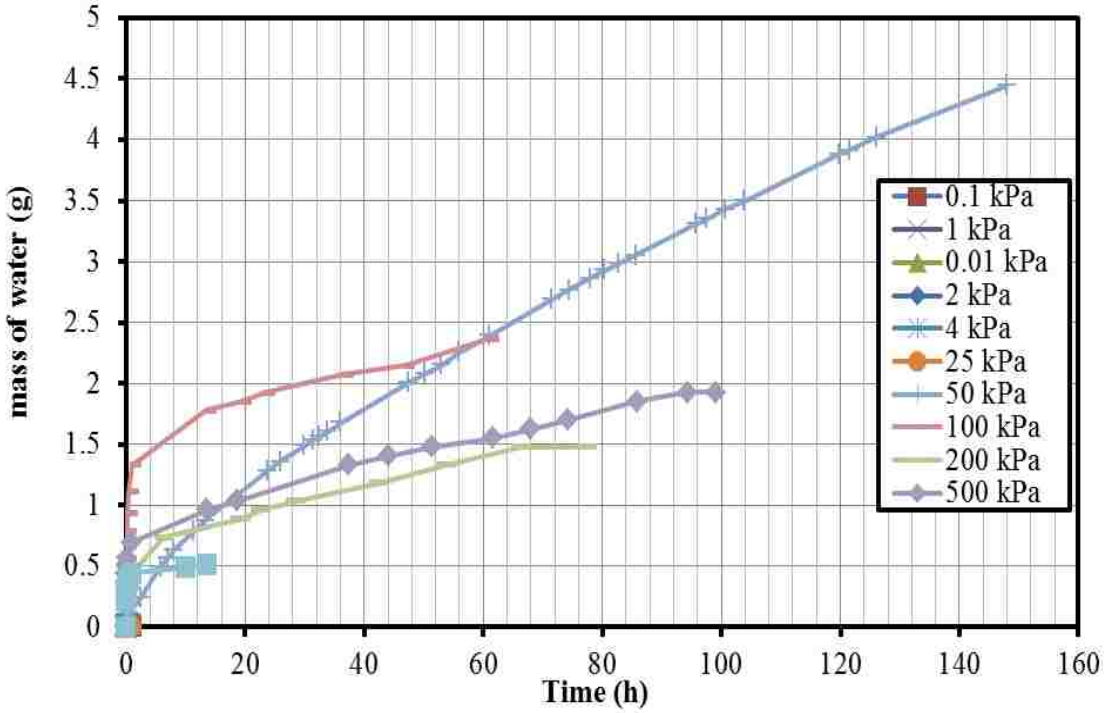

Figure A.12 the mass of outflow under different suction

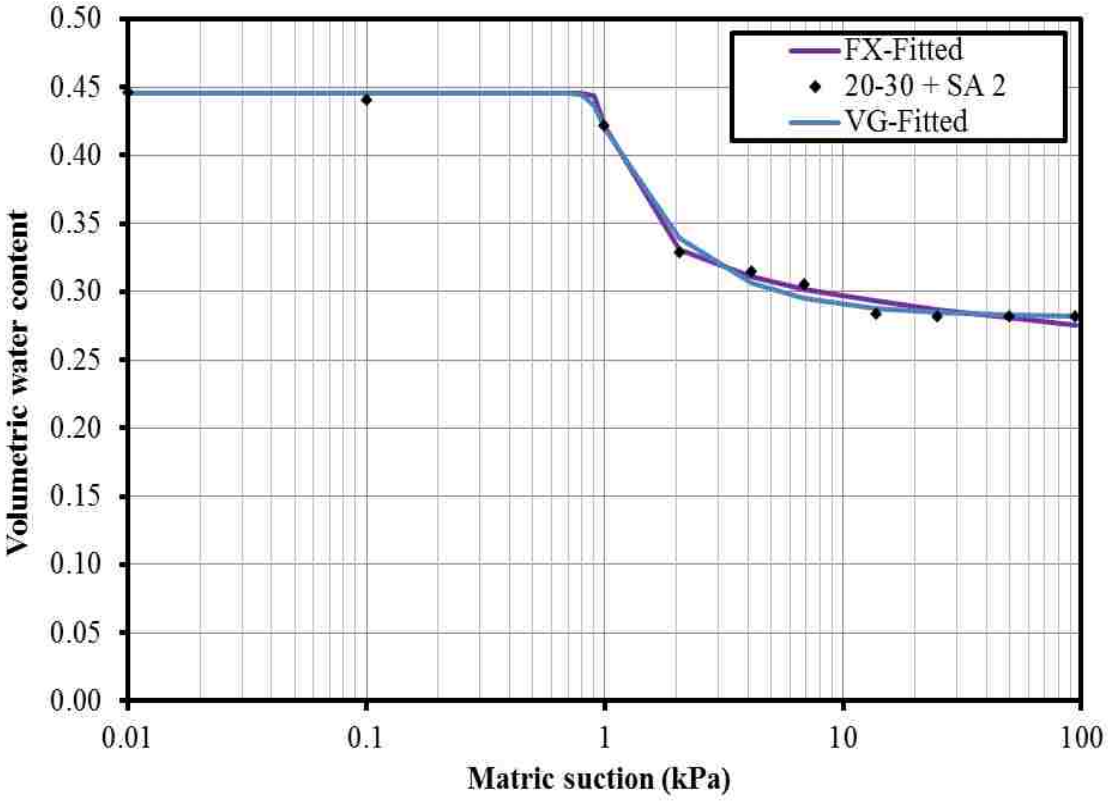

Figure A.13 SWCC result for sand with 2g/L SA

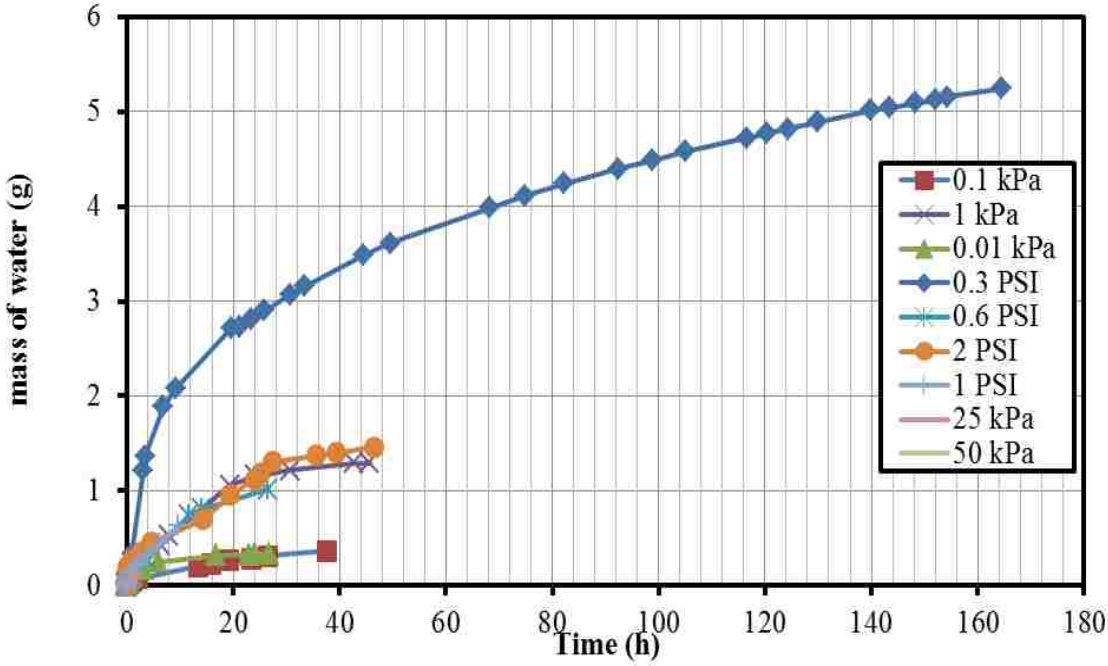

Figure A.14 Flux – Time relation for sand with 2g/L SA

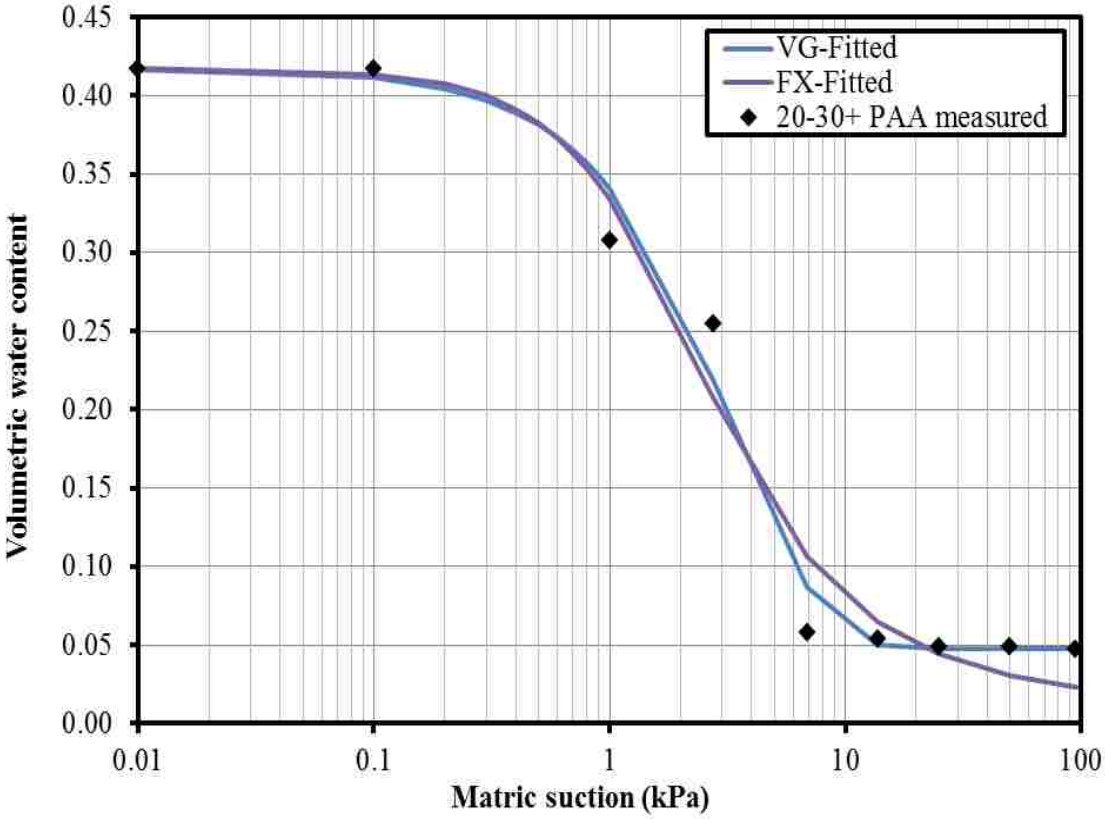

Figure A.15 SWCC result of sand with PAA

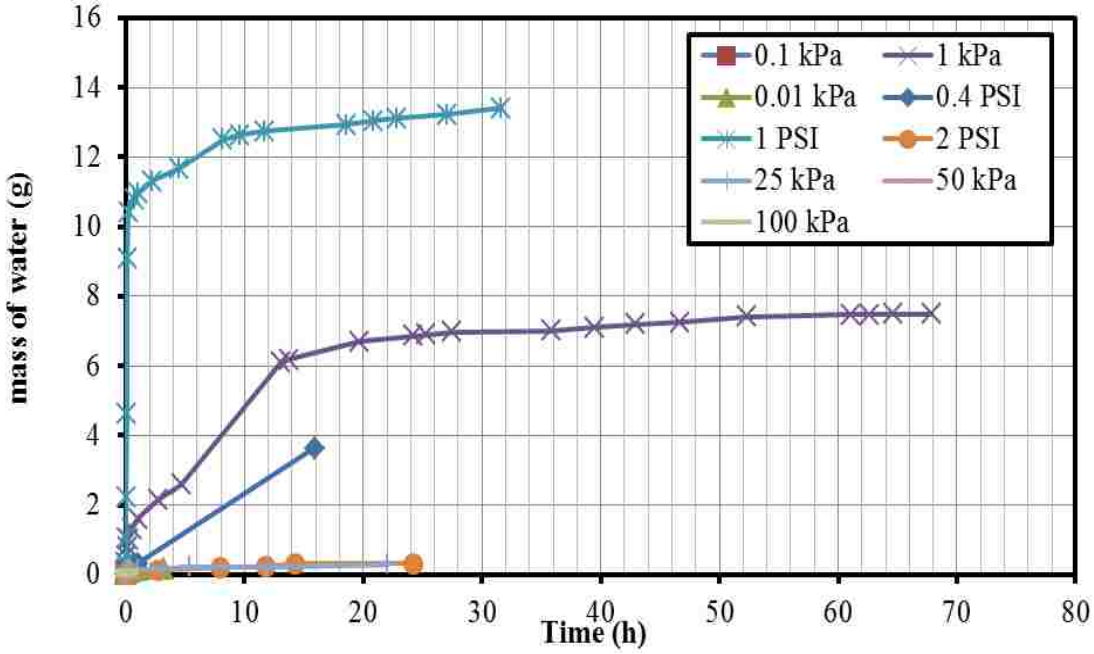

Figure A.16 mass of outflow verse time curve for PAA

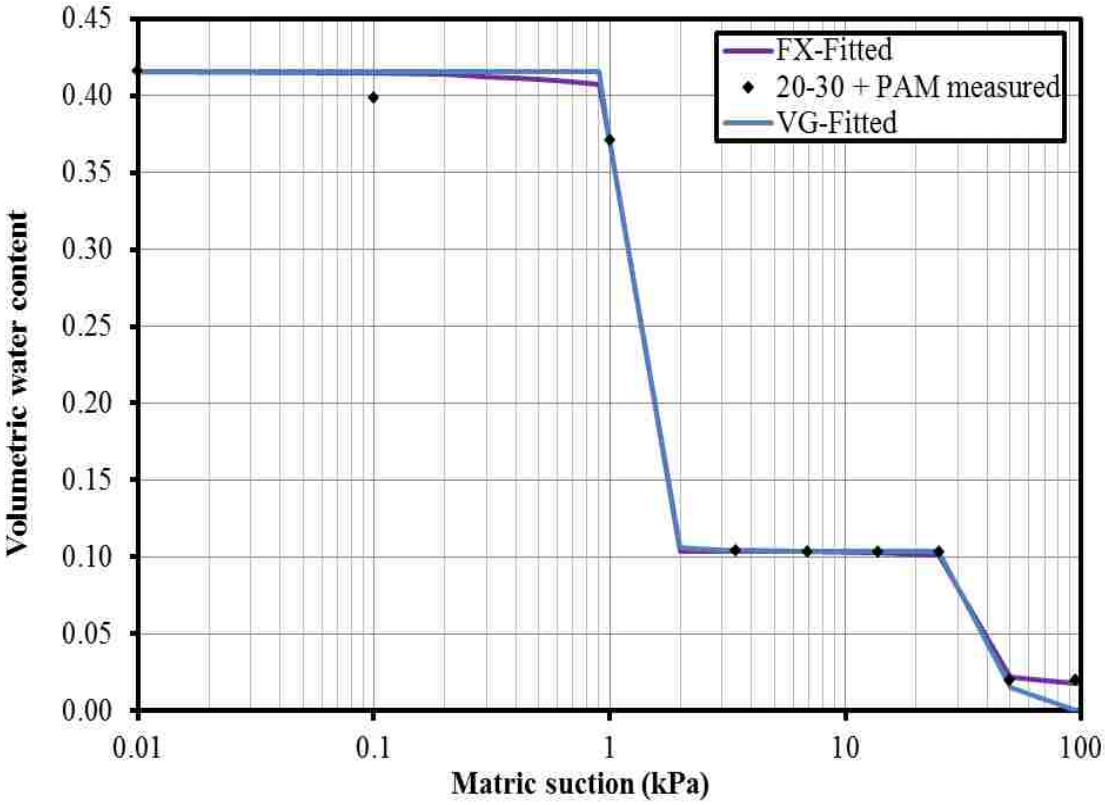

Figure A.17 SWCC result of sand with PAM

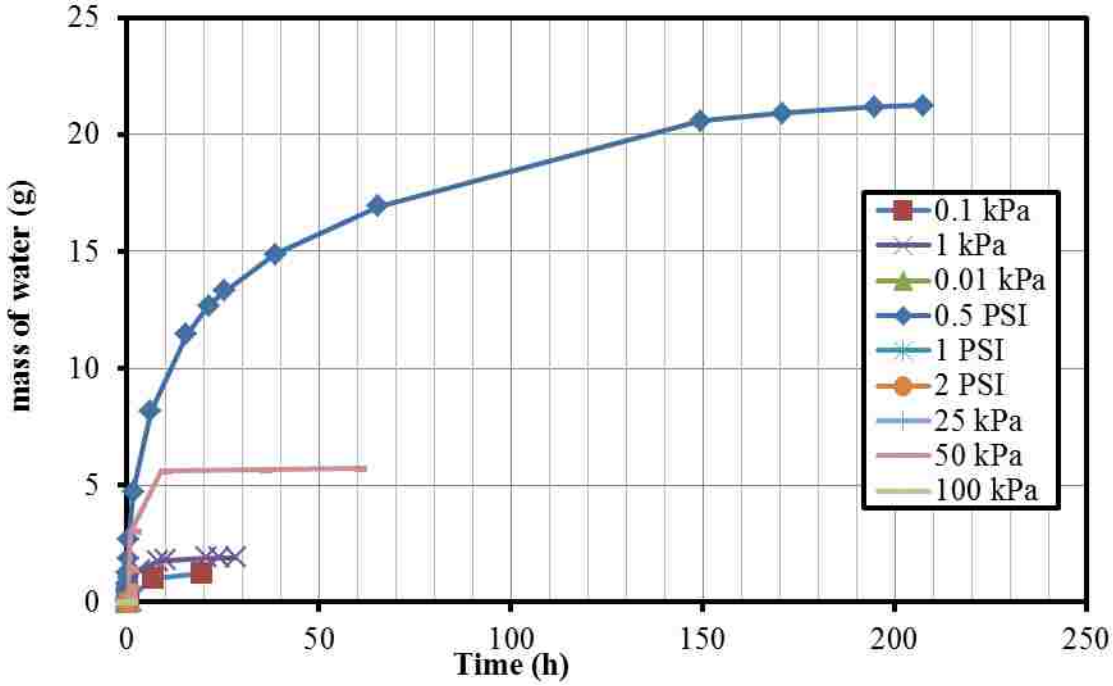

Figure A.18 Flux – Time relationship for PAM

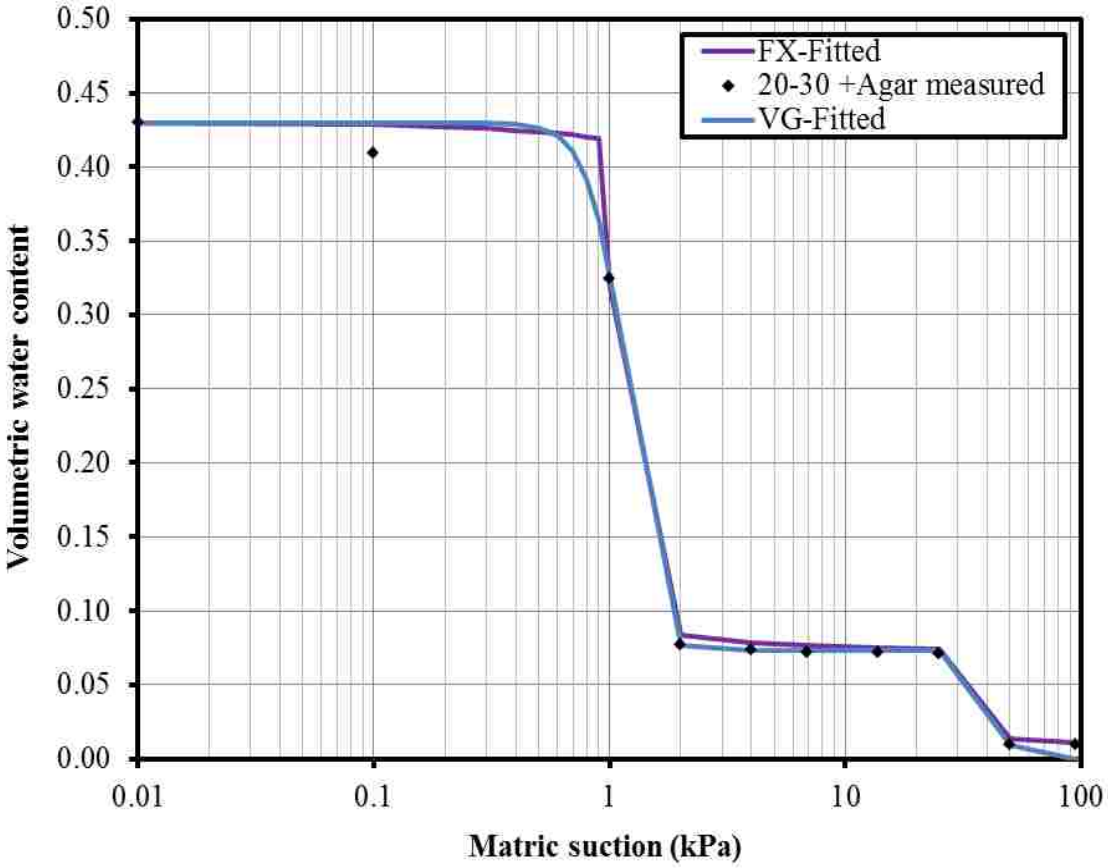

Figure A.19 SWCC result of sand with Agar

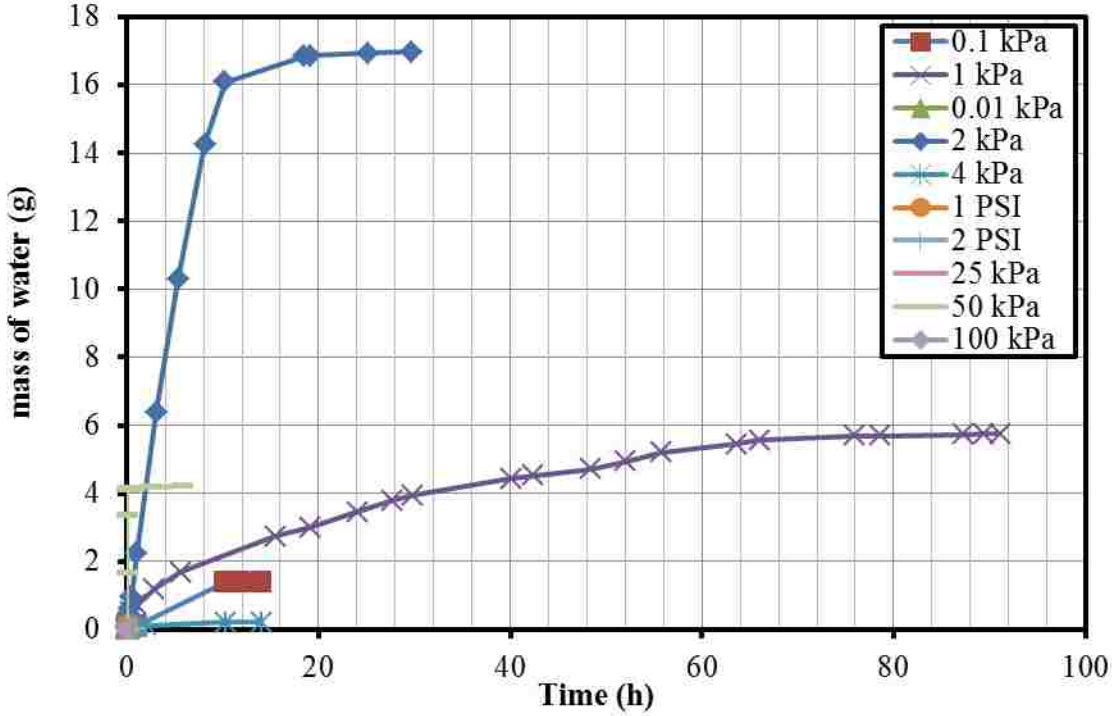

Figure A.20 Flux – Time for Agar

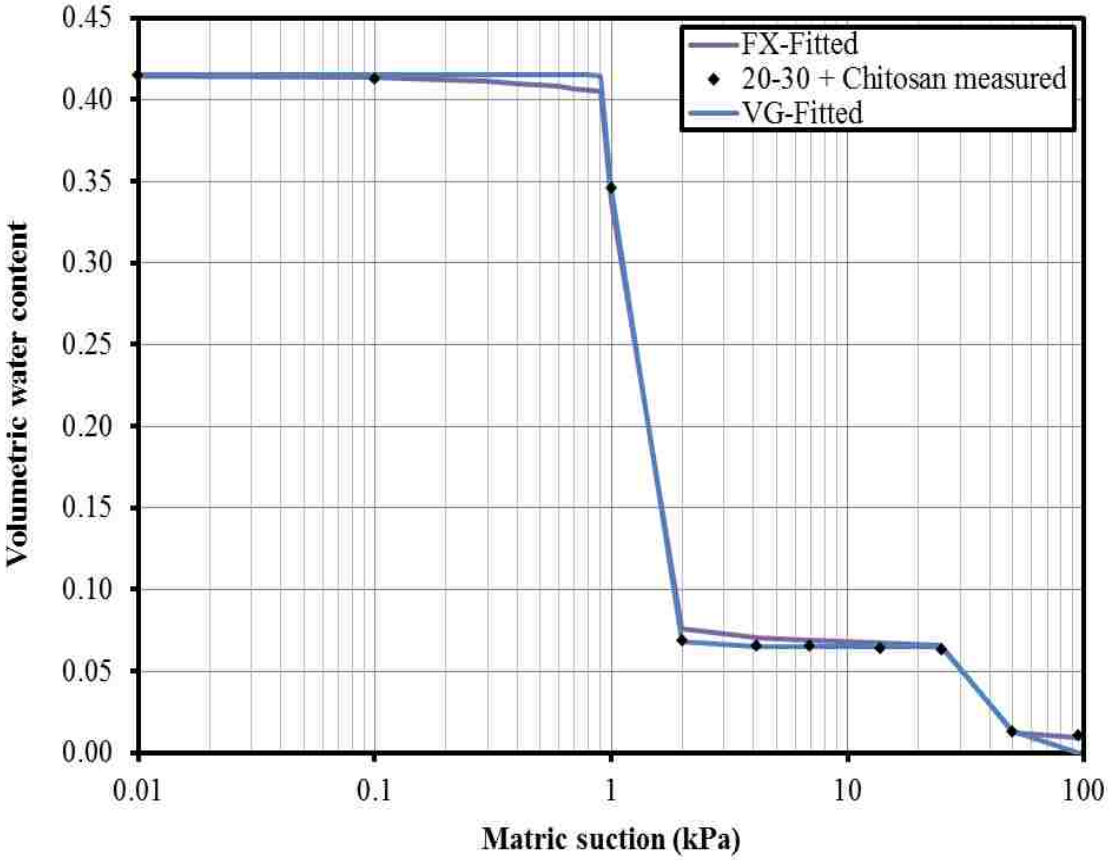

Figure A.21 SWCC result of sand with Chitosan

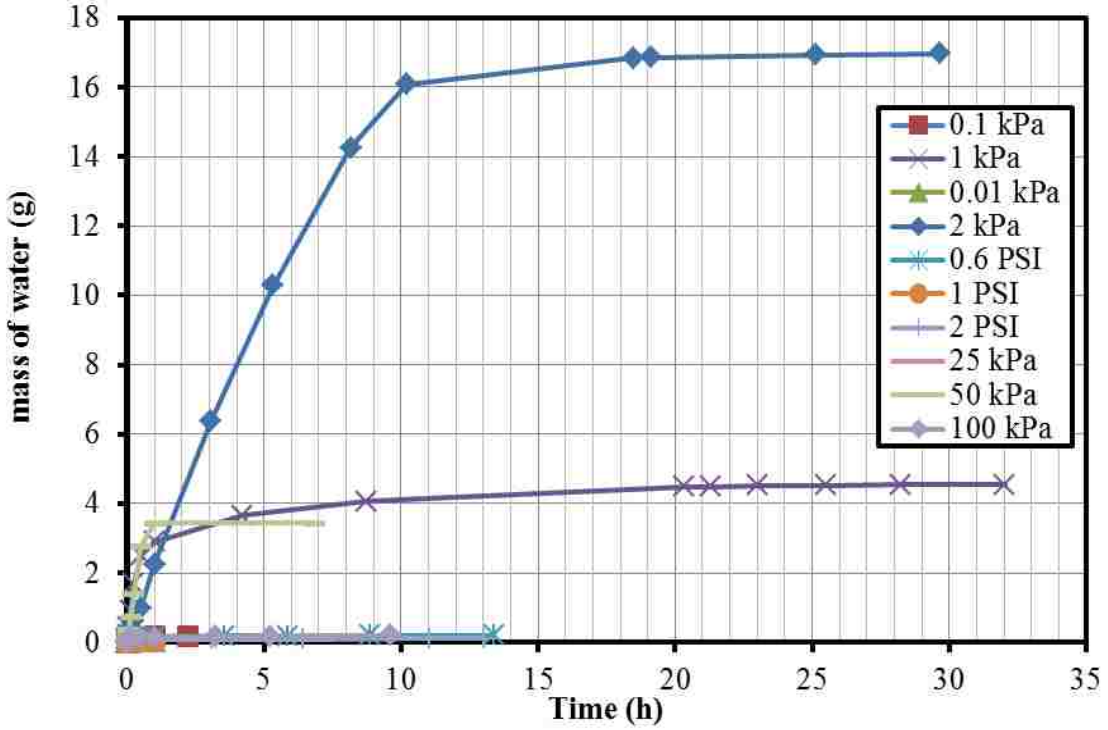

Figure A.22 Flux – Time for Chitosan

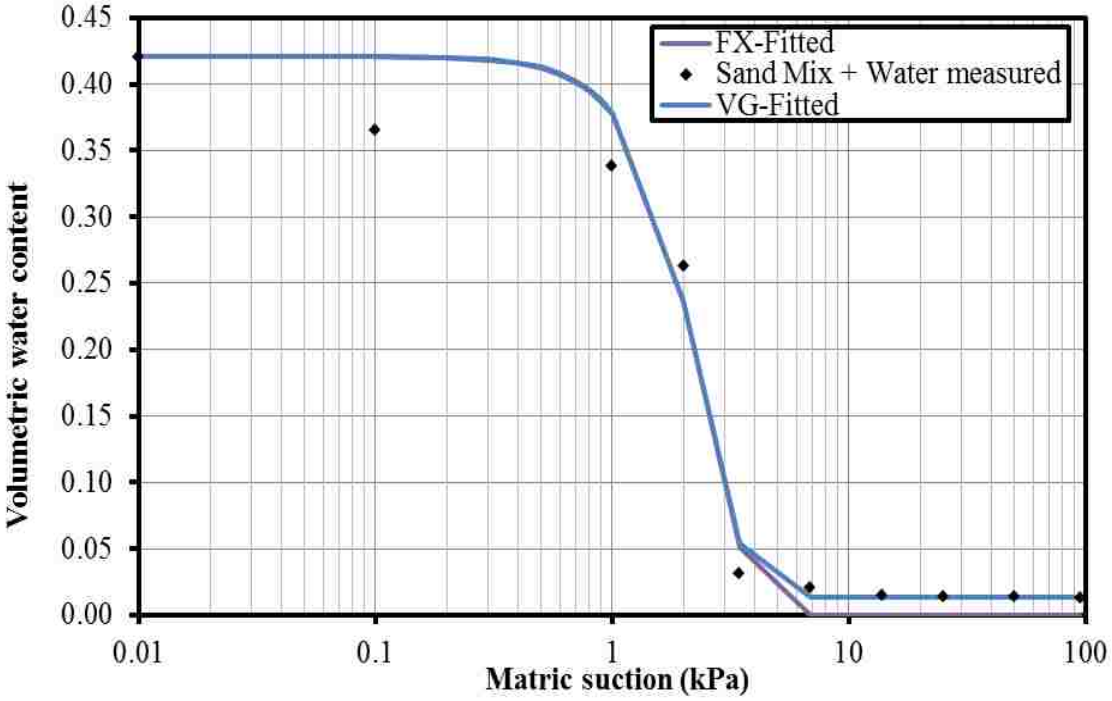

Figure A.23 SWCC result of sand mixture with water

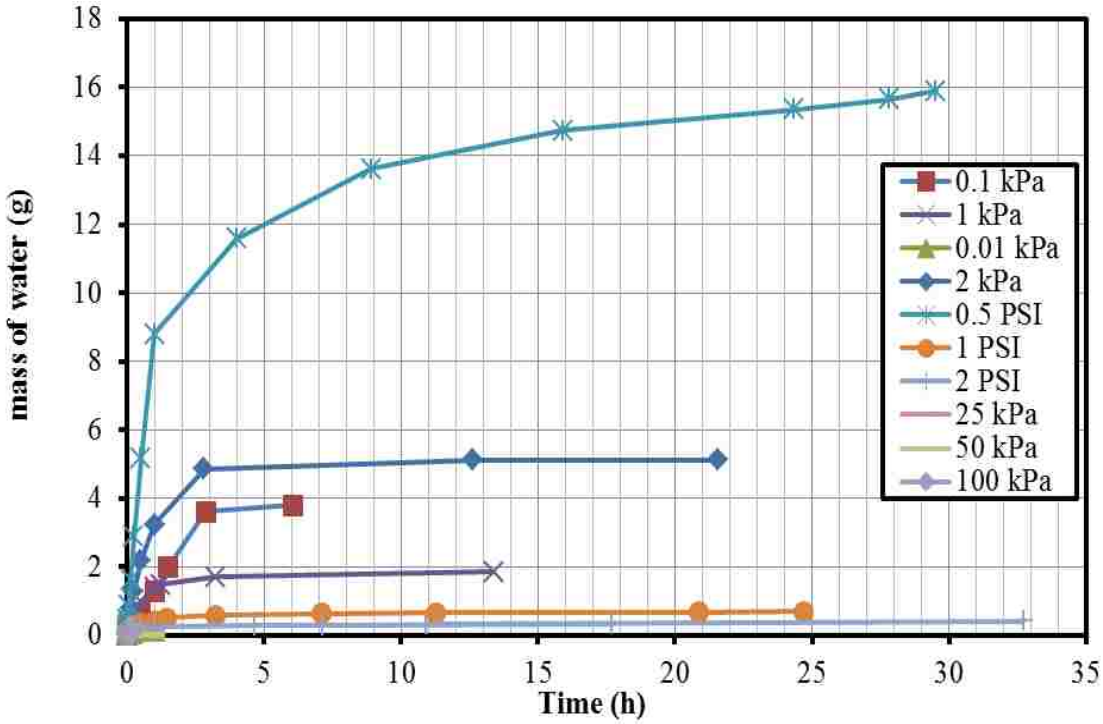

Figure A.24 Flux – Time for sand mixture with water

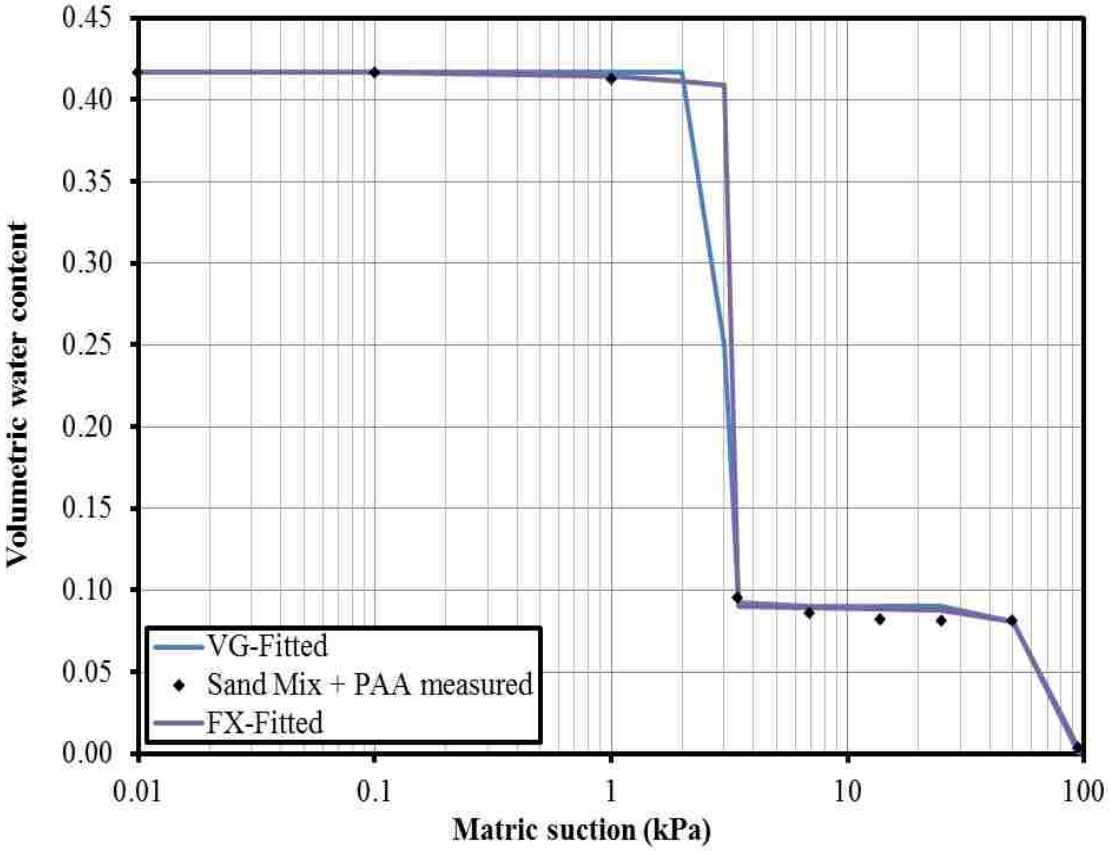

Figure A.25 SWCC result of sand mixture with PAA

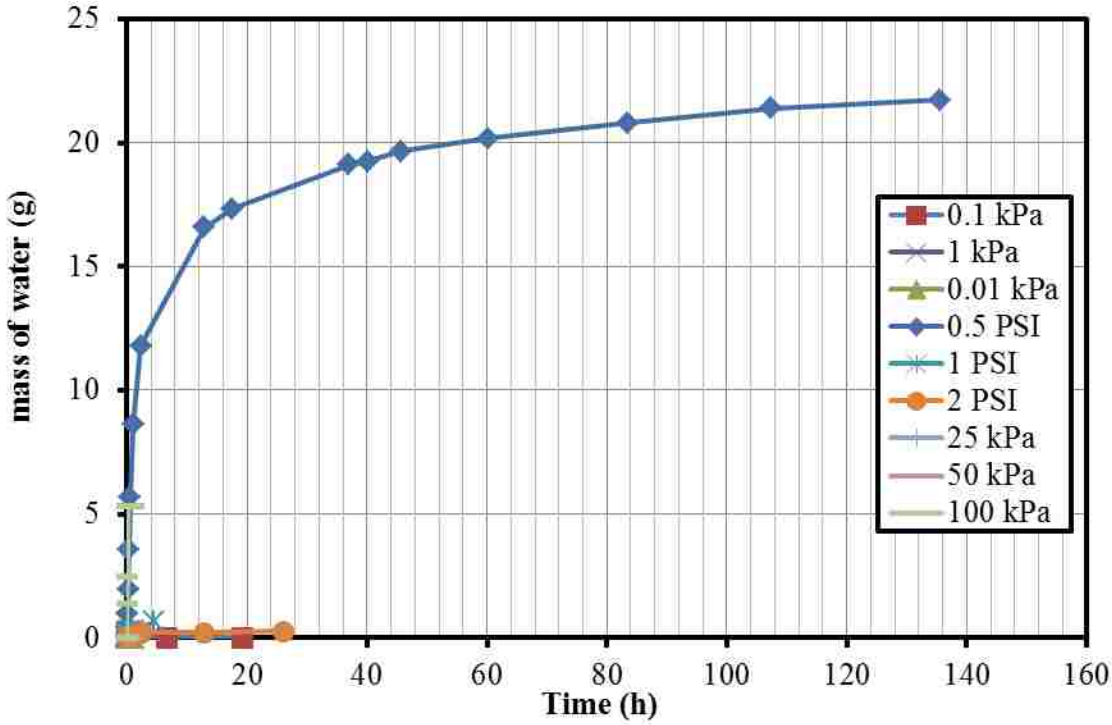

Figure A.26 Flux – Time of sand mixture with PAA

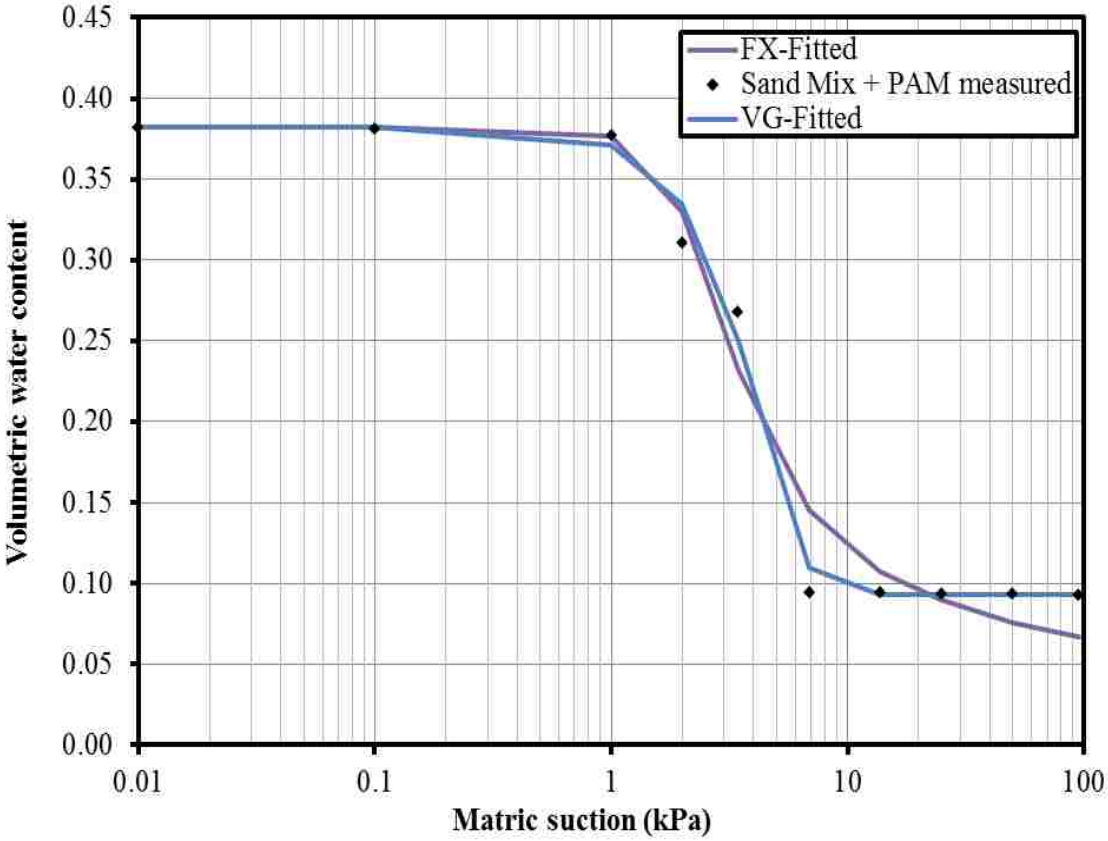

Figure A.27 SWCC result of sand mixture with PAM

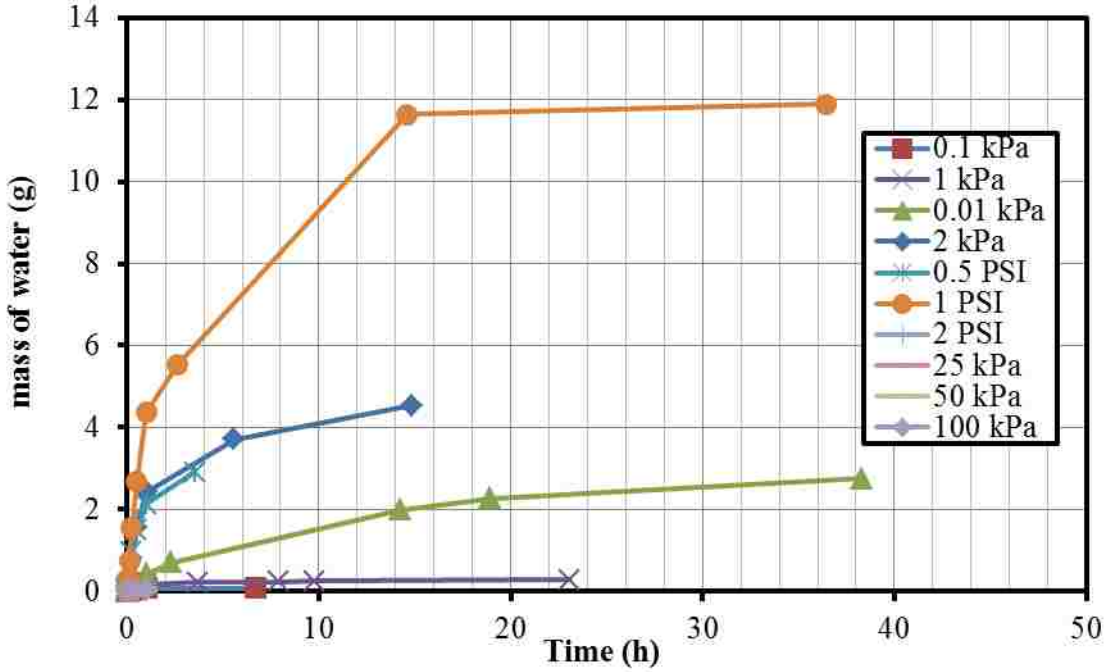

Figure A.28 Flux – Time of sand mixture with PAM

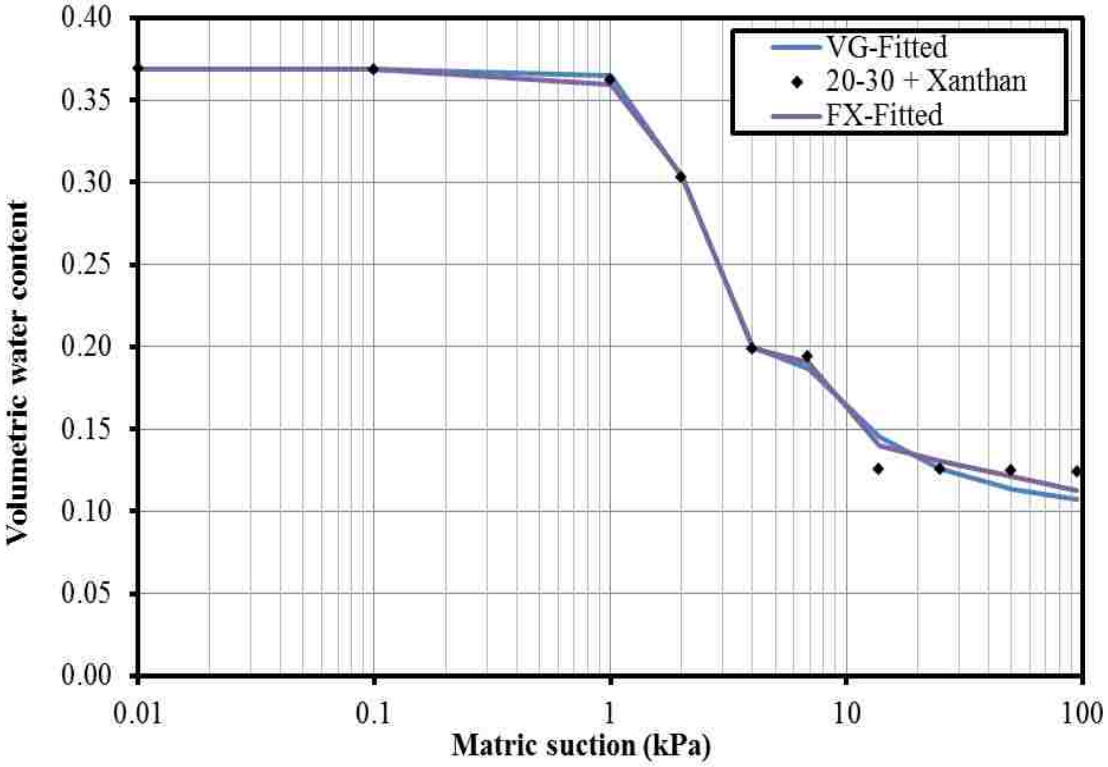

Figure A.29 SWCC result of sand mixture with Xanthan

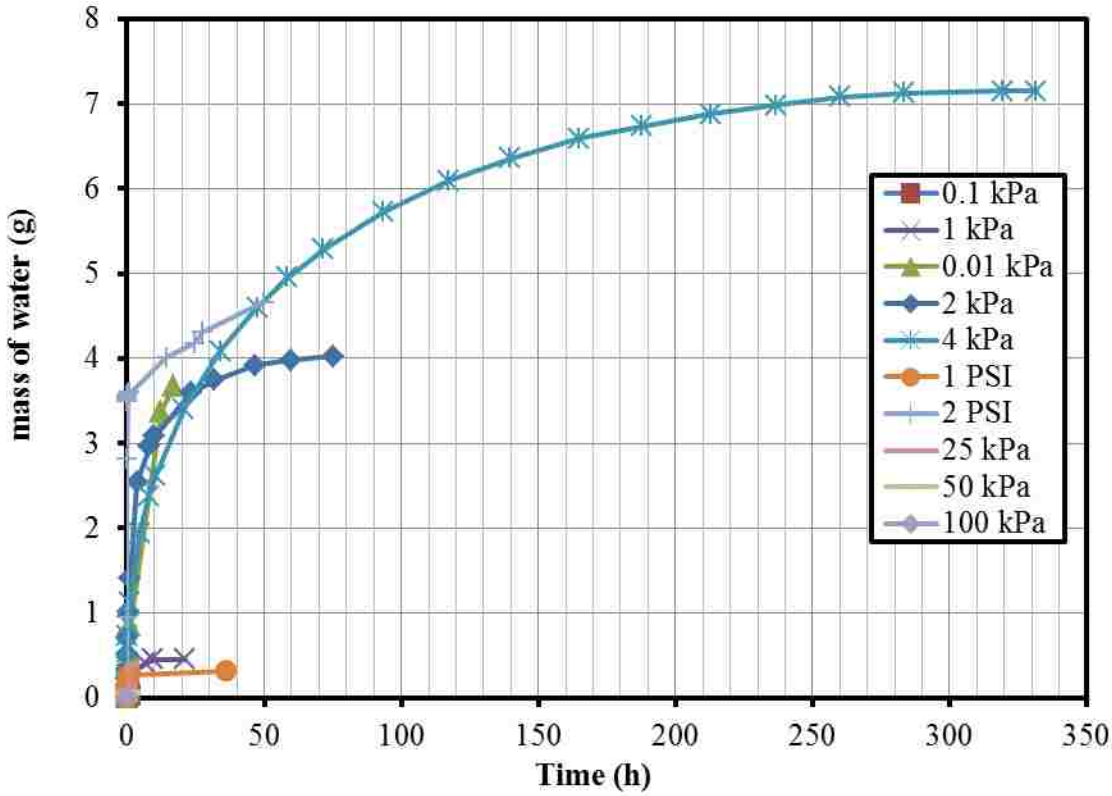

Figure A.30 Flux – Time of sand mixture with Xanthan

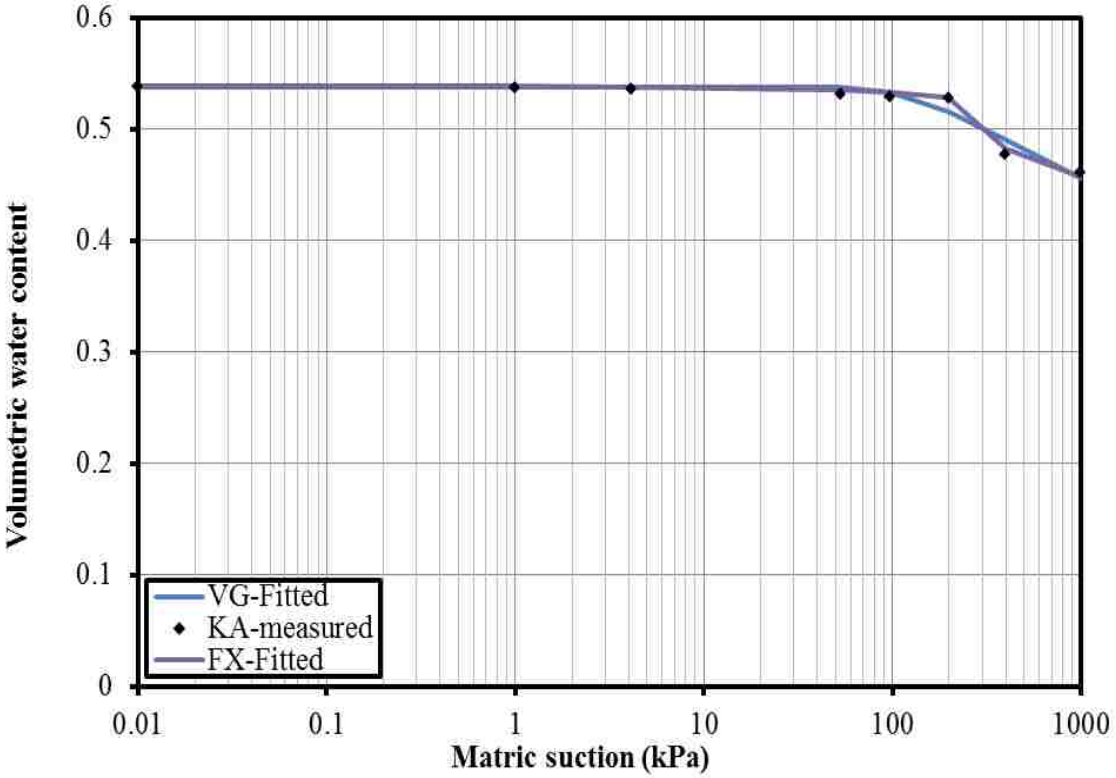

Figure A.31 SWCC result of kaolinite with water

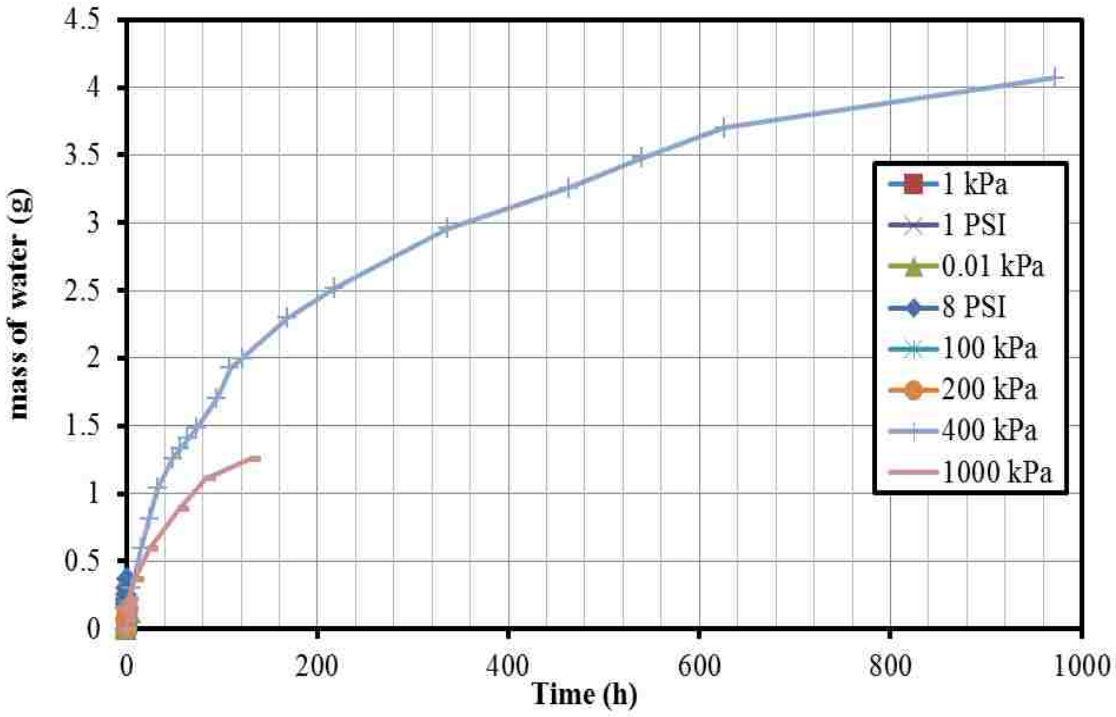

Figure A.32 Flux – Time of kaolinite with water

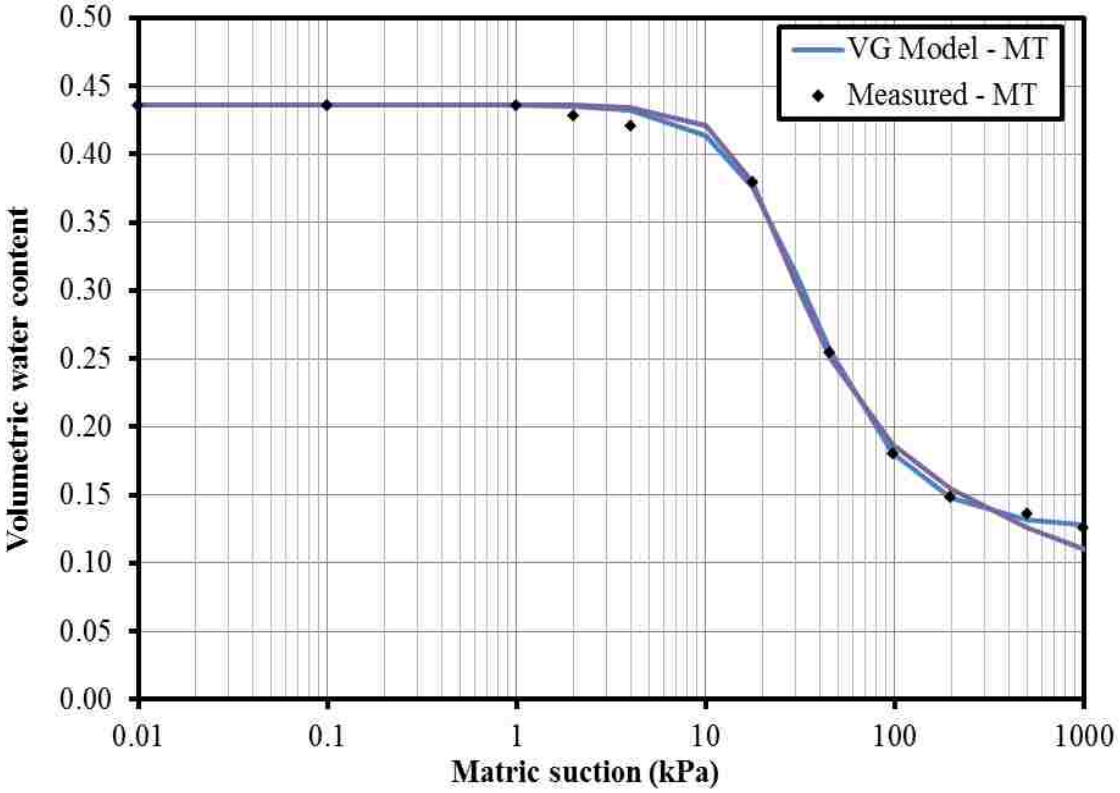

Figure A.33 SWCC result of mine tailing with water

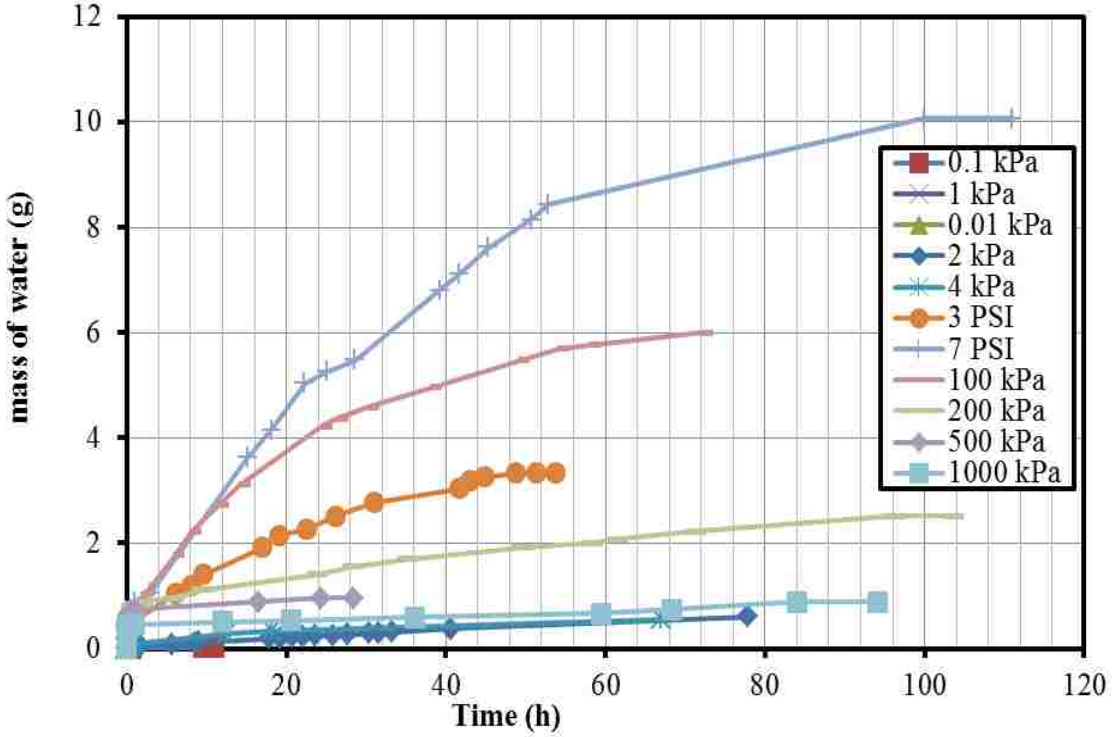

Figure A.34 Flux – Time of mine tailing with water

BIBLIOGRAPHY

Abramento, M., and Carvalho, C. "Geotechnical Parameters for the Study of Natural Slopes Instabilization at 'Serra do Mar'Brazil." *Proc., Proc 12th Int Conf Soil Mechanics and Foundations Engineering. Rio de Janeiro*, 1599-1602.

Adamson, A. W., and Gast, A. P. (1967). "Physical chemistry of surfaces."

Anandarajah, A., and Amarasinghe, P. M. (2011). "Microstructural Investigation of Soil Suction and Hysteresis of Fine-Grained Soils." *Journal of Geotechnical and Geoenvironmental Engineering*, 138(1), 38-46.

Bate, B., Zhao, Q., and Burns, S. (2013). "Impact of Organic Coatings on Frictional Strength of Organically Modified Clay." *Journal of Geotechnical and Geoenvironmental Engineering*, 140(1), 228-236.

Kang, X., Kang, G.-C., and Bate, B. (2014). Shear Wave Velocity Anisotropy of Kaolinite Using a Floating Wall Consolidometer-Type Bender Element Testing System. *Geotechnical Testing Journal*.

Briscoe, W. H., and Klein, J. (2007). "Friction and adhesion hysteresis between surfactant monolayers in water." *The Journal of Adhesion*, 83(7), 705-722.

Brooks, R., and Corey, A. (1964). "Hydraulic properties of porous media, Hydrology Papers, No. 3, Colorado State University, Ft." *Collins, Colo*.

Brutsaert, W. (1966). "Probability laws for pore-size distributions." *Soil Science*, 101(2), 85-92.

Buckingham, E. (1907). "Water retention in soil." *Soil Bulletin*, 38.

Burdine, N. (1953). "Relative permeability calculations from pore size distribution data." *Journal of Petroleum Technology*, 5(03), 71-78.

Cabalar, A., and Canakci, H. (2005). "Ground improvement by bacteria." Taylor and Francis Group, London, England, 707-712.

Chandraprabha, M., Natarajan, K., and Somasundaran, P. (2005). "Selective separation of pyrite from chalcopyrite and arsenopyrite by biomodulation using< i> Acidithiobacillus ferrooxidans</i>." *International Journal of Mineral Processing*, 75(1), 113-122.

Chen, R., Zhang, L., and Budhu, M. (2013). "Biopolymer stabilization of mine tailings." *Journal of Geotechnical and Geoenvironmental Engineering*, 139(10), 1802-1807.

Doering, E. (1965). "Soil-water diffusivity by the one-step method." *Soil Science*, 99(5), 322-326.

Davidson, D.T. (1961) “Soil Stabilization with chemicals,” *Iowa State University Bulletin*, (196), pp. 272-272.

Fam, M., and Santamarina, C. (1995). "Study of geoprocesses with complementary mechanical and electromagnetic wave measurements in an oedometer." *Geotechnical Testing Journal*, 18(3), 307-314.

Figueras, J., and Gribb, M. M. (2009). "Design of a user-friendly automated multistep outflow apparatus." *Vadose Zone Journal*, 8(2), 523-529.

Fredlund, D., Morgenstern, N., and Widger, R. (1978). "The shear strength of unsaturated soils." *Canadian Geotechnical Journal*, 15(3), 313-321.

Fredlund, D. G., and Rahardjo, H. (1993). *Soil mechanics for unsaturated soils*, John Wiley & Sons.

Fredlund, D. G., Rahardjo, H., and Fredlund, M. D. (2012). *Unsaturated soil mechanics in engineering practice*, Wiley.

Fredlund, D. G., and Xing, A. (1994). "Equations for the soil-water characteristic curve." *Canadian Geotechnical Journal*, 31(4), 521-532.

Fredlund, M. D., Wilson, G. W., and Fredlund, D. G. (2002). "Use of the grain-size distribution for estimation of the soil-water characteristic curve." *Canadian Geotechnical Journal*, 39(5), 1103-1117.

Gardner, W. (1956). "Calculation of capillary conductivity from pressure plate outflow data." *Soil Science Society of America Journal*, 20(3), 317-320.

Grimm, W. (1959) “Stabilization by cement, lime and fly ash in road construction,” *Journal of Construction (Arlington)*, 14(11), pp 321-331.

Imre, E., Laufer, I., Rajkai, K., Scheuermann, A., Firgi, T., and Telekes, G. "Water retention functions of sand mixtures." *Proc., 1st European Conference on Unsaturated Soils, E-UNSAT 2008, July 2, 2008 - July 4, 2008*, CRC Press, 299-304.

Kavazanjian Jr, E., Iglesias, E., and Karatas, I. "Biopolymer soil stabilization for wind erosion control." *Proc., Proc. 17th Int. Conf. Soil Mech. Geotech. Engng, Alexandria*, 881-884.

Khatami, H. R., and O'Kelly, B. C. (2012). "Improving Mechanical Properties of Sand Using Biopolymers." *Journal of Geotechnical and Geoenvironmental Engineering*, 139(8), 1402-1406.

Kosugi, K. i. (1994). "Three-parameter lognormal distribution model for soil water retention." *Water Resources Research*, 30(4), 891-901.

Kulhawy, F. H., and Mayne, P. W. (1990). "Manual on estimating soil properties for foundation design." Electric Power Research Inst., Palo Alto, CA (USA); Cornell Univ., Ithaca, NY (USA). Geotechnical Engineering Group.

Lake, C. B., and Rowe, R. K. (2005). "A comparative assessment of volatile organic compound (VOC) sorption to various types of potential GCL bentonites." *Geotextiles and Geomembranes*, 23(4), 323-347.

Li, X., Zhang, L. M., and Li, J. H. (2009). "Development of a modified axis translation technique for measuring SWCCs for gravel soils at very low suctions." *Geotechnical Testing Journal*, 32(6).

Lu, N., and Likos, W. J. (2006). "Suction stress characteristic curve for unsaturated soil." *Journal of Geotechnical and Geoenvironmental Engineering*, 132(2), 131-142.

Martin, G., Yen, T., and Karimi, S. "Application of biopolymer technology in silty soil matrices to form impervious barriers." *Proc., 7th Australia New Zealand Conference on Geomechanics: Geomechanics in a Changing World: Conference Proceedings*, Institution of Engineers, Australia, 814.

Mazzieri, F., Di Emidio, G., and Van Impe, P. O. (2010). "Diffusion of calcium chloride in a modified bentonite: impact on osmotic efficiency and hydraulic conductivity." *Clays and Clay Minerals*, 58(3), 351-363.

McKee, C., and Bumb, A. "The importance of unsaturated flow parameters in designing a monitoring system for hazardous wastes and environmental emergencies." *Proc., Proc. Hazardous Materials Control Research Institute Natl. Conf., Houston, TX*, 50-58.

Mpofu, P., Addai-Mensah, J., and Ralston, J. (2004). "Temperature influence of nonionic polyethylene oxide and anionic polyacrylamide on flocculation and dewatering behavior of kaolinite dispersions." *Journal of Colloid and Interface Science*, 271(1), 145-156.

Mualem, Y. (1976). "A new model for predicting the hydraulic conductivity of unsaturated porous media." *Water resources research*, 12(3), 513-522.

Nugent, R., Zhang, G., and Gambrell, R. "The Effect of Exopolymers and Void Ratio on the Erosional Resistance of Cohesive Sediments." *Proc., Geo-Frontiers 2011@ sAdvances in Geotechnical Engineering*, ASCE, 1493-1502.

Puppala, A. J., Punthutaecha, K., and Vanapalli, S. K. (2006). "Soil-water characteristic curves of stabilized expansive soils." *Journal of Geotechnical and Geoenvironmental Engineering*, 132(6), 736-751.

Raymond, S. (1958). "The utilization of pulverised fuel ash." *Civil Eng Public Works Rev Lond*, 53, 1013-1016.

Russell, H. (1957). "A summary of the fly-ash disposal problem." *Journal of the Air Pollution Control Association*, 7(1), 46-47.

Russo, D. (1988). "Numerical analysis of the nonsteady transport of interacting solutes through unsaturated soil. 1. Homogeneous systems." *Water Resources Research*, 24(2), 271-284.

Simunek, J., and Hopmans, J. W. (2002). "Parameter optimization and nonlinear fitting." *Soil Science Society of America Book Series*, 5, 139-157.

Swanson, D. A., Savci, G., Danziger, G., Mohr, R. N., and Weiskopf, T. (1999). "Predicting the soil-water characteristics of mine soils." *Proceedings of the ... International Conference on Tailings and Mine Waste*, 6, 345-349.

"Stabilization of soil with lime and fly ash."*National Research Council -- Highway Research Board -- Research Record,* (29) pp. 94, 1963.

Toorman, A. F., Wierenga, P. J., and Hills, R. G. (1992). "Parameter estimation of hydraulic properties from one-step outflow data." *Water Resources Research*, 28(11), 3021-3028.

van Dam, J. C., Stricker, J. N. M., and Droogers, P. (1994). "Inverse method to determine soil hydraulic functions from multistep outflow experiments." *Soil Science Society of America Journal*, 58(3), 647-652.

Van Genuchten, M. T. (1980). "A closed-form equation for predicting the hydraulic conductivity of unsaturated soils." *Soil Science Society of America Journal*, 44(5), 892-898.

Vanapalli, S., Sillers, W., and Fredlund, M. "The meaning and relevance of residual state to unsaturated soils." *Proc., 51st Canadian Geotechnical Conference*, Citeseer, 4-7.

Voordouw, G. (2013). "Interaction of oil sands tailings particles with polymers and microbial cells: First steps toward reclamation to soil." *Biopolymers*, 99(4), 257-262.

Wayllace, A., and Lu, N. (2012). "Atransient water release and imbibitions method for rapidly measuring wetting and drying soil water retention and hydraulic conductivity functions." *Geotechnical Testing Journal*, 35(1).

Wheeler, S., and Sivakumar, V. "Development and application of a critical state model for unsaturated soil." *Proc., PREDICTIVE SOIL MECHANICS. PROCEEDINGS OF THE WROTH MEMORIAL SYMPOSIUM, 27-29 JULY 1992, ST CATHERINE'S COLLEGE, OXFORD*.

Whisler, F. D., and Watson, K. K. (1968). "One-dimensional gravity drainage of uniform columns of porous materials." *Journal of Hydrology*, 6(3), 277-296.

Wikipedia (2014). http://en.wikipedia.org/wiki/Contact_angle

Williams, J., Prebble, R., Williams, W., and Hignett, C. (1983). "The influence of texture, structure and clay mineralogy on the soil moisture characteristic." *Soil Research*, 21(1), 15-32.

Williams, P. J. (1982). *The surface of the earth: an introduction to geotechnical science*, Longman London, UK.

Wolf, A. B., Vos, M., De Boer, W., and Kowalchuk, G. A. (2013). "Impact of matric potential and pore size distribution on growth dynamics of filamentous and non-filamentous soil bacteria." *PLoS ONE*, 8(12).

Wright, W., and Ray, P. (1957). "The use of fly ash in soil stabilization." *Magazine of Concrete Research*, 9(25), 27-31.

Wyllie, M., and Gardner, G. (1958). "The generalized Kozeny-Carman equation." *World oil*, 146(4), 210-213.

Xiao, M., Reddi, L. N., and Steinberg, S. L. (2009). "Variation of water retention characteristics due to particle Rearrangement under zero gravity." *International Journal of Geomechanics*, 9(4), 179-186.

Yoshizawa, H., Chen, Y. L., and Israelachvili, J. (1993). "Fundamental mechanisms of interfacial friction. 1. Relation between adhesion and friction." *The Journal of Physical Chemistry*, 97(16), 4128-4140.

Yun, G., and Fredlund, D. G. (1997). "Use of the tensile strength of water for the direct measurement of high soil suction." *Canadian geotechnical journal*, 34(4), 604-614.

VITA

Xiaoyi Zhao was born in 1988 and grew up in Xi' an, Shaanxi Province, China. He received his B.S. in Civil Engineering in July 2010 and began his graduate study in August 2011 at Missouri University of Science and Technology under supervision of Dr. Bate, Bate. He received his Master Degree in Civil Engineering in August, 2014.